DOKUZ EYLÜL UNIVERSITY

GRADUATE SCHOOL OF NATURAL AND APPLIED SCIENCES

MODAL PARAMETER ESTIMATION AND DAMAGE IDENTIFICATION ON PROGRESSIVELY DAMAGED R/C FRAMES

by

Erkan DURMAZGEZER

December, 2019

İZMİR

MODAL PARAMETER ESTIMATION AND DAMAGE IDENTIFICATION ON PROGRESSIVELY DAMAGED R/C FRAMES

A Thesis Submitted to the
Graduate School of Natural and Applied Sciences of Dokuz Eylül University
In Partial Fulfillment of the Requirements for the Degree of Doctor of Philosophy in Civil Engineering, Structural Engineering Program

by

Erkan DURMAZGEZER

December, 2019

İZMİR

Ph.D. THESIS EXAMINATION RESULT FORM

We have read the thesis entitled **"MODAL PARAMETER ESTIMATION AND DAMAGE IDENTIFICATION ON PROGRESSIVELY DAMAGED R/C FRAMES"** completed by **ERKAN DURMAZGEZER** under supervision of **ASSOC. PROF. DR. ÖZGÜR ÖZÇELİK** and we certify that in our opinion it is fully adequate, in scope and in quality, as a thesis for the degree of Doctor of Philosophy.

Assoc. Prof. Dr. Özgür ÖZÇELİK

Supervisor

Prof. Dr. Serap KAHRAMAN

Thesis Committee Member

Asst. Prof. Dr. Serkan GÜNEL

Thesis Committee Member

Doç. Dr. Güvsoy TURAN

Examining Committee Member

Doç. Dr. Emre ERCAN

Examining Committee Member

Prof. Dr. Kadriye ERTEKİN

Director

Graduate School of Natural and Applied Sciences

ACKNOWLEDGEMENTS

The research for this dissertation was performed at Dokuz Eylül University under the direction of Assoc. Prof. Dr. Özgür ÖZÇELİK. His excellent supervision and support has been indispensable to my academic growth over the six years, he has been a rigorous and insightful teacher who enlightened me during my Ph.D study. I will always be grateful to him for his enormous contribution on me.

I also would like to thank Assoc. Prof.Dr. İbrahim Serkan MISIR who helped me to gain significant experience, especially in conducted experimental studies. He spent his valuable time as my temporal Ph.D advisor for more than one year; I benefited from his constructive and inspirational scientific discussions.

My gratitude also extends to all the members of my doctoral committee members, Prof. Dr. Serap KAHRAMAN and Asst. Prof. Dr. Serkan GÜNEL. They had always been willingly to dedicate their time to help me with my research.

The Ph.D fellow, Res.Asst. Umut YÜCEL deserves a very special thanks for sharing his valuable time and friendship with me for all these years. Within this time period, we have passed through many challenging obstacles together and our collaboration will always go on.

My gratitude also extends to all professors & friends who shared with me the moments of the graduate student life in Structural Engineering Department of Dokuz Eylül University, Msc. Özgür GİRGİN, Asst. Prof. Dr. Sadık Can GİRGİN; Research Assistants Burak DURAN, Onur ÖZTÜRKOĞLU and Gökhan YÜCEL and other colleagues. I'm also thankful to former civil engineering department students Muhammed Emin DEMİRKIRAN, Onur BAŞKAYA, Üstun Can MERİÇ, Gokhan OKUDAN, Mazlum YAĞIZ, Umut CANDAN, Fahri TOKGÖZ, Filiz VARGÜN, Mustafa USLU, Bayram KAYA, Samet GÖYMEN, Duygu ŞENOL, İnci TERKAN for their help in experimenal test preperations.

Specifically, I adress my gratitude to Professors Geert LOMBAERT and Guido De ROECK for their hospitality and support during my stay at University of Leuven as an international scholar. I'm indebted to them for their contribution in theoretical knowledge provided in the subject of finite element model updating.

Finally, I would like to thank to my family members Binnaz, Haluk, Melih DURMAZGEZER for their endless, support and guidance. They were by my side whenever I need. They gave me all kind of love and support to receive the Ph.D degree.

I’m greatly acknowledged to the financial support provided by the Scientific and Technological Council of Turkey (TUBITAK) under the grant #112M203 between the years 2013-2016.

Erkan DURMAZGEZER

MODAL PARAMETER ESTIMATION AND DAMAGE IDENTIFICATION ON PROGRESSIVELY DAMAGED R/C FRAMES

ABSTRACT

In the profession of civil engineering, experimental eigenfrequencies and mode shapes estimated by operational modal analysis techniques, are found the most suited parameters used in structural damage identification. The main focus of this study is to perform a damage identification study of an experimentally tested half-scale reinforced concrete (RC) frame by means of degradation of Young's modulus in structural elements; which is done by using the sensitivity-based finite element model updating method. Damage is created by imposing the frame with progressive drift ratios by a displacement-controlled hydraulic actuator using single-cycle quasi-static lateral loading along its in-plane direction. Dynamic tests are conducted using an electro-dynamic shaker and system identification at different damage levels is performed using output-only methods NExT-ERA, EFDD and SSI. The objective function used for damage identification is then constructed by the modal parameter differences constructed between the experimentally identified and finite element (FE) predicted. Results are obtained through the minimization of this function by applying the numerical optimization technique Gauss-Newton method with trust region implementation. Study is performed in three subsequent steps: (i) The system identification results of RC structure at undamaged and various damage levels are obtained (ii) The reference FE model using the experimental modal parameters corresponding to the undamaged test frame is obtained (iii) the reference model is updated for increasing damage levels using the modal parameters corresponding to these levels to identify existence of damage, its location, and extent. Results are presented in terms of stiffness reduction factors on the column(s) bottom and beam ends. In the final part of the thesis, the uncertainty in the damage identification results are investigated using the modal parameters polluted with two levels of noise.

Keywords: System identification, finite element model updating, structural damage identification, vibration-based structural health monitoring, shake table test

ARTAN BİÇİMDE HASARLANMIŞ BETONARME ÇERÇEVELERİN MODAL PARAMETRE TAHMİNİ VE HASAR TANIMLAMASI

ÖZ

İnşaat mühendisliği alanında, operasyonel modal analiz teknikleriyle tahmin edilen deneysel frekans ve mod şekilleri yapısal hasar tespitinde kullanılan en uygun parametreler olarak görülmektedir. Bu çalışmanın ana odağı, deneysel olarak test edilen 1/2 ölçekli betonarme çerçevenin duyarlık-tabanlı sonlu eleman model güncelleme metodu vasıtasıyla hasarlı elemanlarda Young modülü azalması cinsinden hasar tespit tahminin yapılmasıdır. Farklı öteleme oranlarındaki yapısal hasar, deplasman kontrollü hidrolik pistonun çerçeve tepe noktasından düzlem içi doğrultuda tek çevrimli yarı-statik yatay deplasman protokolünün uygulanmasıyla oluşturulmuştur. Dinamik testler, elektro-dinamik sarsma tablası kullanılarak gerçekleştirilmiş olup, farklı hasar seviyelerindeki sistem tanımlama işlemi operasyonel modal analiz yöntemleri olan NExT-ERA, EFDD ve SSI ile gerçekleştirilmiştir. Hasar tespiti aşamasında kullanılan amaç fonksiyonu deneysel olarak elde edilen tahmin modal parametrelerin ve sonlu eleman modal parametrelerinin farkları şeklinde oluşturulmuştur. Sonuçlar, bu fonksiyonun sayısal optimizasyon tekniği olan güven bölgeli Gauss – Newton metodu ile minimizasyonu sağlanarak elde edilmiştir. Çalışma ardışık olarak üç aşamada gerçekleştirilmiştir: (i) Betonarme çerçevenin hasarsız durumda ve farklı hasar seviyelerinde sistem tanımlama sonuçlarının elde edilmesi (ii) betonarme çerçevenin hasarsız durumdaki modal parametreleri kullanılarak referans sonlu eleman modelinin elde edilmesi (iii) referans sonlu eleman modelinin çerçevenin farklı hasar seviyesinde elde edilen deneysel modal parametreleri kullanılarak güncellenmesiyle hasarın lokasyon ve büyüklüğü ile birlikte elde edilmesi. Her bir farklı öteleme oranındaki hasar tespit sonuçları, çerçevenin kolon alt ve kiriş uçlarında rijitlik azalması cinsinden sunulmuştur. Tezin son bölümünde, hasar tespit sonuçlarındaki belirsizlikler iki düzeyde gürültü ile kirletilen modal parametreler kullanılarak incelenmiştir.

Anahtar kelimeler: Sistem tanımlama, sonlu eleman model güncelleme, yapısal hasar tespiti, titreşim-tabanlı yapı sağlığı izleme, sarsma tablası testi

CONTENTS

Page

LIST OF FIGURES

Page

LIST OF TABLES

Page

CHAPTER ONE
INTRODUCTION

1.1 Operational Modal Analysis (OMA)

Modal analysis is developed and well established profession in the identification of inherent dynamic characteristics of systems. Recent innovative developments enabled experimental identification of modal parameters to be used in the fields of vibration control, optimization of design and performance assessment. This field is based on the fact that response of the system can be expressed as a linear combination of harmonic motions, that is the modes of vibration. The methods used for modal testing (also called as experimental modal analysis) mainly employ the measured input-output relationships which are characterized mathematically by frequency response functions (FRFs). Classical modal testing can be performed by various type of excitations, i.e., stepped sinusoids, white noise, frequency sweeping.

Modal analysis has also found a significant attraction in the field of civil engineering; however modal testing was originally developed for smaller structural systems in size. Moreover, difficulties in measurement of input excitations i.e. ambient vibrations (AV), earthquake waves, traffic loads caused civil engineering community to focus on the estimation of dynamic characteristics based on response measurements only. In this context, the operational modal analysis (OMA) belongs to the system identification discipline which is widely used to estimate vibration characteristics of structures (i.e., natural vibration frequencies, mode shapes, and damping ratios, a.k.a. modal parameters) using only-output response data. These tools are generally utilized to identify modal parameters of structures idealized as equivalent viscously damped linear elastic time-invariant systems. A fundamental assumption in OMA techniques is that the structure to be investigated is excited by random broad-band excitation i.e., having white-noise (WN) characteristics, or having band-limited WN characteristics. Broad-band excitation enables various structural modes to be excited sufficiently, and it is also necessary for avoiding the system to be driven at a specific frequency. Consequently, the identified modal

parameters are representing the actual behavior of the structure as the system characteristics are extracted from the data collected in operational conditions.

There are numerous studies available on modal identification of reinforced concrete (RC) structures with different infill conditions tested under dynamic conditions in the literature. Moaveni et al., (2012) performed modal identification study on a progressively damaged three-story building using input-output vibration data. In another study by Moaveni et al., (2010), modal parameters of a seven-story RC building slice tested on a shake table were estimated under progressively increasing damage levels. To do that at each damage level, low amplitude WN tests have been used. Ji et al., (2010) imposed various levels of realistic damage conditions by the E-Defense shake table in Japan. Using frequency response functions (FRF) and auto-regressive exogenous input method (ARX), modal parameters of a four-story real-size RC building were identified at different damage levels. Belleri et al., (2014) performed damage identification work on a 3-story 1/2-scale precast concrete parking structure subjected to various ground motions on a shake table. The recorded input-output data was used with deterministic-stochastic subspace method for modal identification purpose. Astroza et al., (2016) identified modal parameters of a real-size five-story fixed-base RC building subjected to a sequence of earthquake ground motions with increasing intensities on a large outdoor shake table. The recorded data from WN and AV tests were processed by two input-output and three output-only system identification methods. Changes in the modal parameters as a function of increasing damage were reported. Stavridis et al., (2012) performed a series of shake table tests on a 2/3-scale RC frame with un-reinforced solid masonry brick infills. Series of dynamic tests, including AV, WN, and historical earthquake records with increasing intensities, were performed. One of the objectives of the study was to determine the fundamental frequency of the frame experiencing progressively increasing damage.

The modal parameter estimation is not the final objective in SHM. A relevant field of application of the identified modal parameters is finite element (FE) model

validation and damage detection which is generally performed by finite element model updating technique.

1.2 Finite Element Model Updating (FEMU)

Over the recent years, FE method has been widely used as an indispensable tool for structural design and analysis; i.e. to find the force distribution and deformations of structures, vibration responses due to dynamic loading. Accordingly, the physical behavior of the structure can be simulated and predicted in engineering sense. Despite the recent advances in the field of structural modeling, an initial employed FE model may not be a convenient representative of the structure in the context of structural dynamics due to a number of simplifying assumptions depending on engineering judgement e.g. faulty boundary conditions, incorrect values of material properties, discretization of continuum or a poor quality mesh, complexity in modeling real life structures. This result the employed FE model validation is imperative; as these assumptions may result to create deviations between the numerical model and the behavior of real structure. It is widely accepted that, vibrations extracted from experimental data has a better representation of the structural behavior than that of the FE model, despite the presence of experimental errors. Therefore, mathematical tool called "*finite element model updating technique"*, which helps to calibrate the FE model of the structure using the outcomes of the experimental data, is started to be used on various engineering fields commonly (Teughels, 2003; Friswell & Mottershead, 2013). Generally speaking, this technique aims to calibrate design variables which appear as a parameter in numerical model until the discrepancies between the model and experimental modal data.

Model updating techniques are mostly used to find a solution of "inverse problems" since the method aims to produce a certain output which is obtained from the outcome of the experimental data. In the context of structural mechanics, FRFs, acceleration time histories, modal strains (or curvatures) are considered to be best suited tools for calibration of FE models; however in civil engineering profession,

mostly the operational modal parameters, such as eigenfrequencies and mode shapes are preferred; as the structure do not required to be excited by artificial force source. In the field of structural health monitoring (SHM), FE model updating method is also found by the most prominent technique for damage identification problems; as it has capability to identify damage locations together with their extent by calibrating the structural design variables that is related to structural stiffness. Structural damage alters mass, stiffness, and energy dissipation characteristics of structural systems. These changes result in detectable variations in systems' vibration characteristics and detecting these variations is the main principle of vibration-based SHM (Doebling et al., 1998; Sohn et al., 2003).

In literature, the FEMU techniques can mainly be classified into two categories:

- Direct (Matrix) Methods (Non-iterative)
- Iterative Methods (Iterative Sensitivity-Based methods)

1.2.1 Direct Methods

Direct methods can reproduce the measured data exactly within a single-step; therefore these techniques are very efficient in the case of measurement data not contaminated with noise. Despite its effectiveness, these methods have less frequently used in real-life applications since mass and stiffness matrices are updated directly; in-turn their updated values lose their structural meaning which leads difficulties in understanding the system matrices. Positive definiteness and the original model connectivity is no longer guaranteed to be remained.

Appearances of the direct methods are first dated back to late 1970's. Baruch (1978), developed the methodology in which the eigenvectors and stiffness matrices are updated based on the minimization of the weighted norm of the difference between of the FE and measured correspondence. A year later Berman (1979), adopted the mathematical approach of Baruch and contributed the methodology by enabling to update the mass matrices. In literature, these techniques are called as "*reference basis methods*", as one of the quantities among the eigenvectors, mass and

stiffness matrices is assumed to be reference and the other two are updated. Baruch and Berman's method were later combined to update both stiffness and mass matrices of the system sequentially instead of a one quantity at a time (Berman & Nagy, 1983; Wei, 1990). Further, the methodology was extended by Ceasar (1987) who has produced a range of methods that optimizes a number of objective functions. In the recent major developments of direct method, Hu et al., (2007) proposed a direct method called cross-model-cross mode method (CMCM) in which the physical properties of the system matrices is carried out to update the mass and stiffness matrices simultaneously. Effectiveness of the method was demonstrated in two simulated examples of a shear building model and a 3 dimensional frame structural model. Carvalho et al., (2007) proposed a novel method capable of handling the difficulty of the incomplete measured data in an algorithmic way without using standard modal expansion or reduction techniques. Fang et al., (2011) proposed a substructure energy approach based physical property adjustment type direct method in which the structural system is divided into several sub-systems. These sub-structures are then updated using a set of linear simultaneous equations deduced from the energy functional of substructural models and substructure modes. Besides the usage of direct methods in civil engineering structures, Modak (2014), developed a direct method for vibroacoustic systems that involve elastic structure enclosing a medium, like air. Method is then validated by a numerical example of a rectangular-box cavity backed by a flexible-plate. Major contributions related to direct model updating techniques are presented in the study of Sehgal & Kumar (2016).

1.2.2 Sensitivity-Based Model Updating

Sensitivity-based model updating technique is mostly used for parameter identification and damage detection problems in engineering. Method is based on the minimization of an objective function (or called as cost function) which is created by forming the discrepancies between the modal parameters of the FE model and to the one extracted from vibration data. The problem is solved by iterative optimization techniques, since the relation between the modal vibration and physical parameters is

nonlinear. The iterations are stopped when the values of updating parameters stop converging or the error function is reduced to the tolerable level. In these methods, preselected set of design parameters of FE model linked to the relevant physical parameters is updated in order to locate the erroneous regions. In this method, parameterization of the system matrices of the FE model is performed by the design variables which results the components of these matrices are not updated independently from each other; thus the positive definiteness of the system matrices are preserved during the iterations and physically meaningful result is enforced.

Parametrization is important to assure the identifiability in sensitivity based - FE model updating. Model parameters selected for updating needs to clarify the ambiguity of the model and should be sensitive to the structural damage. In order to avoid convergence problems, the number of design variables should be limited. Accordingly, grouping the adjacent structural elements (sub-structuring) that contains the same information in the sense of structural dynamics is widely accepted method in updating (Weng et al., 2011; Mottershead et al., 2011; Simoen et al., 2015). Otherwise, small variations in measurements can lead to a wide changes in updating results, therefore uniqueness (or even existence) of the solution may not be guaranteed (ill-conditioning). Typically, geometrical or material properties of the FE model, e.g. moment of inertia, spring stiffnesses, Young's modulus etc. are involved as design variables in model updating parameter identification and damage detection problems. Theoretical procedure of the technique is explained in Chapter 3.

1.3 Model Updating Studies Used In Parameter Identification and Damage Assessment Problems

1.3.1 Modal Updating for Parameter Identification

Parameter identification refers to process of updating the parameters of a numerical FE model so as to correlate its predicted response with the measured data at observation points. Correcting the numerical models is well-established in structural dynamics profession and there are many studies reported by various

researchers. Brownjohn & Xia (2000), calibrated the FE model of a cable-stayed Safti Link bridge in Singapore by adjusting the geometric properties and Young's modulus. El-Borgi et al., (2005) performed model updating study by updating elastic bearing stiffness, foundation bearing stiffness and Young's moduli values of the reinforced concrete bridge. Teughels & De Roeck (2005), applied the updating method to 2 concrete beams tested in laboratory. Mottershead et al., (2011) showed the effectiveness of the sensitivity-based model updating algorithm by identifying the Young Moduli of the large-scaled helicopter airframe structure by the use of 4 point response measurements. Foti et al., (2012) identified unknown structural FE model parameters of 60m tall historical tower building in Bari/Italy by updating the unknown parameters; Young's moduli of grouped masonry components, densities, concentrated masses and springs. Petersen & Oiseth (2017), performed model updating study to calibrate long-span floating pantoon Bergsøysund bridge located in Norway. Thirty vibration modes are extracted in vibration measurement and FE model is parametrized with a total of 27 elements. Ozcelik et al., (2018) performed parameter identification study of historic masonry courtyard wall of Isabey Mosque located in İzmir/Turkey. In this study, set of design variables set such as mass density, Young's modulus and boundary elements of the FE model is calibrated using 2 sets of measurements. Sun et al., (2018) performed parameter identification study for beam like composite specimen based on model updating using Particle Swarm Optimization technique. Ferrari et al., (2019) employed self-implemented model updating procedure on a historic centennial RC Brivio arch bridge using global optimization technique. In their study, four density and five elastic moduli parameters were successfully identified based on the information gathered from eight modes including modal frequencies and mode shapes.

1.3.2 Modal Updating in Damage Assessment Problems

Modal updating technique is very popular in vibration-based damage identification literature. There exist many different approaches in the field of damage identification. Damage identification is four levelled process (Rytter, 1993): (1) presence of damage is determined, (2) damage localization, (3) determination of

severity of the damage, (4) damage prognosis – remaining service life of the structure. Most of the studies summarized in this chapter reach the 3rd level of damage identification; whereas 4th level is still an objective to pursue in engineering community. In literature, there exists much different type of damage identification methods. Extensive reviews about the various sensitivity-based model updating methods for damage identification purpose can be found on Mottershead & Frisswell (1993); Doebling et al., (1998); whereas recent developments vibration-based damage identification methods are highlighted in the study of Sehgal and Kumar (2016), Das et al., (2016). A comprehensive review on modal parameter-based damage identification methods for simple structures (beam and the plate-type) is presented in the study of Fan & Qiao (2011); and very recently, De Roeck (2019) reviewed model-based methods for damage identification of structures under seismic excitation. The selection of structural damage assessment technique has a significant influence on the efficiency and accuracy of damage diagnosis and prognosis. One of the most effective and precise damage assessment methods is finite element model updating and the thesis mainly focuses on damage identification of RC structure by means of this method.

Weber et al., (2007) performed damage identification study on a 3-dimensional 1-bay 2-story specimen by updating only the stiffness parameters of the elements sensitive to structural damage. They also took into account the symmetric nature of the specimen by assigning common updating parameters to the symmetrically located elements. Different damage levels were introduced by applying progressively increasing lateral force. Their work also contains a discussion of solving ill-posed problems encountered in model updating problems. Bakir et al., (2008) applied coupled local minimizers (CLM) global optimization technique to identify structural damage imposed on a 4-story, 3-bay numerical frame model subjected to 1999 Kocaeli and Düzce earthquakes. Damage results were presented in terms of stiffness reduction of the elements close to beam-column regions. Sheng-En Fang et al., (2008) performed damage identification on a reinforced concrete frame structure. In their paper, the beam damage was inflicted by concentrated load acting at the mid-span of the beam until the first flexural crack occurred. They divided the FE model

of the frame into substructures (i.e. groups of elements) and updated the Young's moduli of these substructures for identifying the location and extent of the damage. The damage identification results were validated by a damage model developed for concrete members using the concept of remnant stiffness. Moaveni et al., (2009) tested a full-scale seven-story reinforced concrete shear wall on UCSD-NEES shake table for uncertainty quantification in damage identification results. They studied the identified damage uncertainty with respect to several factors (e.g. number of sensors, mesh size, and uncertainties in the estimated modal parameters). Yu & Yin (2010) showed the effectiveness of the sensitivity-based damage identification method on a numerical 2-story frame and on two frames tested in laboratory. Moaveni et al., (2012) conducted a damage identification study on a 2/3 scale, 3-story, 2-bay, masonry infilled reinforced concrete frame subjected to a series of progressively increasing ground motions using a shake table. They quantified damage in terms of stiffness loss in column and infill elements. Nozari et al., (2017) applied sensitivity-based FE model updating to identify induced damage in a ten story building; large variability in damage identification results due to changing ambient conditions is reported. Goksu et al., (2017) identified the rate of change in modal parameters of two existing sub-standard full-scale R/C buildings progressively damaged under quasi-static loading. As a part of their study, the extracted modal parameters were used to update the Young's modulus and the slab thickness of the FE model for model validation purpose. Song et al., (2018) studied the performance of the FE model updating method to identify damage on a 2-story reinforced concrete masonry-infilled building using ambient and forced vibration tests. In this study, the results are validated using light detection and ranging (LIDAR) technology.

1.4 Focus and Organization of the Thesis

The objective of the thesis is to help reader to understand the basics of sensitivity-based finite element model method and its applications in civil engineering. As a result of damaging event, identification of unknown stiffness properties of civil engineering structures using robust sensitivity-based FE model updating method

based on experimental (operational) modal data, is mainly addressed. The structure of the thesis divided in 7 main sections as explained below.

2nd Chapter of the thesis is devoted to the clear understanding of signal processing and review of the operational modal analysis (OMA) techniques. Time and domain system identification methods; namely (a) the natural excitation technique combined with eigensystem realization algorithm (NEXT-ERA), (b) Ibrahim Time Domain (ITD) method, (c) Stochastic Subspace Identification (SSI) method (c) AR Models and Poly Reference (PR), and frequency domain decomposition methods (a) Enhanced Frequency Domain Decomposition (FDD and EFDD) and d) Peak Picking (PP) are reviewed. These methods allows analyst to identify structural modal parameters of systems subjected to wide band dynamic excitations.

Chapter 3 deals with the explanation of the FE model updating technique used, along with providing with extensive exposition about the subject. Components of the method such as the definition of objective function, variables in updating process, sensitivity matrix and optimization algorithms are all explained in this section. At the end of this chapter, the effectiveness of the FE model updating method is illustrated and validated through the numerical simulation study.

In Chapter 4, operational modal analysis results of experimentally tested RC structural frame by three different output-only system identification methods (NExT-ERA, SSI and EFDD) are presented. The application of damage identification of large-scaled civil engineering structure is challenging due to difficulties in handling the experimental data analysis and prototype testing; therefore, the implementation is performed through laboratory-scaled single-bay, single-story RC frame specimen. The description of RC frame specimen and the test program are explained with details.

In Chapter 5, the damage identification results of experimentally tested RC frame at various damage levels are presented. The objective function used for damage identification is constructed by the difference between the experimentally identified

and numerically predicted modal parameters. Damage identification results are presented in terms of stiffness reduction factors on the column(s) bottom and beam ends. The identification results correlate very well with the visual damage inspections done during the quasi-static testing.

In Chapter 6, author investigated the variability of damage identification results; accordingly, 20 independent algorithm run is performed by using the 4 structural modes which are polluted with two different noise characteristics. This scenario allowed creating 16 different modal parameter combinations used for model updating. Damage identification results are later then utilized in full factorial analysis of variance (ANOVA) method in order to understand the influence of uncertainties inherent in different structural modes to the mean and standard deviation of the identified damage factors at various substructures.

Finally, Chapter 7 summarizes and highlights the conclusions of the work and provides some suggestions for future work.

CHAPTER TWO
VIBRATION MEASUREMENTS, SIGNAL PROCESSING & REVIEW OF OUTPUT-ONLY SYSTEM IDENTIFICATION METHODS

2.1 Measurement Preparations, Planning

Measurements are one of the most important components of Operational Modal Analysis (OMA); therefore testing session should be carefully planned in advance. For each test setup, good quality of signals is an indispensable factor. For field vibration tests, the preparation process includes the following:

- Measurement grids (location of sensors)
- Definition of the testing sequence
- Workmanship required to complete the tests
- Safety considerations
- Parameters of data acquisition (sampling frequency, number or length of the data segments etc.)

During the field tests, various types of equipments are used; therefore preparing a checklist is best way to ensure the required equipments are ready. Prior to departure, electronic devices such as; data acquisition system, measurement sensors are working appropriately. All the personal involve in the tests should be familiar with the equipments and the operation.

Preparations for a typical ambient vibration testing include:

a) Selection of measurement locations
b) Installation of the reference sensors
c) Acquisition of reference vibration measurements to ensure the settings are appropriate
d) Installation of the roving sensors
e) Review of vibration data
f) Checking of signals from all channels

g) Moving the roving sensors to new measurement locations for the next setup
h) Perform data acquisition in the final case
i) Review preliminary results before packing up the electronic equipments

If unacceptable vibration data is identified during testing procedure, measurement should be repeated. On the other hand, locations of reference sensors can be identified by comparing the peaks of the power spectral densities (PSDs) (Welch, 1967). Sensor locations are considered suitable if spectral peaks identified from the reference sensors cover the peaks identified from the rover sensors. If some peaks are missing in the range of interested frequencies, testing procedure should be repeated until satisfactory results are obtained. For testing preparations, a good guideline is available (ISO/IEC17025, 2006).

2.2 Specifying Dynamic Measurements

2.2.1 Decision of a Required Number of Sensors

The decision of number of sensor is a key factor in OMA tests. If one performs the vibration tests with one or two sensors, the outcomes will be hidden in most of the cases; therefore reasonable number of sensors should be used. The easiest way to understand the number of sensor required is to consider the "*rank of the problem*" which has a direct connection to the frequency domain decomposition technique (FDD). In any frequency band, the *physical rank* of this matrix determines the maximum number of modes contributing to the response. For instance, if there are four closely spaced modes, then the physical rank is four. But engineer also keep in mind that noise factors presented in testing environment is needed to be included in rank calculation. In the case of two noise sources are present, then the rank of the problem is $R_p = 4 + 2 = 6$. Note that rank of the spectral density (SD) matrix of the measurements is limited by the number of measurement points; but if the measurement points are close to each other, they provide the same information; so among them, only one of measurement point contributes to the rank of SD matrix. Therefore, it is important to determine the number of measurement points that is

higher than the problem rank; and the distance between them should be far enough on the structure so as not to repeat spatial information. Thus, it is preferred to use more sensors than the rank of the problem and sensor locations are carefully selected.

The number of independent inputs is also one of the factors that limit the rank of the problem. Considering the input – output relationship of the problem in frequency-domain $\tilde{\mathbf{y}}(f) = \tilde{\mathbf{H}}_{yx}(f)\,\tilde{\mathbf{x}}(f)$ where $\tilde{\mathbf{y}}(f)$ and $\tilde{\mathbf{x}}(f)$ are the vector of response and inputs in frequency domain and $\tilde{\mathbf{H}}_{yx}(f)$ is the frequency response function; if there is one independent input excitation, then the rank of corresponding correlation matrix in time domain $\mathbf{C}_x$ of input $\mathbf{x}(t)$ is one. Moreover, the loading vector $\tilde{\mathbf{x}}(f)$ can be expressed in terms of vector of white noise sources $\hat{\mathbf{e}}(f)$ such that $\tilde{\mathbf{x}}(f) = \tilde{\mathbf{H}}_{xe}(f)\,\tilde{\mathbf{e}}(f)$; where $\tilde{\mathbf{H}}_{xe}(f)$ characterizes the loading color and the spatial distribution of the forces. Thus, if the vector $\hat{\mathbf{e}}(f)$ contains one white noise source, than the rank of the covariance of resulting input vector $\tilde{\mathbf{x}}(f)$ is one, which means that the rank is controlled by the number of independent white noise sources. From this point of view multiple loading sources doesn't always create the multiple independent inputs and a large number of white-noise sources is required in OMA applications.

Regardless of the system identification method used, if there is only one loading source in the testing environment, then it may not possible to identify the closely spaced modes; experiments with single excitation sources e.g. hammers and shakers are not recommended for OMA testing. One can overcome this problem by using multiple shakers or hammers at the same time. There are several cases where the limited sources limit the rank of the problem. For instance, when the large-scale structure is subjected to wind excitation, it is assumed that the structure is excited with many independent input sources. This assumption is valid only when the structure is large enough than the correlation length of wind forces. However, when the structure is small (as in laboratory specimens), the same wind forces might be small compared to the correlation length; which result the rank of the problem

reverted to one. For a second example, consider the structural system excited by a ground shaker. If the excitation directions are shown to be stochastically independent; then the structural properties are extracted properly by using OMA techniques. However, when the rotational components are ignored (for discussion purpose), one might think that the rank of the problem is 3, that is the translational accelerations in these directions. But if all these components of the movement are the result of the same incident wave, the excitation is again limited to a single independent source; therefore this result the rank of the problem to be one. In Table 1, the classification of ideal cases and typical problems in OMA testing in relation to number of excitation sources is summarized. It can also be shown that several different input sources acting on the structures might also create the single independent excitation case if the loading conditions deviate from white noise characteristics. When this is the case, the excitation source should be complemented with some additional artificial loading. In OMA testing, the use of artificial loading might be required if

- the signal to noise ratio measured on the structural system is too small,
- the natural excitation is a single input or near to single,
- the testing is performed on laboratory conditions

Table 2.1 Ideal and problematic cases in relation to number of independent excitation sources in OMA testing (Brincker &Ventura, 2015)

Ideal Cases	Medium Level Prob. Cases	Highly Prob. Cases
Independent inputs (many)	Independent inputs (close to 1)	Independent inputs equal to 1
*Moving stochastic loads	*Small wind loaded struct.	*Hammer and shaker input from 1 point
*Large wind loaded struct.	*Structures only excited by ground motion	
*Structure loaded with traffic loads	*Structure excited by sound from one source	
*Big machines with moving parts	*Simple machines with few moving parts	

Note that, artificial excitations can be created by inducing the additional loading (random in time and space) by the use of moving loading or using different methods that don't change the properties of the structural system. In the book of Brincker & Ventura (2015), theoretical discussion of the subject is comprehensively clarified. For small structures tested in laboratory environment, the application of a kind of scraping tool or brushing the specimen is recommended.

2.2.2 Optimal Sensor Placement in OMA

Optimal positioning of the limited number of sensors is important in OMA testing; but trying to get closer to the optimum locations can only result marginal improvements in the identification procedure. In literature, there exist many optimum sensor placement (OSP) methods; e.g modal kinetic energy method, the effective impedance method, information entropy index method. They are implemented in various types of structures including bridges (Meo & Zumpano, 2005; Guo et al., 2017); buildings (Zhang et al., 2017); high- rise buildings (Yi et al., 2012); space structures (Kammer, 1991); timber structures (Leyder et al., 2018). One of the simplest method in optimal sensor placement problem is presented by Ibanez et al. (1976). Consider the modal decomposition of the dynamic response:

$$\mathbf{y}(t)=\mathbf{A}\mathrm{q}(t) \tag{2.1}$$

Matrix **A** contains the mode shapes of the structure; whereas **q**(*t*) vector contains the modal coordinates. If we have a estimated modal matrix $\hat{\mathbf{A}}$, estimated modal coordinates $\hat{\mathbf{q}}(t)$ is obtained in terms of pseudo inverse of $\hat{\mathbf{A}}$**:**

$$\hat{\mathbf{q}}(t) = \hat{\mathbf{A}}^{+}\,\mathbf{y}(t) \text{ equal to } \hat{\mathbf{q}}(t) = \hat{\mathbf{A}}^{+}\,\mathbf{A}\;\mathbf{q}(t) \tag{2.2}$$

The matrix $\hat{\mathbf{A}}^{+}\,\mathbf{A}$ can be considered as the transformation matrix between the estimated and the real modal coordinates; therefore optimal sensor placement can be satisfied if the product of $\hat{\mathbf{A}}^{+}\mathbf{A}$ is close to identity matrix. Checking the deviation

from identity of measured optimal sensor placement index (OSB) specified in Equation 2.3 is simple and useful method in sensor placements:

$$OSP_{index} = 1 - \left|1 - \det\left(\hat{\mathbf{A}}^{+}\mathbf{A}\right)\right| \tag{2.3}$$

Since we don't know the estimated modal matrix $\hat{\mathbf{A}}$ prior to OMA testing, possible estimations can be adopted by the aid of initial FE model(s) or analytic modal expressions. In this considered case, adding a noise model to the true mode shape vector components yields estimated mode shape vectors $\hat{\mathbf{a}}$ such as:

$$\hat{\mathbf{a}} = \mathbf{a} + \{X_i\} \tag{2.4}$$

where $\{X_i\}$ is the random vector enables to create mode shape estimates with standard deviation $\sigma = \varepsilon \max(a_i)$ where a_i are the individual components of mode vector $\mathbf{a}$ and ε is the uncertainty parameter. Checking deviations from unity of the OSP_{index} given in Equation 2.3 for each different simulated sensor distributions and uncertainty parameters ε, can give a rough useful idea about the optimal sensor placement.

2.2.3 Determination of the Frequency Range, Measurement Duration of Time Series in OMA Testing

2.2.3.1 Frequency Range

Once the decision on the number of sensors and directions are made, next task is to establish frequency range of measurements. The maximum frequency is selected based the maximum significant frequency of the structure in interest. This can also be limited by the standard frequency of the data acquisition system, as the systems testing big-scale structures mostly have a 200 Hz frequency limit. The upper limit of frequency band is defined by the sampling rate of the recorded measurements. Sampling rate is defined as the number of samples per second. If one say that data is

collected in 200 Hz sampling frequency, then the frequency content of the collected signal is limited up to 100 Hz and there exists no information available in the recorded signal beyond this frequency value (called as Nyquist frequency); therefore sampling rate should be high enough so as to capture the enough number of structural modes. One should also take into account that the anti-aliasing filters in data acquisition systems are working efficiently in 0.8 times of the Nyquist frequency; therefore sampling frequency is recommended to be selected approximately larger than at least 1.2 times of the Nyquist frequency.

2.2.3.2 Measurement Duration of Time Series

For random signals, recording duration depends on the allowable bias and variance errors. For example, in the case of 4% bias and 10% variance error, ANSI/ASA S2.47 (1990), recommends standard measurement duration at least $T = 200 / (\xi f)$; where f is the fundamental frequency measured in Hz and ξ is the damping factor. It means that if one is planning to perform measurements on 10-storey structure with an estimated period about 0.5 s and modal damping ratio 1%; each test takes around 3 hours' time. However this standard is considered to be very conservative and the required duration time can be advised to be estimated by the maximum correlation time in the structural response. Expression given by ANSI/ASA S2.47 (1990) is found to be conservative by Brincker (2014) and provided additional formulae obtained based on the reasonable estimation of autocorrelation functions. Accordingly total time series length of measurement duration is specified as $T > 10 / (\xi f_{min})$. This expression results required length of 500 seconds for the example given above $\xi = 0.01$, $f_{min} = 2$Hz.

2.3 Signal Processing

Identification through OMA preliminary requires the estimation of time-domain correlation or frequency-domain SD functions as all the information in the signals are concentrated in second order properties. Both of these functions contain the same information as they form Fourier transform pair. Physical information of the

interested system (modal parameters) are extracted through the use of these functions. In OMA, through the use of signal processing techniques, clear picture of the physical problem is amplified. Processing of the vibration data can be categorized in several consecutive steps including basic preprocessing, filtering and finally estimation of correlation.

2.3.1 Basic Preprocessing

2.3.1.1 Checking of Data Quality

First step involves the quality checking of the data. Ideally this procedure should be performed on-the-spot when the vibration data was collected before the test is over; as it is undesired to recognize the unclear data at office environment. Analog-to-digital convertors may result corruption of the raw data; therefore this step should include checks for spikes, outliers. Outliers are large deviations towards zero; whereas spikes are large deviations towards higher values. Simplest way of checking the data for these phenomenon, checking of moving average $\mu(\tau)$ and standard deviation $\sigma(\tau)^2$ and controlling whether there exist a large deviations from the typical values of these quantities:

$$\mu(\tau) = \frac{1}{T} \int_{\tau - T/2}^{\tau + T/2} \mathbf{y}(t) \mathrm{d}t \tag{2.5}$$

$$\sigma(\tau)^2 = \frac{1}{T} \int_{\tau - T/2}^{\tau + T/2} \left(\mathbf{y}(t) - \mu(\tau)\right)^2 \mathrm{d}t \tag{2.6}$$

2.3.1.2 Detrending & Segmenting

Detrending is the mathematical operation of removing trend in the signal so as to force it to have a zero mean. Measured DC component of the signal (arising due to measured low frequencies) from sensors are generally not trusted; thus analyst should remove these components. From the view of the OMA perspective, we are

already not interested in the response below the lowest frequency value of the structure. A simple way to perform detrending process is segmenting the signal in overlapping data segments of duration *T*; then simply removing the mean value μ_k of each segments. Data segments are generally tapered by windows $w(\tau)$ in order to minimize the discontinuities between the segments, $y_k(\tau)$ is the windowed data segment at time t_k (Figure 2.1). It can be shown that removal the mean value of the windowed data is equivalent to removing the low frequencies of its Fourier transform.

$$\mathbf{y}_k(\tau) = \mathbf{y}(t_k + \tau)\, w(\tau) - \mu_k \tag{2.7}$$

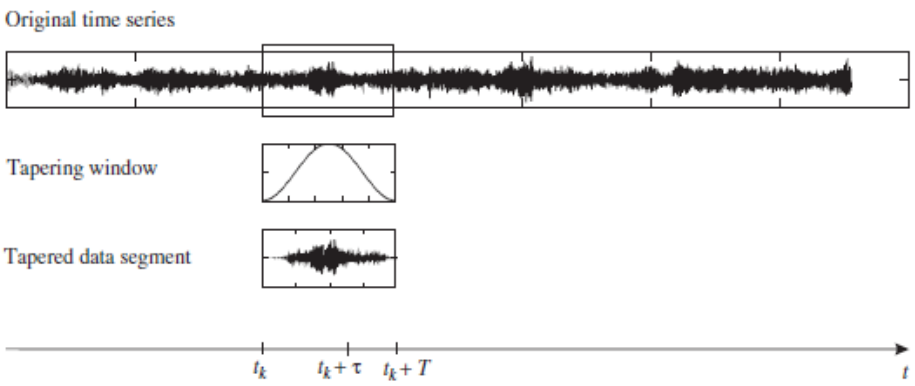

Figure 2.1 Detrending process performed by overlapping and window tapering (Brincker & Ventura, 2015)

2.3.2 Filtering

In OMA, filtering means to exclude undesired frequencies from the signal. After the digitalization of the signal by analog-to-digital converter, only digital types filtering are used in signal processing.

2.3.2.1 Digital Filter Types

There are two main types of digital filtering; the finite impulse response (FIR) and the infinite impulse response (IIR). (FIR) filters are in the form of Equation 2.8. This type of filter is also called as Moving Average (MA) type. **y**(n) is the filtered signal,

b(k) are the constants of the filter, nb is the number of FIR filter coefficients. x(n) represents the input to the filter. It has an advantage of having a frequency independent phase shift.

$$\mathbf{y}(n)=\sum_{k=0}^{nb-1} b(k)\ \mathbf{x}(n-k) \tag{2.8}$$

The infinite impulse response (IIR) filters are in the form of Equation 2.9. This type of filter is also called as Auto Regressive (AR) type. na is the number of IIR filter coefficients and a(k) are the filter constants. It has an advantage of being able to achieve a sharp filter cut-off with limited number of coefficients.

$$\mathbf{y}(n)=\sum_{k=0}^{na} a(k)\ \mathbf{y}(n-k) \tag{2.9}$$

Three classical filter types are commonly used in OMA signal processing:

- High-pass filters are characterized by a single cut-off frequency, which excludes the specified lower frequencies in the Nyquist band.
- Low-pass filters are characterized by a single cut-off frequency, which excludes the specified higher frequencies in the Nyquist band.
- Band-pass filters are characterized by two cut-off frequencies, which include the specified frequency band.

In Figure 2.2, the frequency response function (FRF) representations of these filters are demonstrated. In this figures, f_I represents the cut-off frequencies.

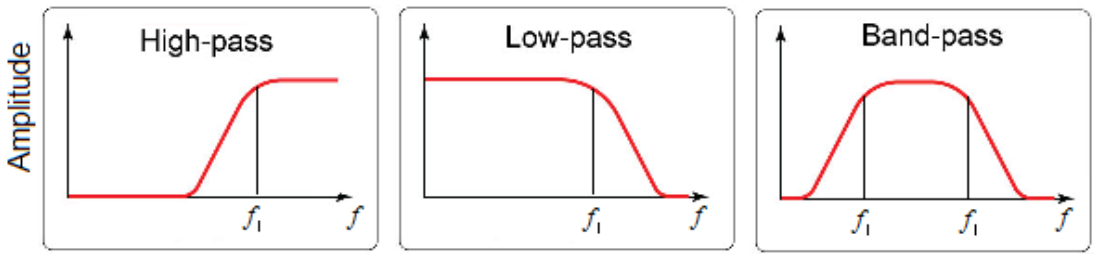

Figure 2.2 Frequency response function representations of the filters commonly used in OMA signal processing: high-pass, low-pass and band-pass filters

2.3.2.2 Down-Sampling & Up-Sampling

Vibration measurements are generally taken with a higher sampling frequency than we needed; therefore a procedure called down-sampling (or decimation) is performed to obtain a smaller suitable sampling frequency for the final analysis. This procedure should be performed carefully. Consider the case in which we want to reduce the sampling frequency by half. At first, one may consider to remove every second data point; but it in this way, energy between the new and the old Nyquist frequency still remains. Therefore; correct solution is first the application of low-pass filtering to the data, then removing every second data point. However, no aliasing problem appears in the process of generation higher resolution data (up-sampling).

2.3.3 Correlation Function Estimation

Estimation of correlation functions is central in OMA. First, they have the same characteristics with the free decays and second, nearly all modal characteristic information are extracted by these functions. Various ways of estimating correlation functions is shown in subsections.

2.3.3.1 Direct Estimation of Correlation Function

For time series vector $\mathbf{y}(t)$, the unbiased correlation function (CF) can be estimated by Equation 2.10.

$$\hat{\mathbf{R}}(\tau) = \frac{1}{T}\int_0^T \mathbf{y}(t)\ \mathbf{y}^{\mathrm{T}}(t+\tau)\,\mathrm{d}t \tag{2.10}$$

However this integral operation given in Equation 2.10 can't be performed numerically as the signal is known in defined interval $t \in [0,T]$; as the integrant is undefined whenever $\tau \neq 0$; therefore reducing this interval to maximum possible size given in Equation (2.11) and in Equation (2.12) discrete time representation is shown. In Equation (2.12), N is the total number of data points, k corresponds time lag ($\tau = k\,\Delta t$).

$$\hat{\mathbf{R}}(\tau) = \frac{1}{T - \tau} \int_0^{T-\tau} \mathbf{y}(t)\,\mathbf{y}^{\mathrm{T}}(t+\tau)\,\mathrm{d}t \tag{2.11}$$

$$\hat{\mathbf{R}}(\mathrm{k}) = \frac{1}{(\mathrm{N}-\mathrm{k})\Delta \mathrm{t}} \sum_{\mathrm{n}=1}^{\mathrm{N-k}} \mathbf{y}(\mathrm{n})\,\mathbf{y}^{\mathrm{T}}(\mathrm{n+k})\,\Delta \mathrm{t} = \frac{1}{(\mathrm{N}-\mathrm{k})} \sum_{\mathrm{n}=1}^{\mathrm{N-k}} \mathbf{y}(\mathrm{n})\ \mathbf{y}^{\mathrm{T}}(\mathrm{n+k}) \tag{2.12}$$

Creating a data series matrix **Y** whose columns are formed with the measured responses from sensors, we can write Equation (2.13)

$$\mathbf{Y} = [\,\mathbf{y}(1),\ \mathbf{y}(2),\ \ldots\,] \tag{2.13}$$

Therefore, the direct estimation of correlation matrix given in Equation (2.12) can be estimated with data series as given in Equation (2.14)

$$\hat{\mathbf{R}}(\mathrm{k}) = \frac{1}{(\mathrm{N}-\mathrm{k})}\,\mathbf{Y}_{(1\,:\,\mathrm{N-k})}\ \ \mathbf{Y}^{\mathrm{T}}_{(\mathrm{k+1}\,:\,\mathrm{N})} \tag{2.14}$$

where $\mathbf{Y}_{(1:N-k)}$ results removing k number of columns from the right part of **Y** matrix; whereas $\mathbf{Y}_{(k+1:N)}$ results removing k number of columns from the left.

2.3.3.2 Unbiased Welch Estimate (Zero Padding)

This method is FFT based correlation function and called as "Roundabout FFT" in Bendat & Piersol (1986). Given the two signals **x**(*t*) and **y**(*t*), the estimation is given by Equation (2.15)

$$\hat{\mathbf{R}}_{\mathrm{xy}}(\tau) = \frac{1}{T - \tau} \int_0^{T-\tau} \mathbf{x}(t)\ \mathbf{y}(t+\tau)\,\mathrm{d}t \tag{2.15}$$

In practice, reduction of the upper integration limit can be introduced by zero padding using Equation (2.16):

$$\hat{\mathbf{R}}_{xy}(\tau) = \frac{1}{T - \tau} \int_0^T \mathbf{x}_0(t)\, \mathbf{y}_0(t+\tau)\, dt \tag{2.16}$$

$\mathbf{x}_0(t)$ and $\mathbf{y}_0(t)$ are the zero padded versions of the signals $\mathbf{x}(t)$ and $\mathbf{y}(t)$ and defined as in Equation (2.17):

$$\mathbf{x}_0(t),\ \mathbf{y}_0(t) = \begin{Bmatrix} \mathbf{x}(t),\ \mathbf{y}(t); \text{ for } t \in [0;T] \\ 0,\ 0; \text{ for } t \in [T;\ 2T] \end{Bmatrix} \tag{2.17}$$

This forces the same reduction of the upper integration limit as in Eq. 15 because the integrand in Equation 2.16 is zero as soon as $t + \tau > T$. Extending the data segments to double size defines the maximum possible time shift τ to be equal to T. Taking into account the convolution property of correlation functions $\mathbf{R}_{xy}(\tau) = \mathbf{x}(-t) * \mathbf{y}(t)$. Equation 2.16 can be adjusted to the form presented in Equation (2.18).

$$\hat{\mathbf{R}}_{0xy}(\tau) = \frac{1}{T} \int_0^T \mathbf{x}_0(t)\, \mathbf{y}_0(t+\tau)\, dt \tag{2.18}$$

This estimation can be directly calculated by FFT. Correlation function estimation can be calculated segmenting the data in the time domain, estimating the corresponding SD as

$$\hat{\mathbf{G}}_{0xy}(\omega) = \mathbf{X}_0(\omega) * \mathbf{Y}_0(\omega) \tag{2.19}$$

The correlation function is called as unbiased; if this estimation is divided by a triangular time window of the form of $w_t(\tau) = (T - \tau) / T$. To sum up, estimation of unbiased correlation function is represented in Figure 2.3, involves the procedures of zero padding, averaging in the frequency domain and finally division of correlation function by the triangular window.

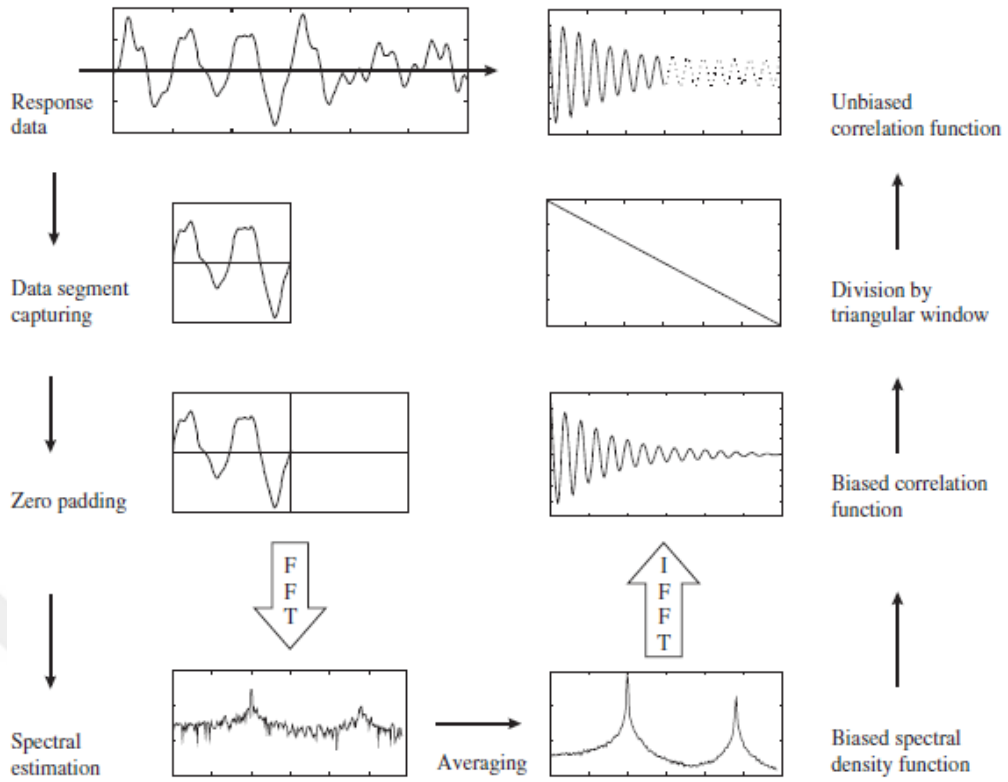

Figure 2.3 Unbiased estimation of correlation functions (Brincker & Ventura, 2015)

2.4 Review of Operational Modal Analysis Methods

Identification of dynamic characteristics has a great importance in engineering fields; there are a vast number of researches available in literature. In OMA, based on the output vibration responses, the algorithms estimating the dynamic characteristics can be investigated in two different domains: time and frequency domain. In time domain methods, analysts mainly deal with the use of correlation functions that has the same characteristics with free decays; whereas frequency domain methods simply employs modal decomposition considering different frequency bands where the structural modes are dominating. In this section, popular OMA methods are presented with their simplified theory, aiming reader to understand the implementation.

2.4.1 Algorithms in Time Domain

In time domain methods, analysts extract the physically related information of the structural system by investigating the correlation functions which have the same form of impulse responses. These functions are derived from the response signal and contain all the structural modes. Modes are basicly identified by fitting the modal model to the correlation functions by various regression methods. They are differentiating from each other by the regression techniques they use. Considering the identified set of poles (eigenfrequencies) arranged in the diagonal matrix $[\lambda_n]$ and the mode shapes are arranged in the matrix $\mathbf{A} = [\mathbf{a}_n]$; one can write the CF of the response at discrete time $\tau = k\Delta t$, for the set of 2N modal parameters as in Equation (2.20).

$$\mathbf{R}_y(k) = 2\pi \sum_{n=1}^{2N} \boldsymbol{\gamma}_n \mathbf{a}_n^T e^{-\lambda_n k\Delta t} \quad \text{or} \quad \mathbf{R}_y(k) = 2\pi \boldsymbol{\Gamma} [\mu_n]^k \mathbf{A}^T \tag{2.20}$$

where the diagonal matrix $[\mu_n]$ contains the discrete time poles $e^{-\lambda_n \Delta t}$ and $\boldsymbol{\Gamma}$ contains the modal participation vectors $\boldsymbol{\gamma}_n$. Both of these matrices forms a set of complex conjugate pairs for each mode. If one arranges the CFs in a block row matrix form, Equation 2.21 is obtained.

$$\mathbf{H} = [\mathbf{R}_y(0),\ \mathbf{R}_y(1),\ \mathbf{R}_y(2), ...] \tag{2.21}$$

If one arranges the modal information as $\mathbf{M} = \left[[\mu_n]^0 \mathbf{A}^T, [\mu_n]^1 \mathbf{A}^T, [\mu_n]^2 \mathbf{A}^T, ... \right]$; Equation (2.21) can then be written as $\mathbf{H} = 2\pi \boldsymbol{\Gamma} \mathbf{M}$ which can be solved by regression or singular value decomposition (SVD). The modal participation vectors can be estimated by Equation (2.22) and the resulting estimation of CF is given in Equation (2.23).

$$\hat{\boldsymbol{\Gamma}} = \frac{1}{2\pi} \mathbf{H} \mathbf{M}^+ \tag{2.22}$$

$$\mathbf{R}_y(k) = 2\pi \hat{\mathbf{\Gamma}} [\mu_n]^k \mathbf{A}^T \quad (2.23)$$

In time domain methods, low modal participation vectors indicate that the corresponding mode might not have a physical meaning; thus these modes can be eliminated. The absolute scalar measure (q_n) of the modal participation vector $\hat{\boldsymbol{\gamma}}_n \in \hat{\mathbf{\Gamma}}$ can then be calculated as $q_n = \sqrt{\hat{\boldsymbol{\gamma}}_n^H \hat{\boldsymbol{\gamma}}_n}$; whereas the relative modal participation factors is calculated as $q_n^2 / \mathbf{q}^T\mathbf{q}$ (where $\mathbf{q}^T = \{q_1, q_2, ...\}$. As known, the sum of relative modal participation factors are equal to one (or 100%) over all the considered modes.

Time domain techniques are developed from the fundamentals of control theory. This allows analyst to separate the noise and the physically related modes from each other by the use of stabilization diagrams. The requisite of minimal realization implies the optimal model order selection. Physical modes are influenced by the noise modes and the model order number is selected so as to minimize this influence. Analyst need to seek for a model which provides the best modal estimation. Furthermore, the stabilization diagrams allow analysts in understanding the number of modes in the frequency band of interest and checking the stability of modal estimations. The reader is referred to Section 3 for the illustration of stabilization diagrams of the experimentally tested RC frame specimen. Here in this section, only the most well-known time domain OMA techniques will be presented.

2.4.1.1 AR Models and Poly Reference (PR)

The first step in the identification procedure is to find the AR matrices of the homogeneous equation given in Equation (2.24) as a function of free decays **y**(n); n = 1,2, …, np of number of samples. Next, the block Hankel matrices, with na number of block rows ($\mathbf{H}_1$) and with a one block matrix with one row ($\mathbf{H}_2$) is formed by the correlation functions (CF) evaluated from response measurements.

$$\mathbf{y}(n) = \mathbf{A}_1 \mathbf{y}(n-1) - \mathbf{A}_2 \mathbf{y}(n-2) - ... - \mathbf{A}_{na} \mathbf{y}(n-na) = 0 \quad (2.24)$$

$$\mathbf{H}_1 = \begin{bmatrix} \mathbf{y}(1) & \mathbf{y}(2) & \dots & \mathbf{y}(\text{np-na}) \\ \mathbf{y}(2) & \mathbf{y}(3) & & \mathbf{y}(\text{np-(na-1)}) \\ \vdots & \vdots & \ddots & \vdots \\ \mathbf{y}(\text{na}) & \mathbf{y}(\text{na+1}) & \dots & \mathbf{y}(\text{np-1}) \end{bmatrix} \tag{2.25}$$

$$\mathbf{H}_2 = \begin{bmatrix} \mathbf{y}(\text{na+1}) & \mathbf{y}(\text{na+2}) & \dots & \mathbf{y}(\text{np}) \end{bmatrix} \tag{2.26}$$

Equation (2.24) can now be formulated in terms of H_1, H_2 and AR matrices as

$$\mathbf{A}\mathbf{H}_1 = \mathbf{H}_2 \quad \rightarrow \quad [\mathbf{A}_{\text{na}}, \mathbf{A}_{\text{na-1}}, \dots, \mathbf{A}_1]\mathbf{H}_1 = \mathbf{H}_2 \tag{2.27}$$

In order to estimate the AR matrices $[\mathbf{A}_{\text{na}}, \mathbf{A}_{\text{na-1}}, \dots, \mathbf{A}_1]$, Equation (2.27) should be transposed and solved by either SVD or least squares as following

$$\hat{\mathbf{A}} = \left(\mathbf{H}_1^{\text{T}+}\, \mathbf{H}_2^{\text{T}}\right) = \mathbf{H}_2\, \mathbf{H}_1^{+} \tag{2.28}$$

Note that, the problem is overdetermined only when np - na >> na x nc; where nc is number of channels used. Finally the modal parameters are obtained by performing the eigenvalue decomposition of the companion matrix $\mathbf{A}_{\text{C}}$, which is shown below.

$$\mathbf{A}_{\text{C}} = \begin{bmatrix} 0 & \text{I} & 0 & 0 \\ \vdots & 0 & \ddots & \vdots \\ 0 & \vdots & & \text{I} \\ \mathbf{A}_{\text{N}} & \mathbf{A}_{\text{N-1}} & \dots & \mathbf{A}_1 \end{bmatrix} \text{ and } \mathbf{A}_{\text{C}}\,\varphi = \mu\,\varphi \tag{2.29}$$

The continuous time poles, modal frequencies and damping values are obtained by Equation (2.30)

$$\lambda_n = \ln(\mu_n)/\Delta t; \quad \omega_n = |\lambda_n|; \quad f = \omega_n/(2\pi); \quad \zeta_n = \frac{\text{Re}(\lambda_n)}{|\lambda_n|} \tag{2.30}$$

2.4.1.2 Natural Excitation Techniques (NExT) Combined with Eigensystem Realization Algorithm (ERA)

The development of NExT was a significant step in the subject of modal parameter estimation. It is shown that, the cross-correlation functions calculated between two response measurements have the same analytical form as the free-vibration response assuming the excitation source has broad band white-noise characteristics (James et al., 1995).

Considering the equation of motion of a multi-degree-of freedom system given in Equation (2.31), the cross-correlation function calculated between two response measurements given in Equation (2.12) satisfy the homogeneous differential equation given in Equation (2.32)

$$\mathbf{M}\ddot{\mathbf{y}}(t) + \mathbf{C}\dot{\mathbf{y}}(t) + \mathbf{K}\mathbf{y}(t) = \mathbf{F}(t) \tag{2.31}$$

$$\mathbf{M}\ddot{\mathbf{R}}_{\ddot{y},\ddot{y}_i}(\tau) + \mathbf{C}\dot{\mathbf{R}}_{\ddot{y},\ddot{y}_i}(\tau) + \mathbf{K}\mathbf{R}_{\ddot{y},\ddot{y}_i}(\tau) = 0 \tag{2.32}$$

In the application of NExT, one sensor is selected as a reference and correlation functions are calculated with respect to this sensor. Application of NExT requires attention in this sense; because if the reference sensor point coincides or located close to a modal node, the response contains no information about that mode. Other important issue is about to estimation of correlation functions; as they are practically obtained through inverse Fourier transformation of the (SD) functions, better results can only be obtained only if measurement durations are long enough (Caicedo et al., 2004; Giraldo et al., 2009; Caicedo, 2011).

From the OMA point of view, ERA was developed by Juang & Pappa (1985). ERA method enables to build a state-space model representation in which the modal characteristics are extracted later. Accordingly, state-space representation for a discrete system is shown in Equation (2.33). In these representation, **x**(k) is the vector of states, **u** is the vector of inputs and **y** is the output vector (i.e. vibration

measurements). Matrices of **A**, **B**, **C** and **D** are called the discrete-time state-space matrices.

$$\begin{aligned} \mathbf{x}(k+1) &= \mathbf{A}\,x(k) + \mathbf{B}\,u(k) \\ \mathbf{y}(k) &= \mathbf{C}\,x(k) + \mathbf{D}\,u(k) \end{aligned} \tag{2.33}$$

ERA algorithm uses the principle of minimum realization; which means that we are interested in smallest number of states. Since the input is not measured in OMA, **B** and **D** matrices can't be estimated. Matrices **A** and **C** can be identified by the use of vibration measurements, enabling modal parameters to be identified. ERA method starts with the formation of block Hankel matrix. Correlation functions that have same formation with free decays, constitutes the entries of the Hankel matrix given in Equation (2.34). For good results, m is advised to be selected approximately ten times the number of modes identified; whereas s should be selected 2-3 times of m (Caicedo et al., 2004). Next step is to perform singular value decomposition of **H**(0) given in Equation (2.35) where $\mathbf{\Sigma}_{mxs}$ is partitioned and minimum realization is obtained by eliminating small singular values produced by the noise; $\mathbf{\Sigma}_g$ square matrix is used in the estimation of system matrices **A** and **C**. System matrices are calculated as in Equation (2.36).

$$\mathbf{H}(k) = \begin{bmatrix} \mathbf{Y}(k+1) & \mathbf{Y}(k+2) & \dots & \mathbf{Y}(k+m) \\ \mathbf{Y}(k+2) & \mathbf{Y}(k+3) & & \vdots \\ \vdots & & \ddots & \vdots \\ \mathbf{Y}(k+s) & \dots & \dots & \mathbf{Y}(k+m+s) \end{bmatrix} \quad \text{where } \mathbf{Y}(k)=[\mathbf{y}_1(k), \mathbf{y}_2(k), \dots] \tag{2.34}$$

$$\mathbf{H}(0) = \mathbf{R}_{mxm}\ \mathbf{\Sigma}_{mxs}\ \mathbf{S}^{T}_{sxs} \qquad \text{under ideal conditions} \qquad \mathbf{\Sigma}_{mxs} = \begin{bmatrix} \mathbf{\Sigma}_g & 0 \\ 0 & 0 \end{bmatrix}_{mxs} \tag{2.35}$$

$$\mathbf{A} = \mathbf{\Sigma}_g^{-1/2} \mathbf{R}^T\ \mathbf{H}(1)\ \mathbf{S}\ \mathbf{\Sigma}_g^{-1/2} \tag{2.36}$$

$$\mathbf{C} = \mathbf{E}^T \mathbf{R}\ \mathbf{\Sigma}_g^{1/2} \qquad \text{where} \qquad \mathbf{E} = [\mathbf{I}_{mxm}\ 0] \tag{2.37}$$

The eigenvalue of matrix **A** has complex conjugate roots which are the poles of the system; the eigenvalues $[\mu_n]$ and eigenvectors $[\boldsymbol{\varphi}']$ of the discrete time system is obtained as follows.

$$\hat{\mathbf{A}}=[\boldsymbol{\varphi}'][\mu_n][\boldsymbol{\varphi}']^{-1} \tag{2.38}$$

The corresponding continuous time eigenvalues λ_n and transformed mode shapes back to physical coordinates is given in Equation (2.39).

$$[\boldsymbol{\varphi}_n]=\mathbf{R}\,\boldsymbol{\Sigma}^{1/2}[\boldsymbol{\varphi}_n'] \tag{2.39}$$

2.4.1.3 Ibrahim Time Domain Method (ITD)

This technique is first introduced by Ibrahim (1977). The technique is based on the idea that any free response (or the correlation functions) can be formulated as a combination of exponential decays as shown in Equation (2.40). In this equation a_1, a_2 ,… represent mode shapes; λ_1, λ_2,... continuous time poles; μ_1, μ_2, … discrete time poles and c_1, c_2, … defines the initial mode shape factors at zero time. Estimation procedure is first initialized by forming block Hankel matrix with four block rows; afterwards partitioned into two block matrices at the middle as shown in Equation (2.42) where N is the number of data points. Considering free decay equation represented in Equation (2.40); one can express the partitioned H_1 block matrix shown in Equation (2.43) and the matrix delayed in time H_2 in Equation (2.44), respectively.

$$\mathbf{y}(t)=\mathbf{y}(k\Delta_t)=c_1a_1e^{\lambda_1 k\Delta t}+c_2a_2e^{\lambda_2 k\Delta t}+\ldots=c_1a_1\mu_1^k+c_2a_2\mu_2^k+\ldots \tag{2.40}$$

$$\mathbf{y}(t=0)=c_1a_1+c_2a_2+\ldots. \tag{2.41}$$

$$\mathbf{H}(k) = \begin{bmatrix} \mathbf{y}(1) & \mathbf{y}(2) & \mathbf{y}(3) & \cdots & \mathbf{y}(N-3) \\ \mathbf{y}(2) & \mathbf{y}(3) & \mathbf{y}(4) & \cdots & \mathbf{y}(N-2) \\ \mathbf{y}(3) & \mathbf{y}(4) & \mathbf{y}(5) & \cdots & \mathbf{y}(N-1) \\ \mathbf{y}(4) & \mathbf{y}(5) & \mathbf{y}(6) & \cdots & \mathbf{y}(N) \end{bmatrix} = \begin{bmatrix} \mathbf{H}_1 \\ \mathbf{H}_2 \end{bmatrix} \tag{2.42}$$

$$\mathbf{H}_1 = \boldsymbol{\Psi}\boldsymbol{\Lambda} \text{ where } \boldsymbol{\Psi} = \begin{bmatrix} a_1 & a_2 & \ldots \\ \mu_1 a_1 & \mu_2 a_2 & \ldots \end{bmatrix} \text{ and } \boldsymbol{\Lambda} = \begin{bmatrix} c_1\mu_1^0 & c_1\mu_1^1 & \cdots & c_1\mu_1^{N-3} \\ c_2\mu_2^0 & c_2\mu_1^1 & \cdots & c_2\mu_2^{N-3} \\ \vdots & \vdots & \vdots & \vdots \end{bmatrix} \tag{2.43}$$

$$\mathbf{H}_2 = \boldsymbol{\Psi}\left[\mu_n\right]^2 \boldsymbol{\Lambda} \tag{2.44}$$

System matrix **A** can be estimated through the subsequent operations shown in Equation (2.45)

$$\boldsymbol{\Psi}^{-1}\mathbf{H}_1 = \left[\mu_n\right]^{-2} \boldsymbol{\Psi}^{-1}\mathbf{H}_2 \quad \rightarrow \quad \boldsymbol{\Psi}\left[\mu_n\right]^2 \boldsymbol{\Psi}^{-1}\mathbf{H}_1 = \mathbf{H}_2 \quad \rightarrow \mathbf{A} = \boldsymbol{\Psi}\left[\mu_n\right]^2 \boldsymbol{\Psi}^{-1} = \mathbf{H}_1^T\mathbf{H}_2 \tag{2.45}$$

Estimation of system matrix **A** can be performed by two ways as shown in Equation (2.46). It is well known that both of these estimations are weakly biased; the final estimation is taking their average.

$$\hat{\mathbf{A}}_1 = \mathbf{H}_2\mathbf{H}_1^T(\mathbf{H}_1\mathbf{H}_1^T)^{-1} \quad \text{and} \quad \hat{\mathbf{A}}_2 = \mathbf{H}_2\mathbf{H}_2^T(\mathbf{H}_1\mathbf{H}_2^T)^{-1}\ ; \quad \hat{\mathbf{A}} = (\hat{\mathbf{A}}_1 + \hat{\mathbf{A}}_2)/2 \tag{2.46}$$

Classic formulation of ITD allows for single output; however this limitation can be solved by introducing block Toeplitz matrices as shown in Equation (2.47).

$$\mathbf{T}_{11} = \mathbf{H}_1\mathbf{H}_1^T; \quad \mathbf{T}_{21} = \mathbf{H}_2\mathbf{H}_1^T; \quad \mathbf{T}_{12} = \mathbf{H}_1\mathbf{H}_2^T; \quad \mathbf{T}_{22} = \mathbf{H}_2\mathbf{H}_2^T \tag{2.47}$$

$$\hat{\mathbf{A}}_1 = \mathbf{T}_{12}\mathbf{T}_{11}^{-1} \quad \text{and} \quad \hat{\mathbf{A}}_2 = \mathbf{T}_{22}\mathbf{T}_{21}^{-1} \tag{2.48}$$

Final step to estimate the modal parameters is the eigenvalue decomposition of $\hat{\mathbf{A}}$ according to Equation (2.49).

$$\mathbf{A}=\mathbf{\Psi}\left[\mu_n\right]^2\mathbf{\Psi}^{-1} \tag{2.49}$$

Accordingly, the columns of the eigenvector matrix yields mode shapes and the square root of the diagonal elements of the eigenvalue matrix yields discrete time poles.

2.4.1.4 Stochastic Subspace Identification (SSI)

These techniques are based on fitting the data to a parametric model. There are two main types of SSI formulation available; correlation driven and the data driven. First technique is well explained in Peeters & De Roeck, 1999 and is very similar to ERA explained in Section 2.4.1.2; therefore not further discussed here. The SSI-DATA method obtains the mathematical model in linear state-space form based on the output-only measurements directly (Overschee & De Moor, 1996). One of the main advantage of the method compared to two-stage time-domain system identification methods such as covariance-driven SSI and NExT-ERA, is that it does not require any pre-processing of the data to calculate auto/cross correlation functions or spectra of output measurements. One other advantage of the method is that QR factorization, singular value decomposition (SVD) and least squares are involved as robust numerical techniques in the identification process. SSI is formulated by control theory terminology; reader can find the understandable version of brief theory behind the SSI in Brincker & Andersen (2006).

First step in identification process by SSI is to form block Hankel matrix based on the measurement responses $\mathbf{y}(t)$ with 2s number of block rows and N number of data points. As indicated in Equation (2.50), two block Hankel matrices are created by splitting into $\mathbf{H}_1$ and $\mathbf{H}_2$; each having s block rows. As a second step the projection matrix **O** defined in Equation (2.51) is calculated.

$$\mathbf{H} = \begin{bmatrix} \mathbf{y}(1) & \mathbf{y}(2) & \dots & \mathbf{y}(N-2s+1) \\ \mathbf{y}(2) & \mathbf{y}(3) & \dots & \mathbf{y}(N-2s+2) \\ \vdots & \vdots & & \vdots \\ \mathbf{y}(s) & \mathbf{y}(s+1) & \dots & \mathbf{y}(N-s) \\ \mathbf{y}(s+1) & \mathbf{y}(s+2) & \dots & \mathbf{y}(N-s+1) \\ \mathbf{y}(s+2) & \mathbf{y}(s+3) & \dots & \mathbf{y}(N-s+2) \\ \vdots & \vdots & & \vdots \\ \mathbf{y}(2s) & \mathbf{y}(2s+1) & \dots & \mathbf{y}(N) \end{bmatrix} = \begin{bmatrix} \mathbf{H}_1 \\ \mathbf{H}_2 \end{bmatrix} \tag{2.50}$$

$$\mathbf{O} = E[\mathbf{H}_2 | \mathbf{H}_1] \rightarrow \mathbf{O} = \mathbf{T}_{21}\mathbf{T}_{11}^{+}\mathbf{H}_1 \quad \text{where} \quad \mathbf{T}_{21} = \mathbf{H}_2\mathbf{H}_1^{T} \qquad \mathbf{T}_{11} = \mathbf{H}_1\mathbf{H}_1^{T} \tag{2.51}$$

The calculation of Toeplitz matrices requires high computational effort in practical applications; therefore projection matrix is generally calculated through the QR decomposition of the transposed Block Hankel matrix. In Equation (2.52), $\mathbf{\Gamma}$ is called observability matrix; $\mathbf{X}$ is the matrix of Kalman states. Taking the QR decomposition and SVD of the projection matrix yields:

$$\mathbf{O} = \mathbf{\Gamma X} \tag{2.52}$$

$$\mathbf{O} = \mathbf{R\,\Sigma\,S}^{T} \tag{2.53}$$

Definition of the observability and the Kalman states matrices according to the singular value decomposed components is given in Equation (2.54). The estimation of these matrices is not unique; however it has no influence on the system matrices.

$$\begin{aligned} \hat{\mathbf{\Gamma}} &= \mathbf{R}\,\mathbf{\Sigma}^{1/2} \\ \hat{\mathbf{X}} &= \mathbf{\Sigma}^{1/2}\mathbf{S}^{T} \end{aligned} \tag{2.54}$$

Discrete time system matrix $\hat{\mathbf{D}}$ and observation matrix $\hat{\mathbf{\Gamma}}$ can then be found by solving the least squares problem as shown in Equation 2.55

$$\hat{\mathbf{D}} = \mathbf{\Sigma}_n^{-1/2}\mathbf{R}_n^{T}\,\mathbf{H}(1)\mathbf{S}_n\,\mathbf{\Sigma}_n^{-1/2} = [\varphi'][\mu_n][\varphi']^{-1} \tag{2.55}$$

The continuous time poles, modal frequencies and damping values are obtained by Equation (2.56).

$$\lambda_n = \ln(\mu_n)/\Delta t;\ \ \omega_n = |\lambda_n|;\ \ f = \omega_n/(2\pi);\ \ \zeta_n = \frac{\mathrm{Re}(\lambda_n)}{|\lambda_n|} \tag{2.56}$$

2.4.2 Algorithms in Frequency Domain

Modal identification estimation can also be performed in frequency domain. These methods are based on investigating the spectral density function (PSD) plots over the frequency range of interest. In these plots, each mode has a frequency band where they dominate, which makes the system identification easier. Therefore, analyst seeks for different frequency bands within one plot for modal estimation. The main drawback of the frequency domain techniques is that the SD estimates may suffer bias; compared to time domain methods the separation of noise and physical modes is rather difficult.

In order to understand the illustration of frequency domain approach, it is useful to show how the SD matrices are fitted to the modal model. Neither the rows, nor the columns of the SD matrix are proportional to the modal displacements. The half spectrum of SD matrix sampled at $\omega = k\,\Delta t$ discrete frequencies can be expressed as a summation for 2N modal parameters set as shown in Equation (2.57), where the $\boldsymbol{\gamma}_n \in \boldsymbol{\Gamma}$ is the nth modal participation vector.

$$\mathbf{G}_y(k) = \sum_{n=1}^{2N} \frac{\boldsymbol{\gamma}_n a_n^T}{i\,k\,\Delta\omega - \lambda_n} \quad \text{or by matrix equation} \quad \mathbf{G}_y(k) = \boldsymbol{\Gamma}\left[\, i\,k\,\Delta\omega - \lambda_n \right]^{-1} \mathbf{A}^T \tag{2.57}$$

The modal information and the SD matrix can be arranged in single block row Hankel matrix for frequency intervals k= k_1, k_1 +1, …, k_2 as shown in Equation (2.58) and Equation (2.59), respectively.

$$\mathbf{H} = [\mathbf{G}_y(k_1), \mathbf{G}_y(k_1+1), \ldots, \mathbf{G}_y(k_2)] \tag{2.58}$$

$$\mathbf{M}=\left[\left[\, i\, k_1\, \Delta\omega - \lambda_n \right]^{-1} \mathbf{A}^T,\ \left[\, i\,(k_1+1)\,\Delta\omega - \lambda_n \right]^{-1} \mathbf{A}^T, \ldots,\ \left[\, i\,(k_2\,\Delta\omega - \lambda_n \right]^{-1} \mathbf{A}^T \right] \quad (2.59)$$

Matrix of modal participation relates these two information, accordingly one can write the relationship

$$\mathbf{H}=\boldsymbol{\Gamma}\mathbf{M} \quad (2.60)$$

Similar to time domain identification, this equation can either be solved by SVD or regression to obtain modal participation vectors, which yields

$$\hat{\boldsymbol{\Gamma}}=\mathbf{H}\mathbf{M}^{+} \quad (2.61)$$

The resulting fit of the estimated half spectrum SD matrix to the modal model becomes

$$\hat{\mathbf{G}}_y(k) =\hat{\boldsymbol{\Gamma}}\left[\, i\, k\, \Delta\omega - \lambda_n \right]^{-1} \mathbf{A}^T \quad (2.62)$$

It should be noted that, only the related modes play a role in the SD matrix in the considered frequency band. Similar to the time domain identification, relative participation factors of the modes are determined by the participation vectors. Here in this section, only the most well-known frequency domain OMA techniques will be presented.

2.4.2.1 Peak Picking (PP) Method (Basic Frequency Domain Method)

Peak picking is based on computation of auto and cross SD functions, also known as ‘Basic Frequency Domain’ method (Felber, 1994). Modes are identified from the peaks of PSD plots. Main assumption is based on the idea that structural modes contribute the structural response only around the natural frequency of the mode considered (Helber, 1994). Accordingly, the structural response $\mathbf{y}(t)$ is only

dominated by a single mode, the response is equal to modal coordinate **q**(*t*) related of that mode times the mode shape a, as shown in Equation (2.63).

$$\mathbf{y}(t) = \mathrm{a}\,\mathbf{q}(t) \tag{2.63}$$

Considering the auto-CF of the modal coordinate $\mathbf{R}_q(\tau)$; the SD matrix of the response $\mathbf{G}_y(f)$ is given by Equation (2.65). Since the rank of the SD is one, mode shape vector is proportional to the any column (or row) of the spectral matrix $\mathbf{G}_y(f)$; therefore any of its columns is an estimation of mode shape $\hat{a}$ (Equation (2.66)). This can be done for all channels (all columns in the spectral matrix).

$$\mathbf{R}(\tau)=\mathrm{E}[\mathbf{y}(t)\ \mathbf{y}^{\mathrm{T}}(t+\tau)] = \mathrm{a}\ \mathbf{E}[\mathbf{q}(t)\ \mathbf{q}^{\mathrm{T}}(t+\tau)]\ \mathrm{a}^{\mathrm{T}} = \mathbf{R}_q(\tau)\,\mathrm{a}\,\mathrm{a}^{\mathrm{T}} \tag{2.64}$$

$\mathbf{G}_y(f) = \mathbf{G}_q(f)\,\mathrm{a}\,\mathrm{a}^{\mathrm{T}}$ the auto spectral density matrix of modal coordinate (2.65)

$\mathbf{G}(f) = [u_1, u_2, ...]$, $\hat{a} = u_c$; u_c is mode shape on the channel c. (2.66)

From a practical point of view, the trace of the PSD matrix (the sum of the auto spectra) at each discrete frequency value is computed first to identify the peaks corresponding to structural resonances. Then, the mode shapes associated to the identified frequencies are obtained from one of the columns of the PSD matrix. In the calculation of the PSD matrix; sensors close to the nodes of the mode shapes shouldn't be selected as a reference sensor; otherwise modes can't be identified. Method can be used effectively when the modes are 'well-separated' which means that frequency distance between two modes is at least half power bandwidth defined as ($2\,f\,\zeta$). This method is advantageous thanks to its simplicity; but one should note that it works accurately only if the above conditions are fulfilled. A more general approach is needed to treat the problems when closely spaced modes or random noise is available. Because, there is no easy way to know if a closely spaced modes are present in the signal in advance.

2.4.2.2 Frequency Domain Decomposition (FDD) and Enhanced Frequency Domain Decomposition Methods (EFDD)

Both PP and FDD are based on the evaluation of the spectral matrix $\mathbf{G}_y(f)$. Frequency Domain Decomposition (FDD) method is an extension of classical peak picking (PP) technique and enables analyzing of closely-spaced modes (Brincker, 2001). The method plots the singular value plot of the SD matrix which allows analyst to see concentrated information within a single plot. Introducing response $\mathbf{y}(t)$ in terms of mode shapes and modal coordinates as in Equation (2.67); CF of response $\mathbf{y}(t)$ is given in Equation (2.68). $\mathbf{A}$ is mode shape matrix and $\mathbf{q}(t)$ modal coordinates vector.

$$\mathbf{y}(t) = a_1 q_1(t) + a_2 q_2(t) + \ldots = \mathbf{A}\ \mathbf{q}(t) \tag{2.67}$$

$$\mathbf{R}_y(\tau) = E[\mathbf{y}(t)\ \mathbf{y}^T(t+\tau)] = \mathbf{A}\ E[\mathbf{q}(t)\ \mathbf{q}^T(t+\tau)]\ \mathbf{A}^T = \mathbf{A}\ R_q(\tau)\ \mathbf{A}^T \tag{2.68}$$

Taking the Fourier transform of both sides of Equation (2.68), corresponding SD matrix is obtained as in Equation (2.69)

$$\mathbf{G}_y(f) = \mathbf{A}\mathbf{G}_q(f)\ \mathbf{A}^T \tag{2.69}$$

Assuming the modal coordinates are uncorrelated, the off-diagonal elements of CF matrix $\mathbf{R}_q(\tau)$ given in Equation (2.68) is zero; therefore SD matrix of modal coordinates $\mathbf{G}_q(f)$ is real valued positive diagonal matrix; the final form of SD matrix is shown Equation (2.69).

$$\mathbf{G}_y(f) = \mathbf{A}[g_n^2(f)]\ \mathbf{A}^T \quad \text{where } g_n^2(f) \text{ are the autospectral densities of } \mathbf{G}_q(f) \tag{2.70}$$

The decomposition shown in Equation (2.70) can be performed by using SVD of the SD matrix $\mathbf{G}_y(f)$ as shown in Equation (2.71). Accordingly, the columns of U are interpreted as mode shapes; whereas the singular values s_n^2 are the ASD of the modal coordinates.

$$\mathbf{G}_y(f) = \mathbf{USU}^H = \mathbf{U}\ [s_n^2(f)]\ \ \mathbf{U}^H \tag{2.71}$$

The SVD technique is useful to separate the noise and the signal space and is used for estimating the rank of $\mathbf{G}_y(f)$ at each frequency with the number of non-zero singular values being equal to the rank. Since the first singular value at each distinct frequency represents the strength of the dominated vibration mode at that frequency, it is suitable to plot frequency - singular values graph can be used as a modal indicator. The identification of modal damping ratio is made through the refinement of the FDD technique, called EFDD. Since, the first singular value around the resonant peak is the ASD of a modal coordinate, taking back the partially identified ASD of the modal coordinate in time domain by inverse FFT yields a free decay time domain function. Modal damping ratio can be estimated by estimating crossing times and logarithmic decrement from the corresponding correlation function as a free decay of the corresponding single-degree-of-freedom system. In literature, the variant of FDD based on EVD instead of SVD is also available (Rodrigues et al., 2004; Jacobsen et al., 2008; Brincker & Zhang, 2009).

CHAPTER THREE
SENSITIVITY-BASED FINITE ELEMENT MODEL UPDATING TECHNIQUE

3.1 Introduction

In general, sensitivity-based FE model updating method can be considered as a mathematical tool which aims to solve the optimization problem of modal parameter discrepancies calculated between the experimentally identified and numerically obtained. The parameters of FE models are generally selected based on plausible assumptions; but it is assumed that knowledge extracted by vibration measurements have a better representation of the dynamic behavior. Thus, in engineering community, the parameters of the initial FE model are preferably adjusted with model updating methods so as to have a better match with the experimental modal parameters. Mostly, the parameters of FE model selected for updating are material or geometrical properties, boundary conditions and connections. Due to the inability in measurement of input excitations in engineering structures, modal parameters identified from the ambient (AV) or white noise (WN) vibrations extracted by OMA techniques, are used for tuning in civil engineering applications. In the case of matching one or two structural modes is acceptable, structural parameters relates modal properties can be adjusted manually; however the updating procedure are mostly performed computer-aided, since there are significant difficulties in trying to obtain a good correlation between the analytical and experimental modal parameters, especially for complex engineering structures.

This section deals with the technique of tuning FE models based on experimentally identified modal parameters. First, the definition of objective function for the optimization problem is explained. Parameters related to physical of the FE model are selected as the design variables of the optimization problem. Next, the concept of sensitivity matrix and its use in optimization problem is introduced. The entries of the sensitivity matrix are the modal sensitivities calculated analytically based on the equation of motion of the undamped FE model. Finally the optimization

algorithm is discussed. Optimization problem is solved iteratively by using sensitivity-based trust region Gauss-Newton algorithm. Methodology is well-explained in Teughels (2003) and adopted in this study for damage identification purpose. The flowchart of the updating method is shown in Figure 3.1. The effectiveness of the algorithm is shown by numerical damage identification study applied on three dimensional (3D) structural frame simulation where the damage is modelled with reduction in translational spring coefficients located at two structural nodes in Section 3.3.

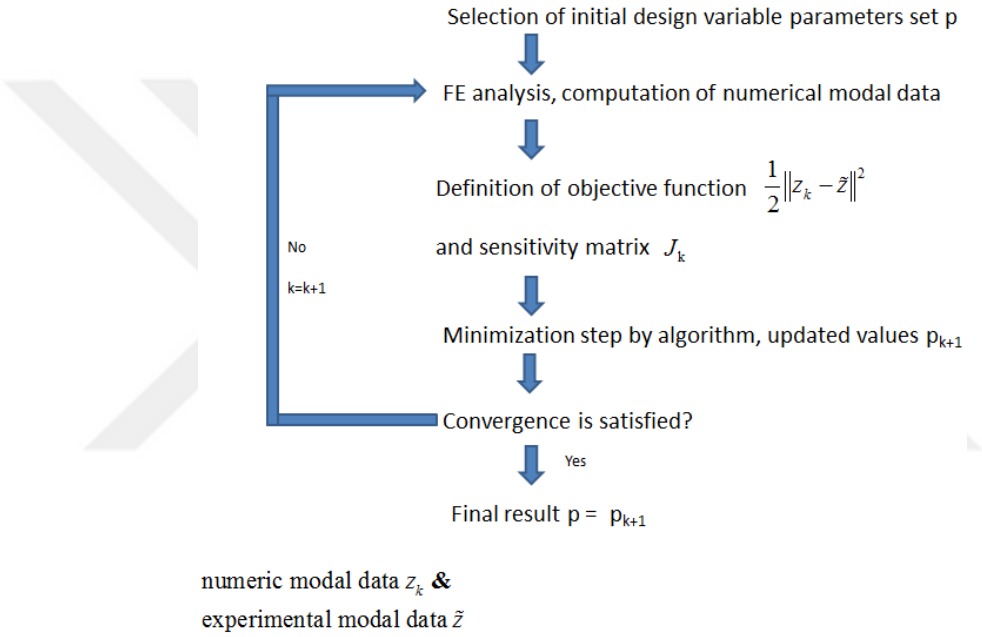

Figure 3.1 The flowchart of FE model updating method

3.2 Theoretical Procedure of FEMU

First, the modal parameters (eigenfrequencies and mode shapes) are calculated based on the initial estimate of FE model parameters (ie. Young's Modulus, spring constants, etc.). Next, the experimental modal data of the structure are obtained by OMA. Third step consists in evaluation of modal parameter discrepancies evaluated between the experimental and the FE model. Final step consists of iterative procedure to correct FE model by updating the unknown model parameters by optimization algorithm.

3.2.1 Definition of Objective Function

The objective function is constructed as a least squares problem as shown in Equation (3.1). The problem is non-linear since the modal parameters are a nonlinear function of design parameters **p**.

$$f(\mathbf{p}) = \frac{1}{2}\sum_{j=1}^{m}\left[z_j(\mathbf{p}) - \tilde{z}_j \right]^2 = \frac{1}{2}\sum_{j=1}^{m}\left[\mathbf{r}_j(\mathbf{p}) \right]^2 \tag{3.1}$$

where $\mathbf{r}_j$ is the j^{th} residual (difference of modal component j); m is the number of residuals; $z_j(\mathbf{p})$ is the quantity of modal parameters belongs to FE model; $\tilde{z}_j$ is the components of experimental modal data; and $\mathbf{p} \in \mathbb{R}^n$ is the design variables of optimization problem which is explained in Section 3.2.3.

3.2.2 Residual Vector (r)

This thesis focuses on eigenfrequency and mode shape residuals only which means that residual vector **r** is formed with $\mathbf{r}_f(\mathbf{p})$ and $\mathbf{r}_s(\mathbf{p})$. By considering Equation (3.1), residuals which measure the discrepancies of modal parameters calculated between FE model and experiments can be represented in vectoral form.

$$\min \frac{1}{2}\left\| \mathbf{r}(\mathbf{p}) \right\|^2 = \min \frac{1}{2}\left\| \begin{matrix} \mathbf{r}_f(\mathbf{p}) \\ \mathbf{r}_s(\mathbf{p}) \end{matrix} \right\|^2 \tag{3.2}$$

Depending on the frequency domain or modal domain, different types of residuals exist; in this chapter latter type of residuals are addressed; since the first type of residuals (for instance FRFs) are generally not available in civil engineering application over a wide frequency domain. Eigen frequencies, mode shapes and modal curvatures are used as modal domain residuals in FEMU. Note that, before the experimental and numerical modal data can be compared, they must be paired correctly so as to relate the correct modes during the iterations. To this end, the

Modal Assurance Criterion (MAC) (Allemang, 2003) is applied in order to match experimental and FE modal data; however this approach may result erroneous results in the case of closely-spaced modes. Accordingly, Simoen et al., (2015) offered MAC based equation to match modes efficiently; they are paired correctly when the lowest value of Equation (3.3) is obtained (i.e value close to zero indicates perfect correlation). ϕ_i and $\bar{\phi}_j$ corresponds to numerical and experimental mode shapes.

$$1 - \mathrm{MAC}\left(\phi_i, \bar{\phi}_j\right) + \left|1 - \frac{\lambda_i}{\bar{\lambda}_j}\right| \tag{3.3}$$

Residual vector in optimization problem consists of eigenfrequency and mode shape residuals which are explained in subsections 3.1.2.1 and 3.1.2.2. Modal strains and modal strain energies can also be used; but not discussed herein.

3.2.2.1 Eigenfrequency Residuals $r_f(p)$

Eigenfrequency type of residuals is indispensable in model updating and formulated as in Equation (3.4). The use of normalized eigenfrequencies simplifies the sensitivity formulations. In this equation, there are m_f number of eigenfrequencies used in FEMU process. Note that, taking relative eigenfrequencies in updating problem enable similar weighting of modal frequencies. This type of residual is very sensitive with respect to the stiffness property and they can be measured accurately.

$$\mathbf{r}_f(\mathbf{p}) = \frac{\lambda_j(\mathbf{p}) - \bar{\lambda}_j}{\bar{\lambda}_j}; \quad \text{with } \lambda_j = \left(2\pi f_j\right)^2 \qquad \mathbf{r}_f : \mathbb{R}^n \rightarrow \mathbb{R}^{m_f} \tag{3.4}$$

3.2.2.2 Mode Shape Residuals $r_s(p)$

The condition of the problem is improved by addition of mode shape residuals; it contains valuable information to complement eigenfrequency residuals with spatial information. As there is no measurable input excitation in OMA, only the

translational degree-of-freedoms (DOFs) is available. Mode shape residuals can be formulated as in Equation (3.5). In this equation, m_s is the number of mode shape components used in FEMU process. ϕ_j^l and ϕ_j^{ref} denotes single mode shape components of mode shape vector ϕ_j. Since an absolute scaling factor is missing for the experimental mode shapes, the numerical and experimental mode shapes are normalized to 1 in a reference node, which is a node at which the mode shapes have their largest amplitude (Figure 3.2). Compared to eigenfrequencies, mode shape components have less sensitivity and they are contaminated with noise. Nevertheless, it is desirable to provide them in FEMU algorithm since they provide spatial information. Note that, the uniqueness of the problem can only be achieved if the number of residuals $m=m_f + m_s$ are greater than the number of design variables n.

$$\mathbf{r}_s(\mathbf{p}) = \frac{\phi_j^l(\mathbf{p})}{\phi_j^{ref}(\mathbf{p})} - \frac{\tilde{\phi}_j^l}{\tilde{\phi}_j^{ref}}; \quad \mathbf{r}_s : \mathbb{R}^n \rightarrow \mathbb{R}^{m_s} \tag{3.5}$$

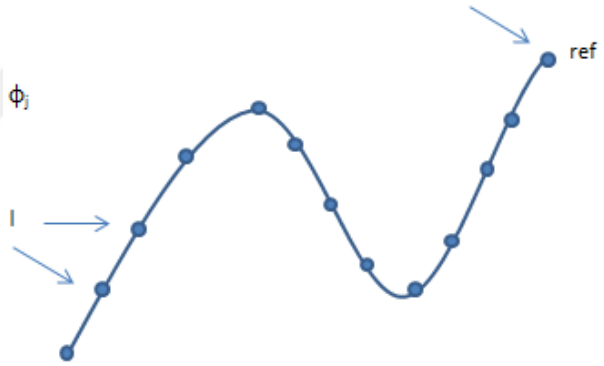

Figure 3.2 Mode shape ϕ_j with reference component “ref” and other components “l”

3.2.2.3 Weighting of Residuals

The components of the nonlinear least squares problem defined in Equation (3.2) can be weighted according to their importance. Accordingly, weighted least squares problem can be formed as shown in Equation (3.6). W is diagonal weighting matrix i.e. $W_{mxm} = \text{diag}(\ldots, w_j^2, \ldots)$, where w_j is the weighting factor of $\mathbf{r}_j$. It is noticeable

that only the relative ratio of weighting factor is meaningful; not their absolute values.

$$\min \frac{1}{2}\mathbf{r}(\mathbf{p})^{T}\ \mathrm{W}\ \mathbf{r}(\mathbf{p}) = \frac{1}{2}\left\|\mathbf{W}^{1/2}\ \ \mathbf{r}(\mathbf{p})\right\|^{2} = \min \frac{1}{2}\sum_{j=1}^{m}\left(\mathrm{w}_{j}\ \mathrm{r}_{j}(\mathbf{p})\right)^{2} \qquad (3.6)$$

Engineering insight helps analyst to find appropriate weighting factors. If mode shapes are considered to be identified accurately, a higher weight can be assigned to them. As stated in Section 3.1.2.2, eigenfrequencies can in general be more accurately identified and are more sensitive to structural changes; therefore most of the case, it is appropriate to assign relatively higher weighting factors to them compared to mode shape residuals. Depending on the modeling and measurement errors, multiple results is obtained for different weight factors; therefore the most realistic result needs to be selected by the analyst insight.

3.2.3 Variables of FEMU Problem & Concept of Damage Function

FE model of the structure are generally generated based on the knowledge of geometric and material properties; analyst first need to choose appropriate physical variables to update. In civil engineering applications, Young's Modulus of structural elements (E), mass densities (ρ), moment of inertia values (I) and thickness (H) of the slabs are the most convenient physical variables **X** to be updated. In the updating problem, although the number of potential erroneous parameters is high, variables should be limited in number to ensure a well-conditioned problem and to obtain physically reasonable results. Moreover, selected variables should influence the modal data sensitively, yet it doesn't imply that all the sensitive parameters should be included in the updating process; if the parameter is already represented by a true value, then there is no reason to update it.

The physical variables can have different orders of magnitude; therefore it is preferable to perform the updating process by updating a dimensionless parameter a^{e} derived by the normalization of physical parameters. If $\mathbf{X}^{e}$ represents the physical

parameter value in element e and its reference value $\mathbf{X}^e_{ref}$, the *dimensionless correction factor* a^e_X is defined as in Equation (3.7).

$$a^e_X = -\frac{\mathbf{X}^e - \mathbf{X}^e_{ref}}{\mathbf{X}^e_{ref}} \quad \text{or equivalently updated parameter} \quad \mathbf{X}^e = \mathbf{X}^e_{ref}(1 - a^e_X) \qquad (3.7)$$

The correction factor a^e_X can affect one element or can be assigned to element groups. In model updating, any parameter in system matrices can be updated by the algorithm; if the physical parameter is linearly related to the stiffness matrix of the element, the relationship between the reference and updated stiffness matrices can be written as in Equation 3.7. Updated global stiffness matrix is then formed by assembling the element stiffness matrices as represented in Equation 3.9; where **K** is the global stiffness matrix, $\mathbf{K}^U$ is stiffness matrix of elements properties remain unchanged and n^e is the number of elements (or group of elements) which are updated.

$$\mathbf{K}^e = \mathbf{K}^e_{ref}(1 - a^e); \mathbf{K}^e \text{ and } \mathbf{K}^e_{ref} \text{ are updated and ref element stiffness matrices} \qquad (3.8)$$

$$\mathbf{K} = \mathbf{K}^U + \sum_{e=1}^{n_e} \mathbf{K}^e_{ref}(1 - a^e) \qquad (3.9)$$

Correcting the erroneous parts of the FE model by updating submatrices of the global stiffness matrix using dimensionless correction factors has two merits in dealing with the problem. First, the connectivity of the FE model is preserved. Additional advantage is that the components of the sensitivity matrix (derivatives of residuals with respect to the correction factors) are calculated easily. In model updating, it is desirable to keep the number of design variables limited to create a well-conditioned problem; otherwise algorithm update the neighboring elements separately, hence the physically meaningful result is not guaranteed. Number of design variable is reduced by the concept of damage functions which defines a mapping between the design variables **p** to correction factors **a** (Teughels et al., 2002). Accordingly, the distribution of correction factors a^e is approximated by

combining a set of fixed triangular-shaped shape (damage) functions N_i and obtained with the linear combination presented in Equation (3.10). In this equation, n is the number of damage functions N_i with their multiplication factor p_i and x^e is the central coordinate of element e. Matrix notation of Equation (3.7) is represented in Equation (3.11); it should be noted that n should be much smaller than the number of elements to be updated n_e. Each damage function differs from zero in that and its adjacent elements; whereas it is equal to zero in other elements.

$$a^e = \sum_{i=1}^{n} p_i N_i(x^e) \tag{3.10}$$

Accordingly, a mesh of damage elements is defined on top of the mesh of finite elements, with each damage element simply consisting of a set of neighboring finite elements (Figure 3.3). To be able to obtain a continuous smoother distribution of correction factors throughout the FE model, the number of damage functions is needed to be increased. According the linear relationship presented in Equation (3.10), once the design variable vector **p** is obtained by the algorithm, dimensionless correction factors is found uniquely by applying the transformation given. Therefore the set of design variables **p** helps problem to reduce in size and are the only unknowns in optimization problem. In Section 5, the methodology is demonstrated with an explanatory simulation example first, and implemented on experimentally tested structural frame for damage identification purpose.

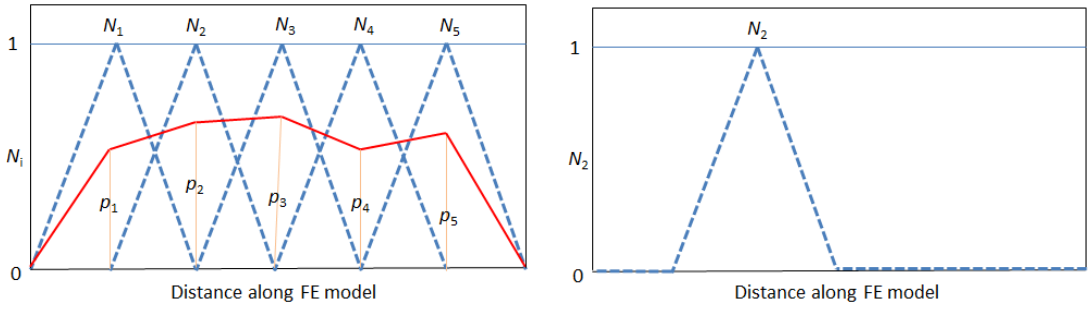

Figure 3.3 (a) Fixed damage functions N_i are used to approximate the distribution of the element correction factors a^e. (b) Isolated representation of fixed damage function N_2

$$\begin{bmatrix} a^1 \\ a^2 \\ a^3 \\ a^4 \\ \vdots \\ a^{n_e} \end{bmatrix}_{n_e x 1} = \begin{bmatrix} N_1(x^1) & \cdots & N_n(x^1) \\ N_1(x^2) & \cdots & N_n(x^2) \\ N_1(x^3) & \cdots & N_n(x^3) \\ N_1(x^4) & \cdots & N_n(x^4) \\ \vdots & \cdots & \vdots \\ N_1(x^{n_e}) & \cdots & N_n(x^{n_e}) \end{bmatrix}_{n_e x n} \begin{bmatrix} p_1 \\ p_2 \\ p_3 \\ p_4 \\ \vdots \\ p_n \end{bmatrix}_{nx1} \quad \text{or} \quad \mathbf{a}_{n_e x 1} = [\mathbf{N}]_{n_e x n} \ \mathbf{p}_{nx1} \quad (3.11)$$

3.2.4 Sensitivity Matrix

The residuals $\mathbf{r}_f(\mathbf{p})$ and $\mathbf{r}_s(\mathbf{p})$ specified in Equation (3.4) and Equation (3.5) have a nonlinear relationship with set of design variables; therefore the objective function $f(\mathbf{p})$ is minimized with an iterative sensitivity-based optimization methods (Nocedal & Wright 1999). Accordingly at each iteration, the Jacobian matrix (or sensitivity matrix) which defines the rate of change between the residuals r to each of the design variables p_i is needed to be calculated (Equation 3.12). As shown in Equation 3.13, chain rule can be applied to obtain the elements of Jacobian matrix $\frac{\delta \mathbf{r}_j(\mathbf{p})}{\delta p_i}$.

$$[J_P]_{m x n} = \begin{bmatrix} \frac{\delta \mathbf{r}_1(\mathbf{p})}{\delta p_1} & \frac{\delta \mathbf{r}_1(\mathbf{p})}{\delta p_2} & \cdots & \frac{\delta \mathbf{r}_1(\mathbf{p})}{\delta p_n} \\ \frac{\delta r_2(\mathbf{p})}{\delta p_1} & \frac{\delta r_2(\mathbf{p})}{\delta p_2} & \cdots & \frac{\delta r_2(\mathbf{p})}{\delta p_n} \\ \vdots & \vdots & \ddots & \vdots \\ \frac{\delta r_m(\mathbf{p})}{\delta p_1} & \frac{\delta r_m(\mathbf{p})}{\delta p_2} & \cdots & \frac{\delta r_m(\mathbf{p})}{\delta p_n} \end{bmatrix}_{m x n} \quad (3.12)$$

$$\frac{\delta \mathbf{r}_j(\mathbf{p})}{\delta p_i} = \sum_{e=1}^{n_e} \frac{\delta \mathbf{r}_j}{\delta a^e} \frac{\delta a^e}{\delta p_i} \overset{\text{Eq.(3.11)}}{=} \sum_{e=1}^{n_e} \frac{\delta \mathbf{r}_j}{\delta a^e} N_i(\mathbf{x}^e) \quad (3.13)$$

$\frac{\delta \mathbf{r}_j}{\delta a^e}$ is obtained for frequency and mode shape residuals in Equation (3.14) and Equation (3.15) by taking derivatives of Equation (3.4) and Equation (3.5) with respect to correction factors, respectively.

$$\frac{\delta \mathbf{r}_f}{\delta a^e} = \frac{1}{\tilde{\lambda}_j} \frac{\delta \lambda_j}{\delta a^e} \tag{3.14}$$

$$\frac{\delta \mathbf{r}_s}{\delta a^e} = \frac{1}{\phi_j^r} \frac{\delta \phi_j^l}{\delta a^e} - \frac{\phi_j^l}{(\phi_j^r)^2} \frac{\delta \phi_j^r}{\delta a^e} \tag{3.15}$$

Modal sensitivities $\frac{\delta \lambda_j}{\delta a^e}$ and $\frac{\delta \phi_j^l}{\delta a^e}$ should be calculated to evaluate Equation (3.14) and Equation (3.15). Sensitivities of eigenvalues with respect to the change in correction factors were already developed by Fox & Kapoor (1968) in closed form for the undamped FE problem; exposition given below is adopted from Maia et al., (1997); Teughels (2003). Considering the undamped eigenvalue problem given in Equation (3.16) and differentiating with respect to a^e results Equation (3.17). The derivations given below are valid under the assumption that analytical mode shapes are mass-normalized.

Eigenvalue Sensitivity

$$\mathbf{K}\phi_j = \lambda_j \mathbf{M}\phi_j \rightarrow \phi_j^T [\mathbf{K} - \lambda_j \mathbf{M}]\, \phi_j = 0 \tag{3.16}$$

where λ_j and ϕ_j are functions of correction factor

$$\frac{\delta \phi_j^T}{\delta a^e} [\mathbf{K} - \lambda_j \mathbf{M}]\, \phi_j + \phi_j^T \frac{\delta [\mathbf{K} - \lambda_j \mathbf{M}]}{\delta a^e} \phi_j + \phi_j^T [\mathbf{K} - \lambda_j \mathbf{M}] \frac{\delta \phi_j}{\delta a^e} = 0 \tag{3.17}$$

The first and the last expression in Equation (3.17) is equal to zero; therefore it is equal to:

$$\phi_j^T \frac{\delta[\mathbf{K} - \lambda_j \mathbf{M}]}{\delta a^e} \phi_j = \phi_j^T [\frac{\delta \mathbf{K}}{\delta a^e} - \frac{\delta \lambda_j}{\delta a^e} \mathbf{M} - \lambda_j \frac{\delta \mathbf{M}}{\delta a^e}] \phi_j = 0 \quad (3.18)$$

Applying mass orthogonality conditions, results modal sensitivity of eigenvalue:

$$\phi_j^T \frac{\delta \mathbf{K}}{\delta a^e} \phi_j - \frac{\delta \lambda_j}{\delta a^e} - \lambda_j \phi_j^T \frac{\delta \mathbf{M}}{\delta a^e} \phi_j = 0 \quad \rightarrow \quad \frac{\delta \lambda_j}{\delta a^e} = \phi_j^T \left[\frac{\delta \mathbf{K}}{\delta a^e} - \lambda_j \frac{\delta \mathbf{M}}{\delta a^e} \right] \phi_j \quad (3.19)$$

Eigenvector Sensitivity

Differentiating Equation (3.16) with respect to dimensionless element correction factor a^e yields Equation (3.20).

$$\frac{\delta[\mathbf{K} - \lambda_j \mathbf{M}]}{\delta a^e} \phi_j + [\mathbf{K} - \lambda_j \mathbf{M}] \frac{\delta \phi_j}{\delta a^e} = 0 \quad (3.20)$$

The mode shape sensitivity $\frac{\delta \phi_j}{\delta a^e}$ can be expressed as basis vectors as shown in Equation (3.21); where d is the number of DOFs in FE model (equal to the number of mods) and j is the mods. Substituting Equation (3.21) into Equation (3.20), results Equation (3.22). Pre-multiplication of Equation (3.22) by ϕ_s^T (s^{th} mode different from mode j) leads to Equation (3.23).

$$\frac{\delta \phi_j}{\delta a^e} = \sum_{q=1}^{d} \alpha_{jq}^e \phi_q \quad (3.21)$$

$$\sum_{q=1}^{d} \alpha_{jq}^e [\mathbf{K} - \lambda_j \mathbf{M}] \phi_q = -\frac{\delta[\mathbf{K} - \lambda_j \mathbf{M}]}{\delta a^e} \phi_j \quad (3.22)$$

$$\sum_{q=1}^{d} \alpha_{jq}^e \phi_s^T [\mathbf{K} - \lambda_j \mathbf{M}] \phi_q = -\phi_s^T \frac{\delta[\mathbf{K} - \lambda_j \mathbf{M}]}{\delta a^e} \phi_j \quad (3.23)$$

Orthogonality property implies that left hand side of the equation is equal to zero except for q = s.

$$\alpha_{jq}^{e}\left[\lambda_q-\lambda_j\right]=-\phi_q^T\frac{\delta[\mathbf{K}-\lambda_j\mathbf{M}]}{\delta a^e}\phi_j \tag{3.24}$$

Expanding the right-hand side of Equation (3.24), results Equation (3.25). Since q ≠ j, second term of Equation (3.25) is equal to zero, therefore α_{jq}^{e} is obtained in Equation (3.26). The coefficient α_{jq}^{e} is to be calculated separately in the cases of q = j and j = j

$$\alpha_{jq}^{e}\left[\lambda_q-\lambda_j\right]=-\phi_q^T\frac{\delta\mathbf{K}}{\delta a^e}\phi_j+\frac{\delta\lambda_j}{\delta a^e}\phi_q^T\mathbf{M}\ \phi_j+\lambda_j\phi_q^T\frac{\delta\mathbf{M}}{\delta a^e}\phi_j \tag{3.25}$$

$$\alpha_{jq}^{e}=-\frac{1}{\left[\lambda_q-\lambda_j\right]}\phi_q^T\left[\frac{\delta\mathbf{K}}{\delta a^e}-\lambda_j\frac{\delta\mathbf{M}}{\delta a^e}\right]\phi_j \quad \text{for } j\neq q \tag{3.26}$$

Differentiating $\phi_j^T\mathbf{M}\phi_j=1$ results in Equation (3.27) and using orthogonality property one obtains Equation (3.28).

$$2\phi_j^T\mathbf{M}\frac{\delta\phi_j}{\delta a^e}=-\phi_j^T\frac{\delta\mathbf{M}}{\delta a^e}\phi_j \quad\rightarrow\quad 2\sum_{q=1}^{d}\alpha_{jq}^{e}\phi_j^T\mathbf{M}\phi_q=-\phi_j^T\frac{\delta\mathbf{M}}{\delta a^e}\phi_j \tag{3.27}$$

$$\alpha_{jj}^{e}=-\frac{1}{2}\phi_j^T\frac{\delta\mathbf{M}}{\delta a^e}\phi_j \tag{3.28}$$

Results obtained at Equation (3.26) and Equation (3.28) should be put into Equation (3.21) for final results, hereby:

$$\frac{\delta\phi_j}{\delta a^e}=\sum_{q=1;\ q\neq j}^{d}\left(\frac{\phi_q}{\lambda_j-\lambda_q}\phi_q^T\left[\frac{\delta\mathbf{K}}{\delta a^e}-\lambda_j\frac{\delta\mathbf{M}}{\delta a^e}\right]\phi_j\right)-\frac{\phi_j}{2}\phi_j^T\frac{\delta\mathbf{M}}{\delta a^e}\phi_j \tag{3.29}$$

Equation (3.29) is simplified to Equation (3.30) if one assume that mass properties are preserved $\frac{\delta\mathbf{M}}{\delta a^e}$=0.

$$\frac{\delta\phi_j}{\delta a^e} = \sum_{q=1;\, q\neq j}^{d} \left(\frac{\phi_q}{\lambda_j - \lambda_q} \phi_q^T \left[\frac{\delta \mathbf{K}}{\delta a^e} \right] \phi_j \right) \tag{3.30}$$

In sensitivity analysis, sufficiently enough number of modes d are needed to be considered. It is also recommended to cross check the sensitivity results obtained by Equation (3.19) and Equation (3.30) with finite difference method to ensure that analytic expressions are coded in programming sense appropriately.

3.2.5 Solution of the Problem by Optimization Algorithm

As the problem given in Equation (3.1) is a nonlinear function of design parameters $\mathbf{p}$, it is preferred to be solved by iterative optimization algorithms. Accordingly, the problem can be solved by Gauss-Newton Method which approximates the function f($\mathbf{p}$) by a quadratic model $q_k(\mathbf{z})$ of truncated Taylor series at the current iterate $\mathbf{p}_k$.

$$q_k(\mathbf{z}) = f(\mathbf{p}_k) + \nabla f(\mathbf{p}_k)^T \mathbf{z} + \frac{1}{2} \mathbf{z}^T \nabla^2 f(\mathbf{p}_k) \mathbf{z} \tag{3.31}$$

If the Hessian matrix $\nabla^2 f(\mathbf{p}_k)$ is positive definite, then there exist a unique solution $\mathbf{p}^*$ given by Newton equations (Equation 3.32). By letting $\mathbf{p}_{k+1} = \mathbf{p}_k + \mathbf{z}_k^{GN}$, the process is repeated until the convergence is satisfied.

$$\nabla^2 f(\mathbf{p}_k) \mathbf{z}_k^{GN} = -\nabla f(\mathbf{p}_k) \tag{3.32}$$

The gradient $\nabla f(\mathbf{p})$ and the Hessian $\nabla^2 f(\mathbf{p})$ of the objective function, which can be expressed in terms of Jacobian matrix and residual vector, are represented in Equation (3.33) and Equation (3.34), respectively. Accordingly, the step vector $\mathbf{z}_k$ is calculated in algorithm by solving set of linear equations given in Equation (3.35)

which requires the calculation of only the first order derivatives given in Equation (3.12).

$$\nabla f(\mathbf{p})=\sum_{j=1}^{m}\mathbf{r}_j(\mathbf{p})\nabla\mathbf{r}_j(\mathbf{p})=J_p(\mathbf{p})^T\mathbf{r}(\mathbf{p}) \tag{3.33}$$

$$\nabla^2 f(\mathbf{p})=J_p(\mathbf{p})^T J_p(\mathbf{p})+\sum_{j=1}^{m}\mathbf{r}_j(\mathbf{p})\nabla^2\mathbf{r}_j(\mathbf{p})\approx J_p(\mathbf{p})^T J_p(\mathbf{p}) \tag{3.34}$$

$$\left(J_k^T J_k\right)\mathbf{z}_k^{GN}=-J_k^T\mathbf{r}_k \tag{3.35}$$

In this method, convergence is guaranteed if the design variables p_0 initially is selected sufficiently close to the solution where $\nabla^2 f(\mathbf{p})$ is positive definite. For the cases of bad estimation in initial point, methodology is generally improved by additional mathematical tool called 'trust region implementation' (Conn et al., 2000). Accordingly, algorithm determines a surrounding region around p_k and a new candidate p_{k+1} is then searched by minimizing model function $q_k(\mathbf{z})$ inside the trust region which is generally represented by a sphere $\|z\|\le\Delta$ which can be modified during iterations based on the agreement between the approximated and actual functions, $q_k(\mathbf{z})$ and $f(\mathbf{p}_k)$ respectively. If the ratio given in Equation (3.36) is close to unity, then Δ_k can be increased; however if the agreement is poor, rate is smaller than one or negative means that Δ_k should be decreased. $\mathbf{z}_k$ is accepted as a candidate for next iteration if Ω exceeds a small positive number. In Figure 3.4, trust region implementation is illustrated on a 2-dimensional curved valley function f. The optimization process was performed by Matlab (2017) function 'fmincon'. In addition, applying the bound constraints on design variables have favorable effect on the solution by reducing the search space which allows to avoid divergence.

$$\Omega=\frac{f(\mathbf{p}_k)-f(\mathbf{p}_k+\mathbf{z}_k)}{f(\mathbf{p}_k)-q_k(\mathbf{z}_k)} \tag{3.36}$$

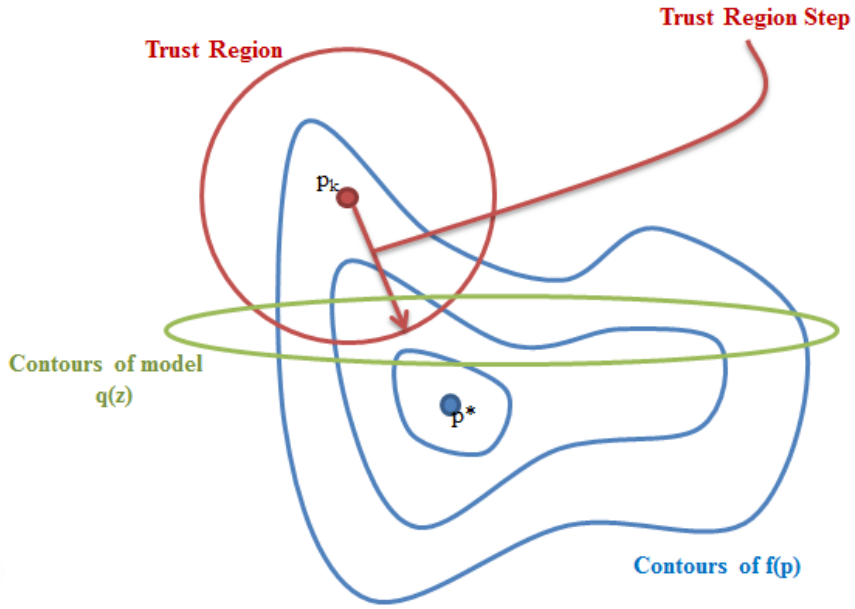

Figure 3.4 The visualization of the trust region implementation. The trust region step always remains inside the radius Δ_k . Model function is defined based on the information extracted by the function and its derivatives at p_k

3.3 Model Updating Simulation Example Applied on Numerical Structural Frame

In this section, the effectiveness of the model updating algorithm programmed in MATLAB based FEDEASLab environment is shown on numerical simulation study. Accordingly, model updating study is performed on single-story, single-bay numerical FE frame type structure consists of 12 elements (6 frame + 6 translational springs) which is shown in Table 3.1. Algorithm run is performed in order to calibrate the undamaged model to the damaged scenario. The stiffness coefficients of translational springs located at nodes 4 and 6 in structural frame are adjusted; whereas no damage is provided to the frame elements. The performance of model updating algorithm is checked based on the updating of 6 spring element coefficients. First six structural modes are used in this example; therefore residual vector **r** have $6\mathbf{r}_f$ + (6mode x 3DOFs x 5 free nodes)$\mathbf{r}_s$ = 96 components (the dimension of the Jacobian matrix *J* is [96x6]). At each iteration, Jacobian is re-calculated. Stiffness of

the springs are corrected with dimensionless parameter $a_{spr} = -\frac{k-k_0}{k_0}$ where k denotes updated spring coefficients and k_0 is initial values. Each node of the FE model totally have 6 DOFs (3 translational, 3 rotational DOFs); accordingly, each frame element has 12 DOFs. Both eigenfrequency and mode shape vectors of 6 modes are included in the optimization process; results are given for all the modes in Table 3.2. Weighting factor for all the residual components (frequency and mode shapes) are selected as 1; hence, all modal components effect by the same weight. Note that, algorithm pairs the structural modes of the undamaged frame to the damaged one according to Equation 3.3; thus undamaged FE model frequencies for the first two modes given in Table 3.2 are not represented in increasing order. In Table 3.3, spring coefficients of undamaged, damaged and updated cases is given; note that algorithm can obtain better results if the updating is performed by taking into account more structural modes. Figure 3.5 shows the convergence history of dimensionless spring factors a_{spr} by iterations. The least squares problem is solved with the trust region Gauss-Newton method; the process converges in 10 iterations. The final norm of the residual vector $\|\mathbf{r}\|$ is calculated as 8.2×10^{-10}, whereas its initial value is 1.17.

Table 3.1 Parameters of single - bay, single - story numerical structure

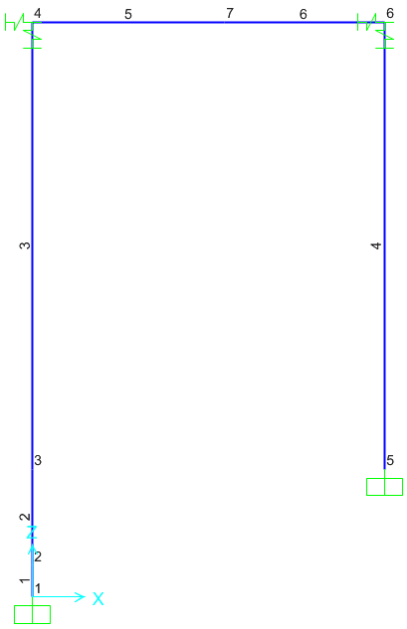

Table 3.1 continues

Element no:	Node Numbers and [x,y,z Coordinates] of Frame		Cross Sections [cm x cm]	Young's Moduli E of the Undamaged Frame [tonf/cm2]	Young's Moduli E of the Damaged Frame [tonf/cm2]
1	1 [0,0,0]	2 [0,0,50]	63 x 63	2141.40	2141.40
2	2 [0,0,50]	3 [0,0,200]	63 x 63	2141.40	2141.40
3	3 [0,0,200]	4 [0,0,900]	63 x 63	2141.40	2141.40
4	5 [550,0,200]	6 [550,0,900]	63 x 63	2141.40	2141.40
5	4 [0,0,900]	7 [300,0,900]	63 x 63	2141.40	2141.40
6	7 [300,0,900]	6 [550,0,900]	63 x 63	2141.40	2141.40
	Node Numbers and [x,y,z Coordinates] of Springs		Cross Sections [cm x cm]	Undamaged Spring Coefficients k [tonf/cm]	Damaged Spring Coefficients k [tonf/cm]
7	4 [0,0,900]	8 [1,0,900]	-	57	10
8	4 [0,0,900]	9 [0,1,900]	-	112	40
9	4 [0,0,900]	10 [0,0,901]	-	2860	350
10	6 [550,0,900]	11 [551,0,900]	-	21	4
11	6 [550,0,900]	12 [550,1,900]	-	57	13
12	6 [550,0,900]	13 [550,0,901]	-	1540	60

Table 3.2 Frequency and MAC values of simulation example before and after updating

Mode	FE model frequencies of undamaged model ($f_{undamaged}$)	FE model frequencies of damaged model ($f_{damaged}$)	Updated FE model frequencies ($f_{updated}$)	Frequency differences before updating (a-b) [%/100]	Frequency differences after updating (b-c) [%/100]	MAC before updating (a-b)	MAC after updating (b-c)
	(a)	(b)	(c)	(d)	(e)	(f)	(g)
	[Hz]	[Hz]	[Hz]	[(a-b)/b]	[(b-c)/c]		
1	11.10	7.50	7.50	0.48	7.26E-08	0.981	1
2	10.85	8.77	8.77	0.24	-3.4E-07	1.000	1
3	15.68	12.08	12.08	0.30	4.51E-08	0.973	1
4	58.19	58.04	58.04	0.00	3.54E-08	1.000	1
5	59.47	59.41	59.41	0.00	1.08E-10	0.993	1
6	60.53	60.42	60.42	0.00	2.25E-10	0.994	1
7	68.23	67.86	67.86	0.00	3.51E-08	0.999	1
8	138.76	124.66	124.66	0.11	2.22E-06	0.998	1
9	155.30	147.13	147.13	0.06	-2.8E-07	1.000	1
10	224.91	224.79	224.79	0.00	1.2E-07	1.000	1

Table 3.3 Undamaged, damaged and updated spring coefficients of FE model

Undamaged Spring Coefficients k [tonf/cm]	Damaged Spring Coefficients k [tonf/cm]	Updated Spring Coefficients k [tonf/cm]
57	10	10.55
112	40	40
2860	350	350.05
21	4	3.45
57	13	13.00
1540	60	59.99

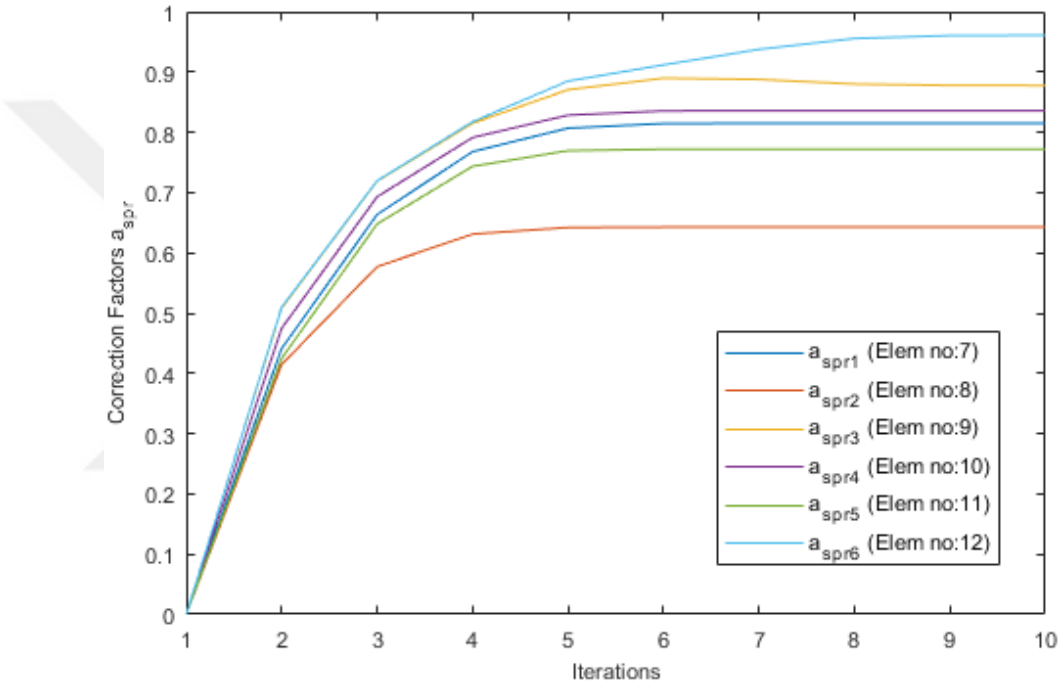

Figure 3.5 History of dimensionless spring coefficients a_{spr} by iterations

Algorithm successfully set frequency differences to zero and MAC values to 1 for all the structural modes; hence good correspondence with the simulated modal data is obtained by after the modal updating application. Note that, the results are obtained by adjusting all 6 spring coefficients independently.

CHAPTER FOUR
OPERATIONAL MODAL ANALYSIS RESULTS OF PROGRESSIVELY DAMAGED RC FRAME

4.1 Introduction

In extensive laboratory test programme, eight RC structural frames are subjected to quasi-static loading in order to create progressive damage; the project is supported by The Scientific and Technological Council of Turkey (TUBITAK) under the Grant #112M203. More information on the test programme is given by Ozcelik et al., 2016, 2018. In this chapter, modal parameter estimation results of one of them, single-bay single-story half-scale bare frame is presented. The frame was quasi-statically tested under progressively increasing in-plane drifts and then dynamic measurements are performed at the end of specific drift levels. At different damage states, AV and WN tests were conducted for modal parameter identification. An electro-dynamic shaker, positioned on top of the slab, was used to perform WN tests. Three different output-only system identification methods, namely, Natural Excitation Technique combined with Eigensystem Realization Algorithm (NExT-ERA), Data-Driven Stochastic Subspace Identification (SSI-DATA), and Enhanced Frequency Domain Decomposition (EFDD) are used with the recorded response data at different damage states. Detailed visual damage inspections, made during quasi-static tests (i.e., at discrete damage states), and their evolution with respect to increasing drift levels are coupled with the corresponding modal identification results. This allows correlation study to be made among identified modal parameters, damage types, their locations, and their extent. The presented OMA results in this chapter are then later used in Chapter 5 for finite element model updating based damage identification purpose.

4.2 Test Setup & Specimen

The quasi-static loading was applied along the frame in-plane direction. The average 28th day compressive strength of the concrete used is ~38 MPa, and the nominal yield strength of the steel bars is 420 MPa. The column and beam elements

have cross-sectional dimensions of 15 cm x 25 cm. The frame has a height of 150 cm measured from foundation top to slab top, and center-to-center column span was 225 cm. It has 6 cm thick partial slabs. The schematic view and rebar detailing of the frame are presented in Figure 4.1(a) and (b), respectively. A vertical load of approximately 10% of columns' axial load capacity was applied on each column by two separate but parallel connected hydraulic pistons. This load represents the weight of the upper stories. The pressure level in these pistons was monitored during the tests by a manometer attached to the supply line to check the level of axial load applied on the columns. In addition to the axial load applied by these pistons, 4 concrete pads (each weighing 1.38 kN) and 16 steel plates (each weighing 0.18 kN) were placed on the slab for representing gravity loads on the beams. The actuator was attached on the frame at the slab level. The actuator used is a double-acting actuator capable of applying cyclic displacements. The general view drawing of the test setup is shown in Figure 4.1(c) and the test frame itself with components is shown in Figure 4.2. The displacement pattern applied for the test is based on ACI 374.1.05 (2005) which is shown in Figure 4.3(a); accordingly, the frame is subjected to lateral cyclic displacements ranging from 0.075% (1.04 mm) to 3.5% (48.65 mm).

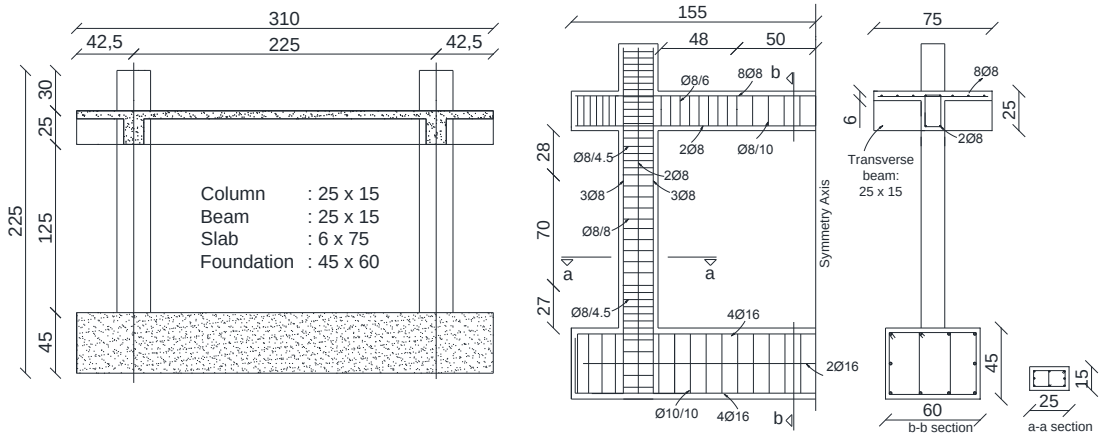

Figure 4.1 (a) Schematic view, (b) reinforcing details, (c) test setup

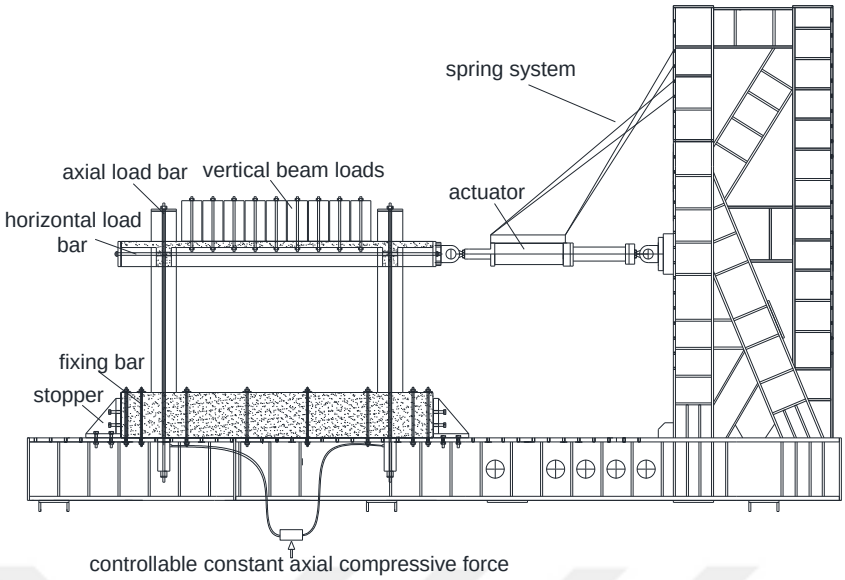

(c)

Figure 4.1 continues

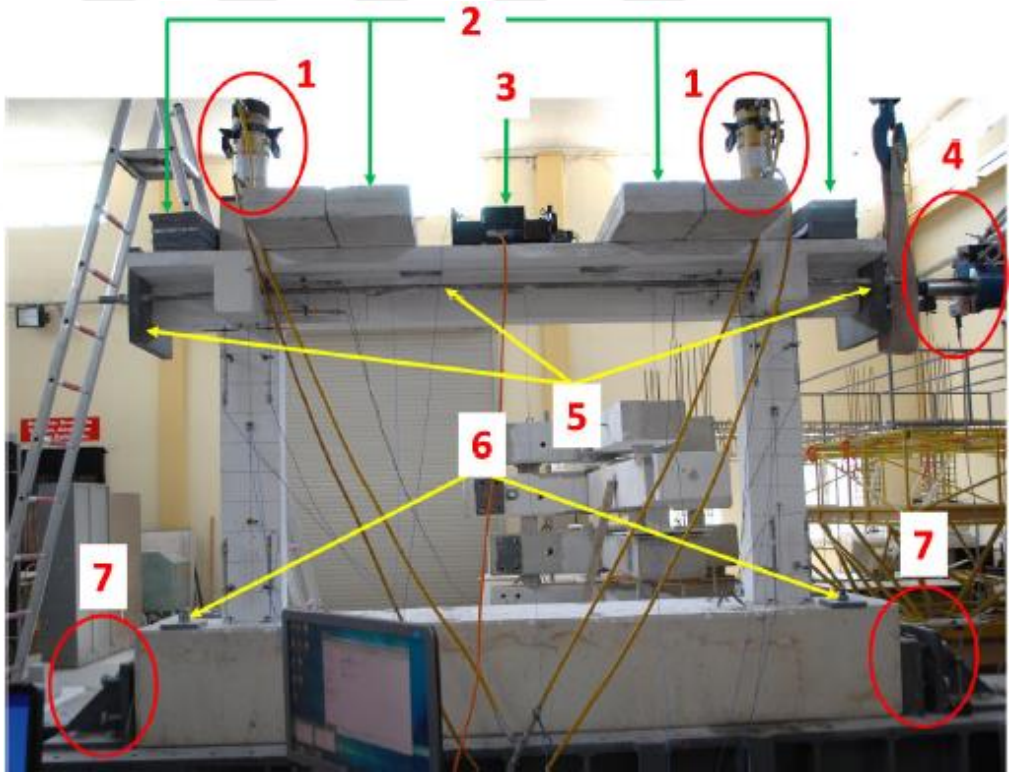

Figure 4.2 General view of the test setup with installed sensors and equipments: (1)hydraulic pistons used to provide axial load to the column system, (2) concrete pads provides additional masses to the frame (3) electro-dynamic shaker, (4) hydraulic displacement controlled actuator, (5) horizontal rod & head plater system used to transfer lateral load to the structural system, (6) studs used to connect the structural frame, (7) stopper system used to prevent sliding (Personal archive, 2016)

4.3 Quasi Static & Dynamic Tests and Operational Modal Analysis Results

In-plane displacement loading pattern shown in Figure 4.3(a) was applied to the RC frame by a computer-controlled hydraulic actuator; whereas hysteretic lateral force-floor displacement response of the RC frame obtained by quasi-static cyclic tests are shown in Figure 4.3(b). A set of photographs of the frame at the end of some specific drift ratios, are presented in Figure 4.4. At the end of each pre-determined in-plane drift ratios: 0%, 0.2%, 0.5%, 1.0%, 1.4%, 2.2%, and 3.5% (i.e., at gradually increasing damage levels), a series of WN, AV tests were performed on the frame; these dynamic test points are indicated in with the circle symbol (Figure 4.3a). Dynamic test points were selected so that significant changes in modal parameters as damage level increases can be captured. The frame was densely instrumented with 5 uni-axial and 4 tri-axial piezo-electric type accelerometers. The accelerometer stations with their positive polarities are shown in Figure 4.5(a). Additionally, 2 string potentiometers and 12 linear variable displacement transducers (LVDTs) were used on the structural members (i.e., columns, beams, and infill walls) for response measurements during quasi-static testing. In Figure 4.5(b), an accelerometer and LVDT mounted on the structural frame is shown. For WN tests, an electro-dynamic shaker with an increased reaction mass positioned at the slab mid-line (on top of the frame) was used for applying in-plane broad-band dynamic excitation on the RC frame with an intention to excite in-plane mode(s). Also, one uni-axial accelerometer was deployed on the electro-dynamic shaker's reaction mass for measuring the level of input excitation along the in-plane direction. Accelerometers used have ±5g amplitude range, frequency bandwidth of 0.25 Hz to 3000 Hz, sensitivity of 1000 mV/g. Three 18-bit A/D converters with 8 channels each were used. Multiple A/D modules were all synchronized. Spatial distribution of the accelerometers was decided based on the modal analysis results using the initial numerical model. Since the response of the structure is governed mainly by the modes in the frequency band of interest, sensor placement was performed by investigating the fundamental in-plane mode of the numerical model. The input signal to the shaker was designed so that it had a frequency bandwidth of 0.1 – 100 Hz. Due to setting the shaker's excitation direction along the in-plane direction, the recorded structural response was

predominantly along this direction; therefore the WN tests were mainly used to track the changes in the fundamental in-plane mode with respect to gradually increasing structural damage. The actuator was detached from the frame before the dynamic tests were performed. This was done to ensure that the restraining effect of the actuator on the specimen along the in-plane direction could be avoided. 8 minutes long AV and WN response data at the end of the predetermined drift ratios were recorded at a rate of 1000 Hz. Prior to performing modal identification work, the recorded time series were filtered between 0.5 – 100 Hz using a band-pass finite impulse response filter to increase estimation accuracy by focusing the estimation effort on the frequency range of interest. This bandwidth was deemed sufficiently broad-band to excite first few modes obtained based on preliminary numerical model studies. Figure 4.6 shows the acceleration time histories recorded in stations during the white-noise tests at 3.5% drift ratio together with the corresponding Fourier Amplitude Spectra. The spectrogram of the acceleration data collected on the beam member (in-plane -x direction of Sta3) for WN excitation case at 3.5% drift ratio, is shown in Figure 4.7. The variation of energy of various harmonics in a signal with respect to time is color coded with large amplitudes shown as red to very small amplitudes shown in yellow-green color. The spectrogram graph reveals that the structural frame is excited with a wide-frequency band and has time invariant characteristics. Since, the excitation direction provided by the electro-dynamic shaker is in in-plane direction, the power of the signal is found to be insufficient for OMA in estimation of the fundamental out-of-plane mode. Moreover, the out-of-plane structural mode couldn't be identified by NExT-ERA method due to low signal-to-noise (SNR) ratio is identified by EFDD method by simply performing a peak-picking on the frequency-singular value plot around the frequency of interest. The existence of the out-plane mode is also justified by Fourier Amplitude Spectra plots of accelerations channels in -y direction (Figure 4.6). Chapter 4.3.1 mainly focuses on only the identification of in-plane mode, however the out-of-plane mode is at each incremental damage state is identified in Chapter 4.3.2.

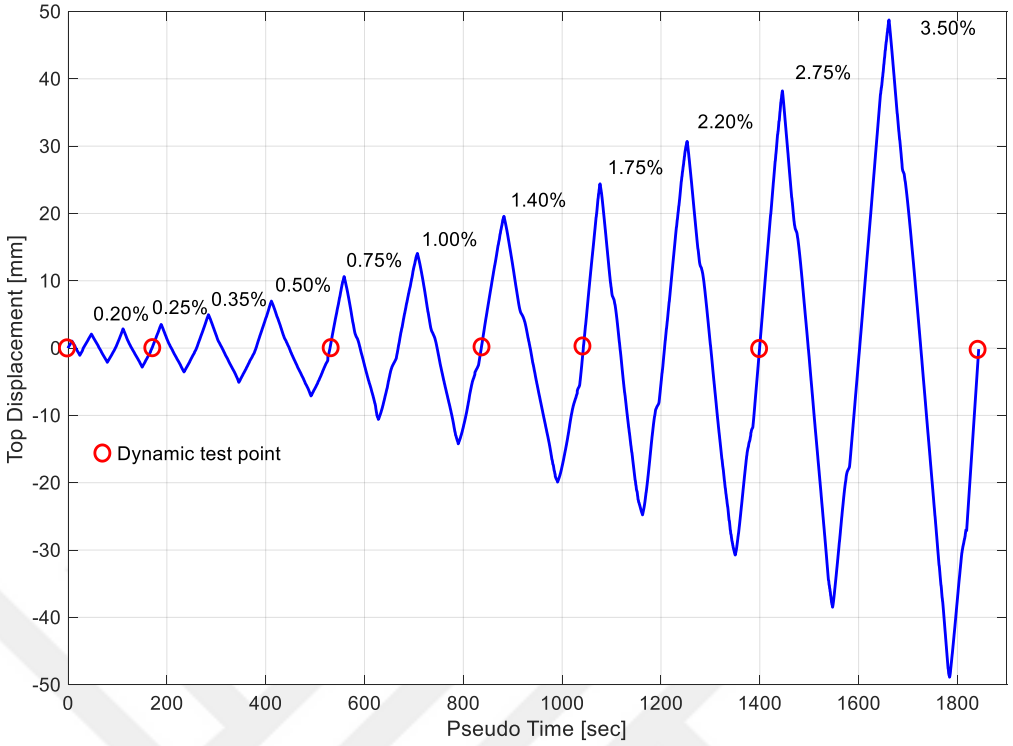

(a)

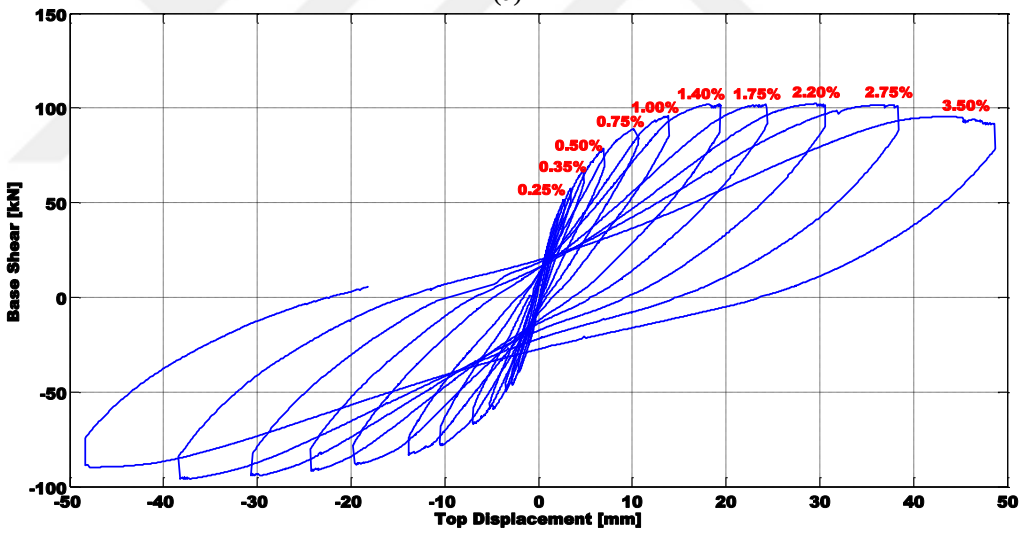

(b)

Figure 4.3 (a) Single-cycle displacement history drifts applied to the structure, (b) base shear – top displacement response of the structural frame

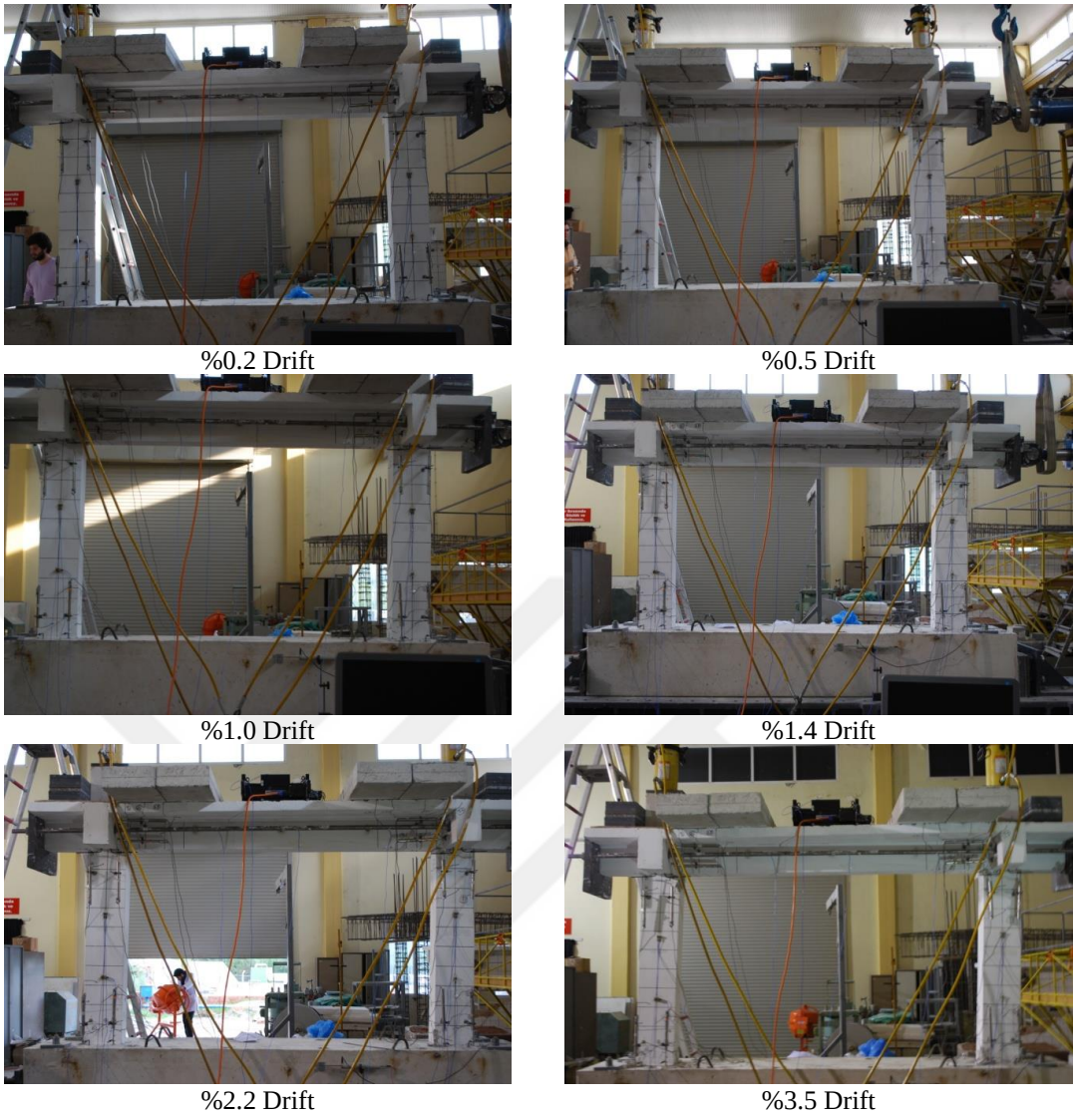

Figure 4.4 Photographs of the frame at the end of specific drift ratios (Personal archive, 2016)

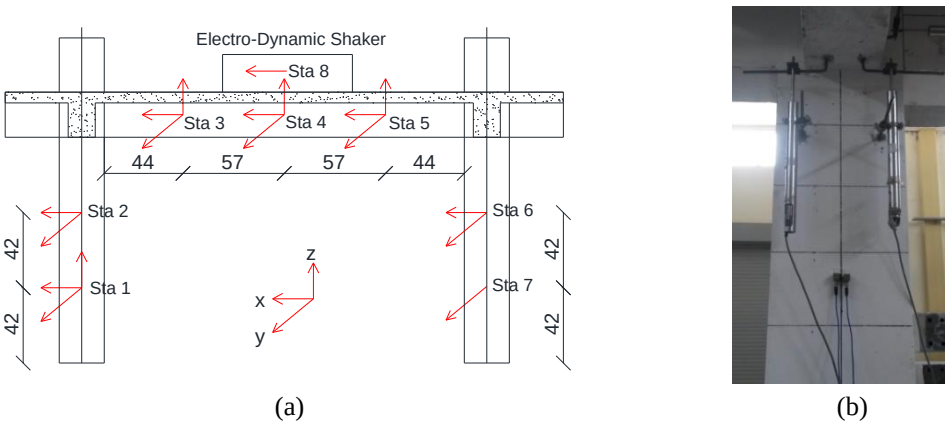

(a) (b)

Figure 4.5(a) Accelerometers on the frame and their positive directions (dimensions are in cm), (b) displacement transducer and accelerometer (Sta6) mounted on the frame system

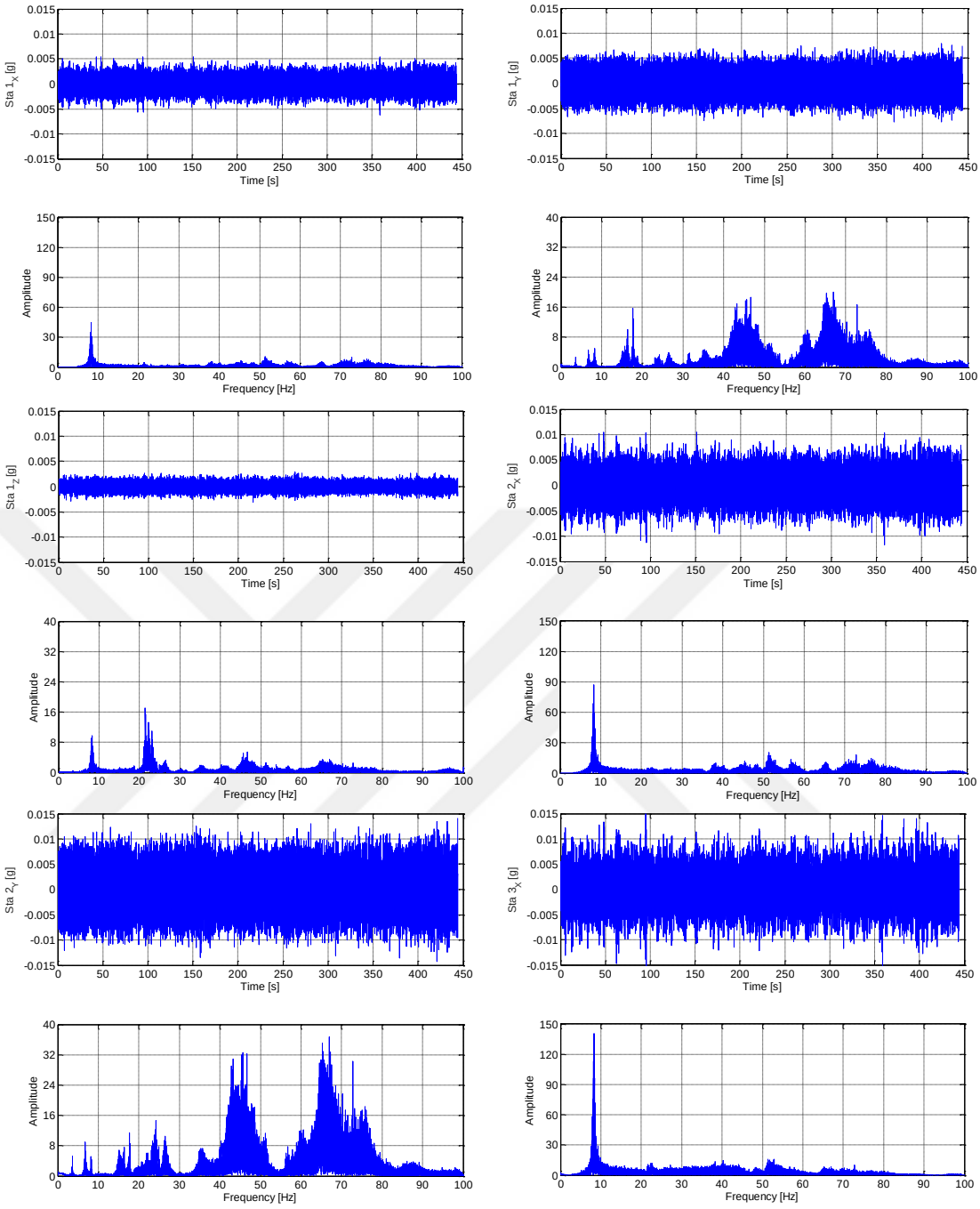

Figure 4.6 Acceleration time histories and Fourier amplitude spectra of the stations due to white-noise excitation

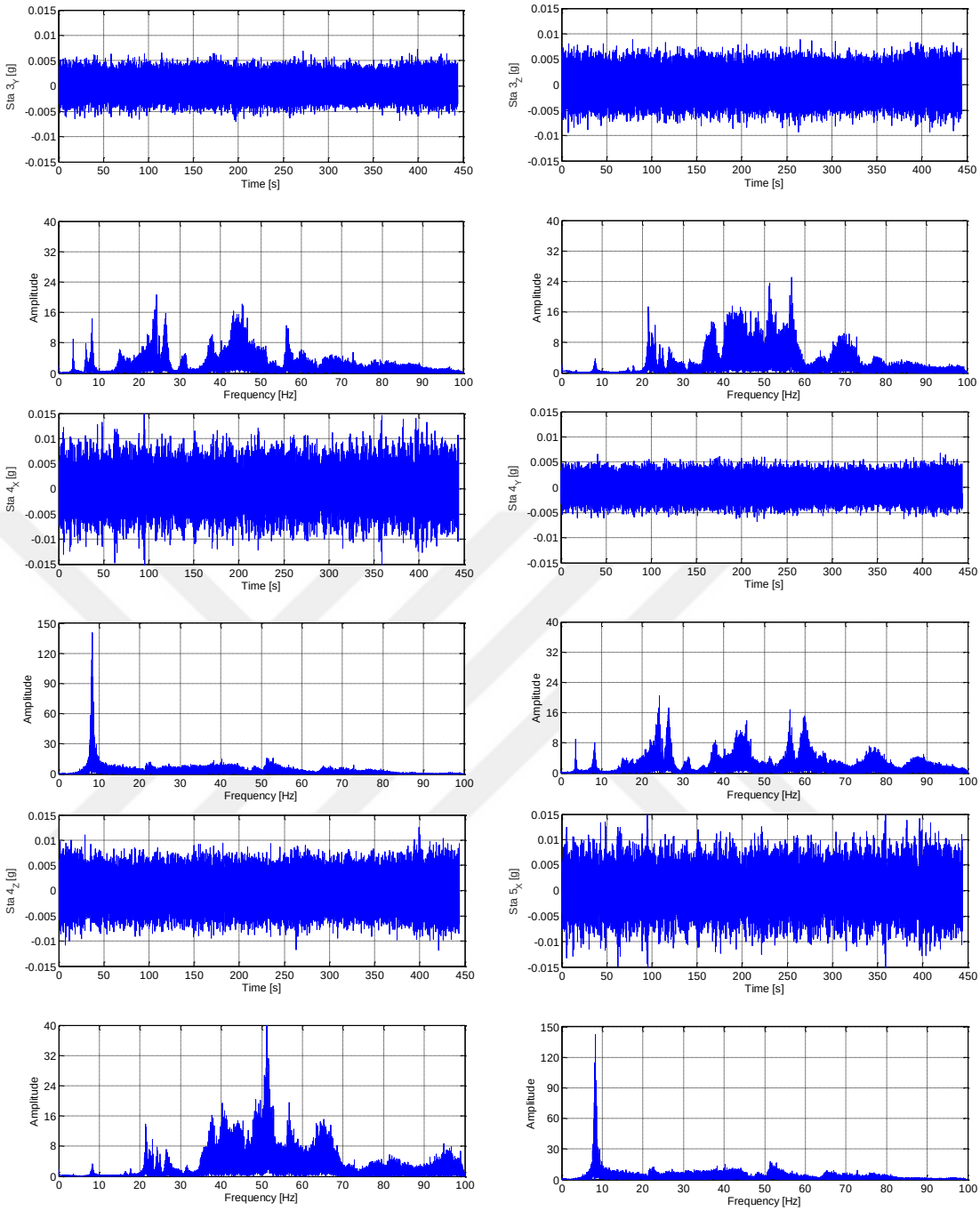

Figure 4.6 continues

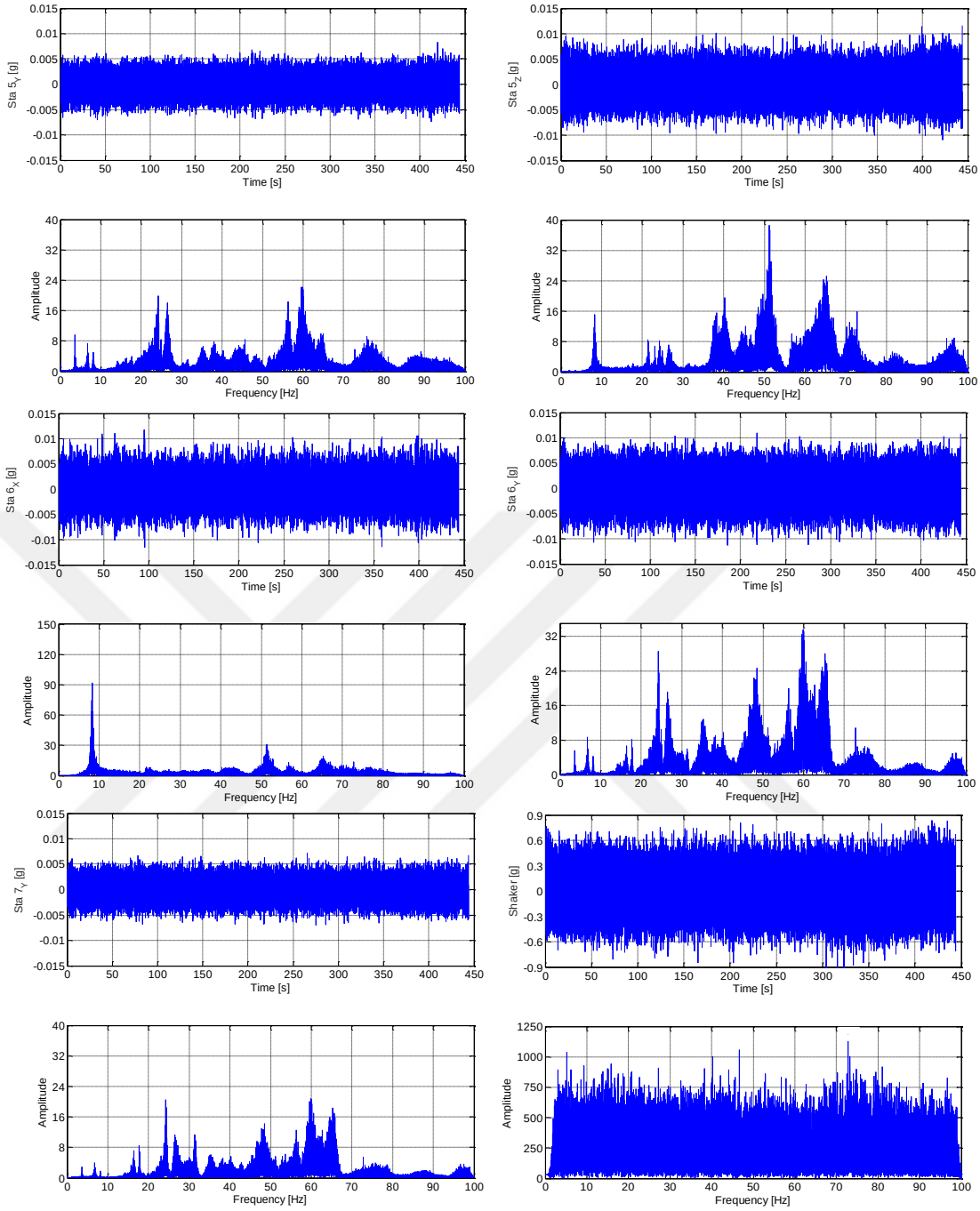

Figure 4.6 continues

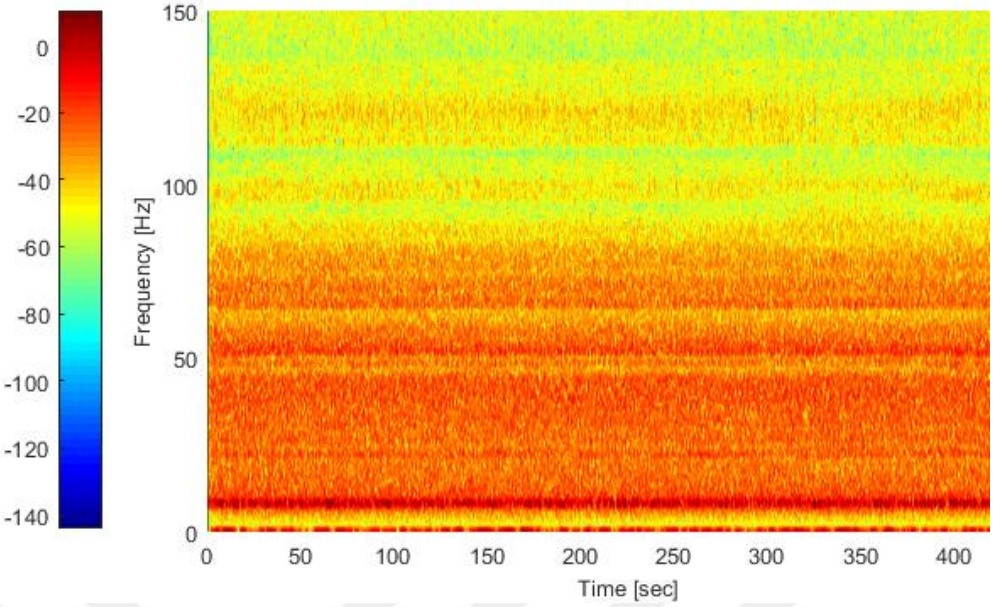

Figure 4.7 Spectrogram of the acceleration data on beam member at 3.5% drift ratio

4.3.1 Identification of Fundamental In-Plane Mode

Modal identification results obtained by NExT-ERA for the fundamental in-plane mode at different damage states using two different excitation types (AV and WN) are presented in Figure 4.8. Here, the selection of the modes at different damage states are done by the aid of stabilization diagrams. These diagrams are helpful tools to be used with parametric system identification methods (e.g., SSI-DATA and NExT-ERA). They are used for determining proper system orders and for distinguishing stable and unstable modes (Peeters & De Roeck, 2001), (Zhang et al., 2014). As an illustrative example, the stabilization diagram of the frame at each drift ratios is shown in Figures 4.9 - 4.15 for WN excitation. The following stability criteria are used to obtain the diagram

$$\frac{\left|f_i - f_j\right|}{f} \le 1\% \; ; \qquad \frac{\left|\xi_i - \xi_j\right|}{\xi_j} \le 5\% \; ; \qquad \left|1 - \mathrm{MAC}_{\phi_i,\phi_j}\right| \le 1\% \tag{4.1}$$

where the estimated frequencies and the damping ratios for models of successive orders are denoted as (f_i, f_j) and (ξ_i, ξ_j), respectively. MACϕ_i,ϕ_j term represents the modal assurance criteria of a pair of mode shapes identified for two different models

of successive orders (Allemang, 2003). The symbols shown in the stabilization diagram denote "⊕": a pole with stable frequency, damping, and mode shape, ".d": a pole with stable frequency and damping, ".v": a pole with stable frequency and mode shape, and "*.f*": a pole with stable frequency only. In the figure, also smoothened and amplitude scaled power spectral density functions (PSDs) are shown which are calculated using the response data recorded at "Sta 1" along x, y, and z-directions from a tri-axial accelerometer. From the stabilization diagrams, model order of 14 was found appropriate for modal identification. From the NExT-ERA results presented in Figure 4.8, as expected, similar frequency values are estimated for a particular damage level and estimated values become smaller for both AV and WN tests as damage increases; results are also represented quantitatively in Table 4.1.

In order to investigate the method-to-method variability in estimation results, the recorded response data at different damage states was processed by three different system identification methods; results are presented in Figure 4.16. The MAC values shown in the figures are calculated between the undamaged mode shapes (using the WN tests and estimated by NExT-ERA method) and the damaged ones (using the WN and estimated by SSI-Data and EFDD methods). It can be said that frequency estimations and MAC values by different methods are very similar for each damage state (i.e., negligible differences), therefore the estimated values are independent of the method used.

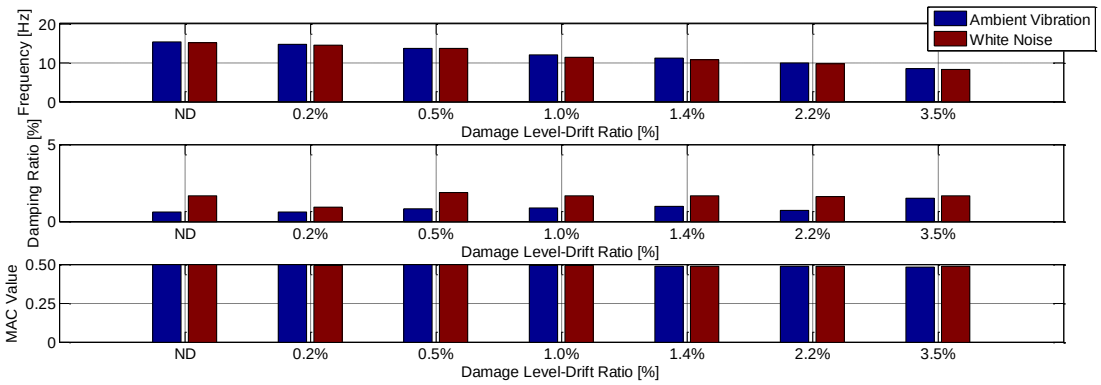

Figure 4.8 Modal identification results of in-plane mode for the test frame under different excitation conditions at progressively increasing damage levels (processed by NExT-ERA method)

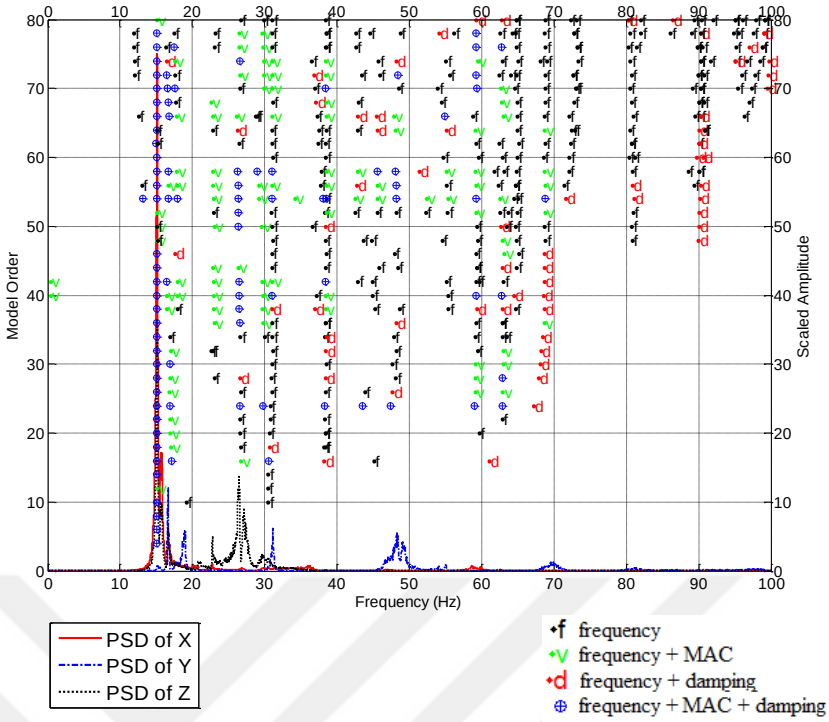

Figure 4.9 Stabilization plot of frame at the undamaged state obtained by NExT-ERA method using WN test data

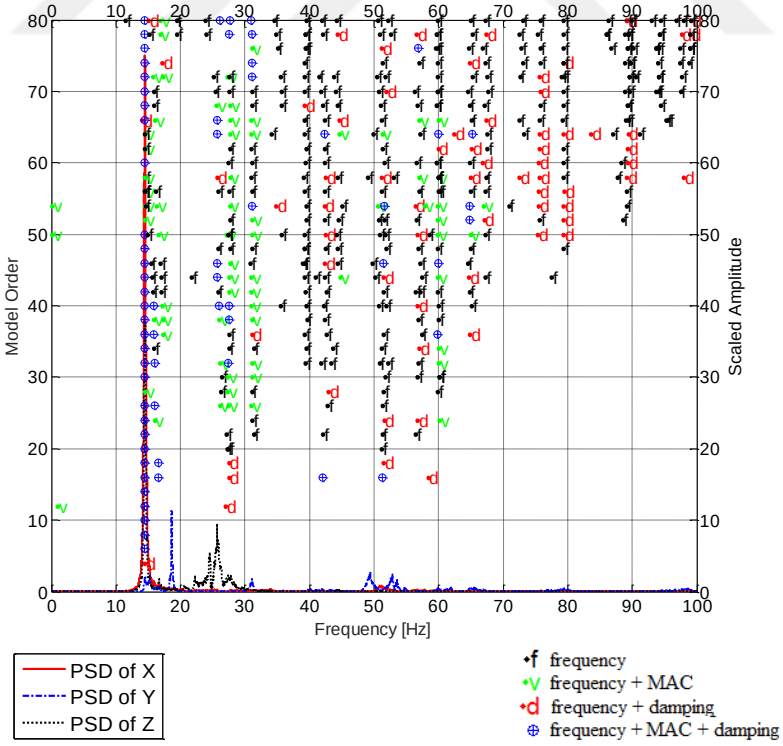

Figure 4.10 Stabilization plot of frame at 0.2% drift ratio obtained by NExT-ERA method using WN test data

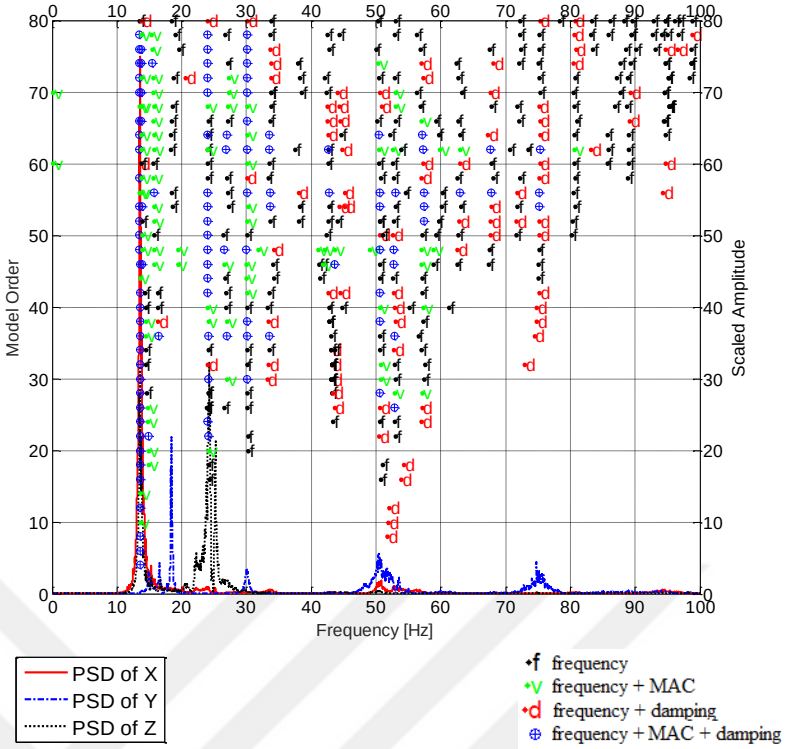

Figure 4.11 Stabilization plot of frame at 0.5% drift ratio obtained by NExT-ERA method using WN test data

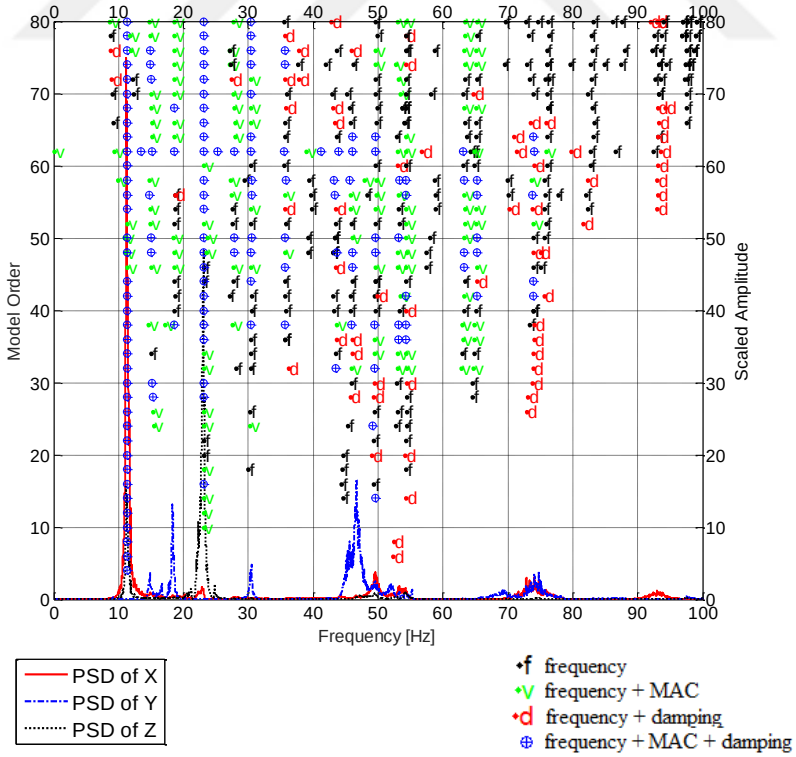

Figure 4.12 Stabilization plot of frame at at 1.0% drift ratio obtained by NExT-ERA method using WN test data

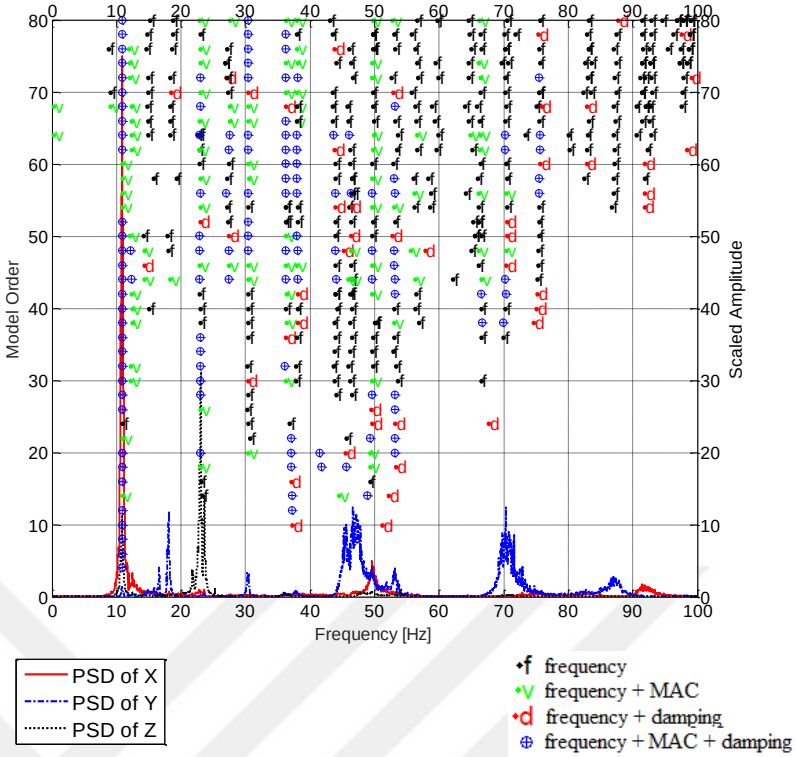

Figure 4.13 Stabilization plot of frame at 1.4% drift ratio obtained by NExT-ERA method using WN test data

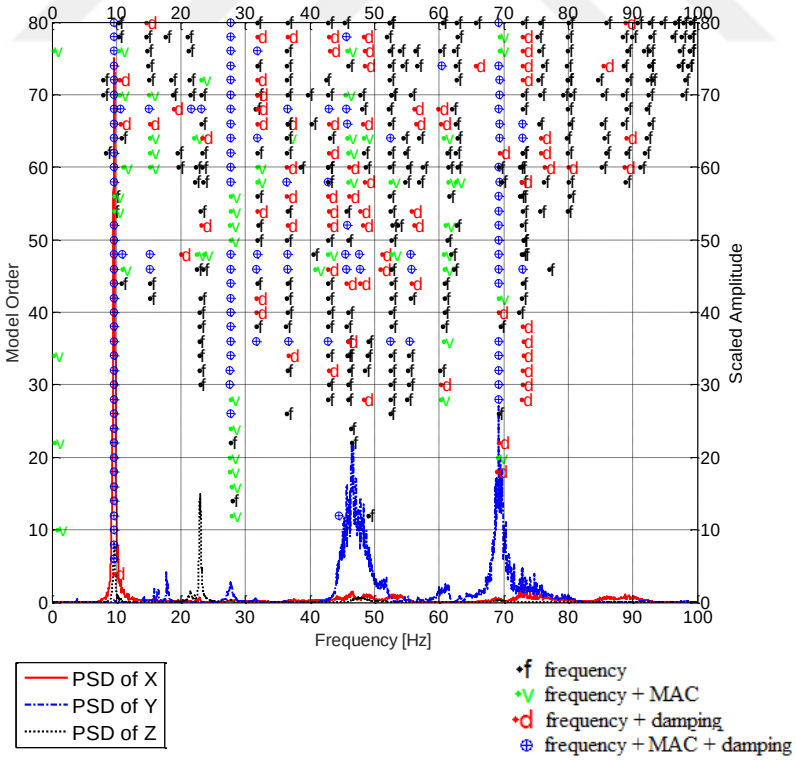

Figure 4.14 Stabilization plot of frame at 2.2% drift ratio obtained by NExT-ERA method using WN test data

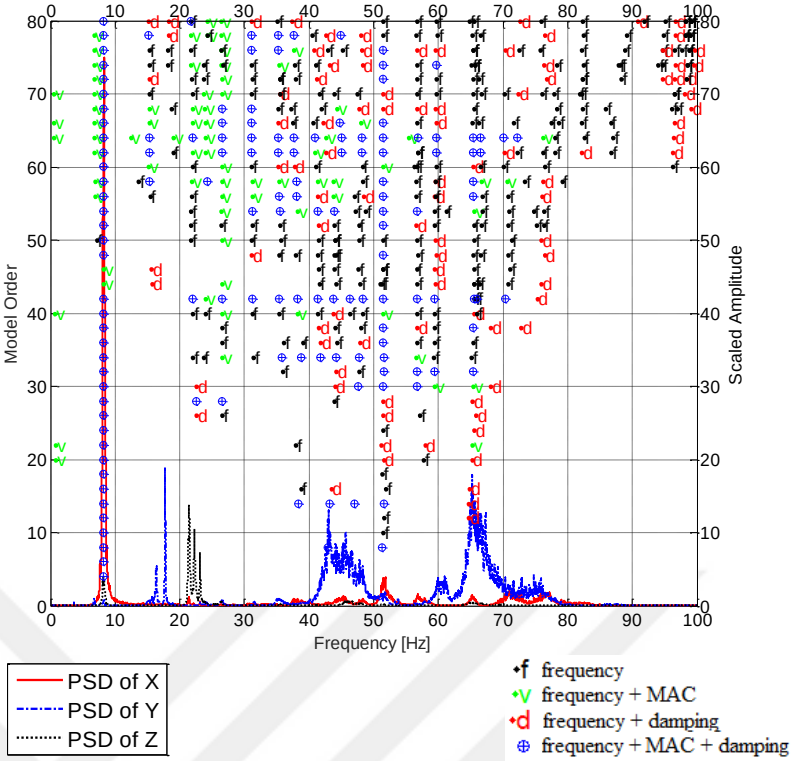

Figure 4.15 Stabilization plot of frame at 3.50% drift ratio obtained by NExT-ERA method using WN test data

Table 4.1 Modal identification results of in-plane mode for the bare test frame under different excitation conditions at progressively increasing damage levels (processed by NExT-ERA method).

Excitation Type	Modal Params	No Damage	0.2%	0.5%	1.0%	1.40%	2.20%	3.50%
AV	ω [Hz]	15.26	14.62	13.72	12.04	11.15	9.81	8.44
	ξ [%]	0.59	0.59	0.81	0.88	0.98	0.73	1.51
	MAC	1.00	1.00	0.99	0.98	0.97	0.97	0.96
WN	ω [Hz]	15.11	14.49	13.55	11.29	10.83	9.62	8.23
	ξ [%]	1.65	0.92	1.85	1.66	1.67	1.58	1.65
	MAC	1.00	0.98	0.99	0.98	0.97	0.97	0.97

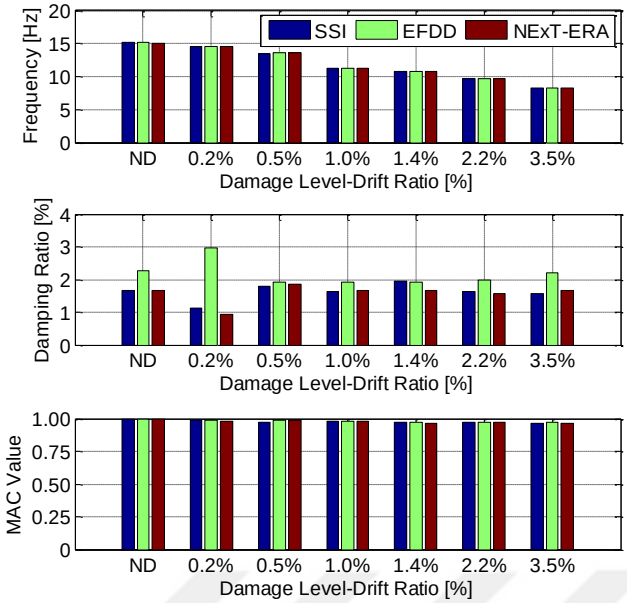

Figure 4.16 Fundamental in-plane modal parameters by different system identification methods using WN data

MAC values presented in Table 4.1 and Figure 4.16 are calculated between the mode shapes of the undamaged state and the different damaged state of the frame. The MAC values show the changes taking place in mode shapes as structural damage increases. It is clearly seen that the MAC values consistently decrease as damage increases indicating that the estimated mode shape at different damage states differ increasingly more with respect to the mode shape of the undamaged case. Mode shape estimations obtained from WN test data using NExT-ERA method are represented in Figure 4.17 for each damage state. Figure 4.18 shows the polar plot representations of the estimated mode shapes with complex components. These plots show the level of non-classical damping in the frame. Based on the results, it can be said that the mode shapes are classically damped (characterized by negligible complex parts) because the vector components are almost perfectly collinear and aligned along the real axis.

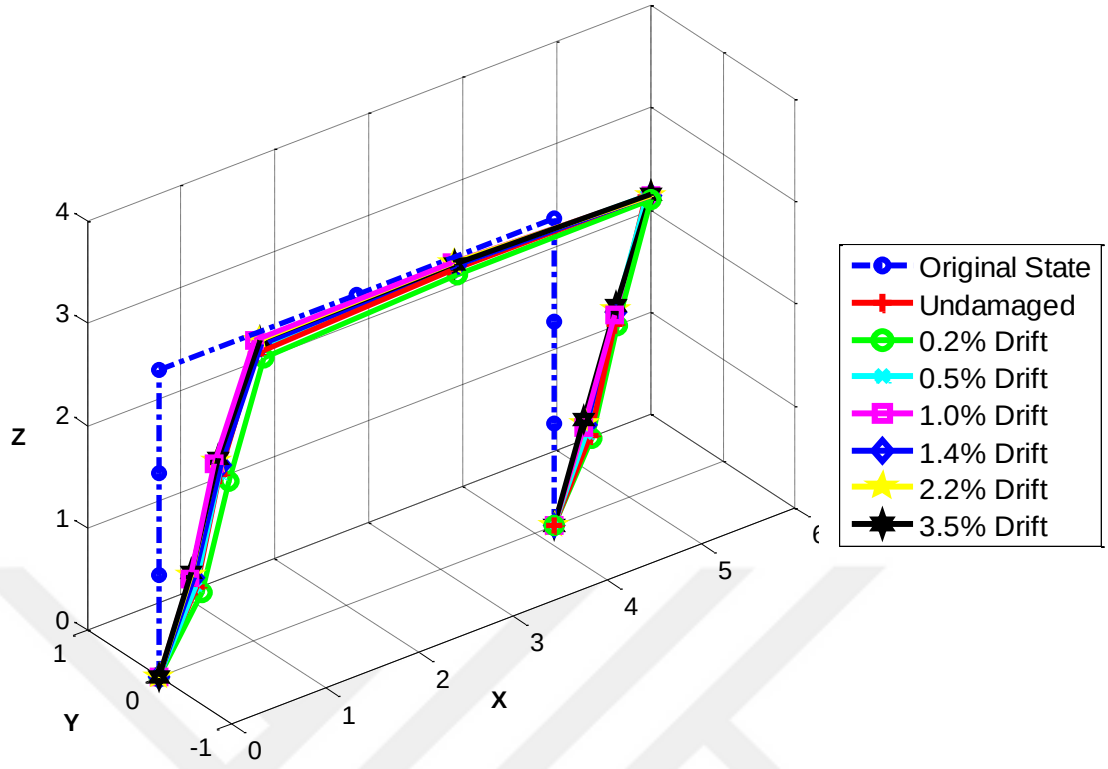

Figure 4.17 Evolution of mode shape at incremental damage states

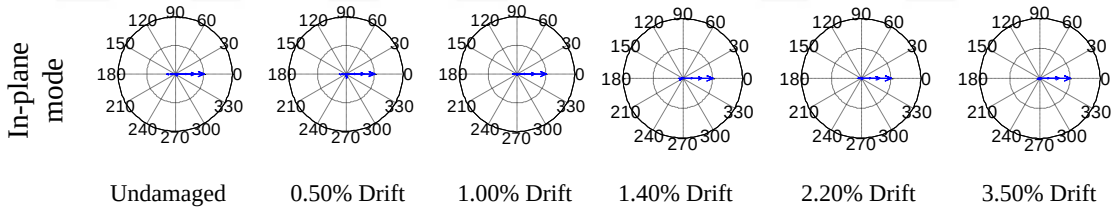

Figure 4.18 Polar plot representation of the in-plane mode shape

4.3.2 Identification of Fundamental Out-Of-Plane Mode

Due to low SNR ratio in out-of-plane direction, fundamental out-of-plane mode couldn't be estimated by using WN and AV test data with parametric time domain methods NExT-ERA and SSI; the stabilization plots presented in Figure 4.9 to 4.15 reveals this fact. However, since the weakest direction of the structure is in out-of-plane direction, frame structure most likely to have a structural mode in lower frequencies than that of the fundamental in-plane mode presented in Section 4.3.1. This idea is supported by the spectrogram plot presented in Figure 4.7 and

investigation of Fourier Amplitude Spectra plots of –y direction sensors given in Figure 4.6. Although it is highly biased, the out-of-plane mode is estimated by non-parametric EFDD technique at each incremental damage state; in Figure 4.19, singular values of the spectral matrix is demonstrated for 3.5% drift ratio. It is obvious that singular values are much smaller for out-of-plane mode compared to in-plane mode. Since the excitation to the frame is in the in-plane direction only, higher estimation uncertainty in the out-of-plane mode is expected (lower signal-to-noise ratio along the not excited out-of-plane direction). Figure 4.20 shows the polar plot representation of the complex valued mode shapes with estimated frequency values. From these plots, it is seen that the out-of-plane mode has large complex components; so it can concluded that, the out-of-plane mode shape should be excluded in the updating process in order to reduce its unfavorable effect on the stability of the optimization problem.

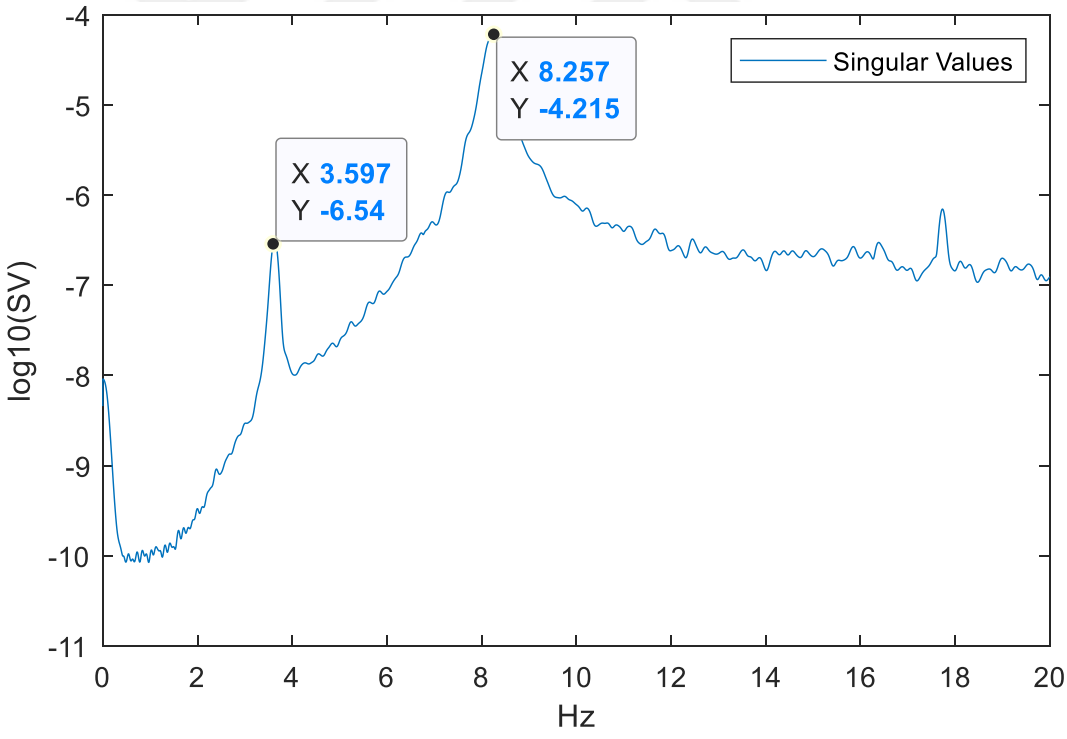

Figure 4.19 Singular value plot of the spectral matrix at 3.5% drift ratio

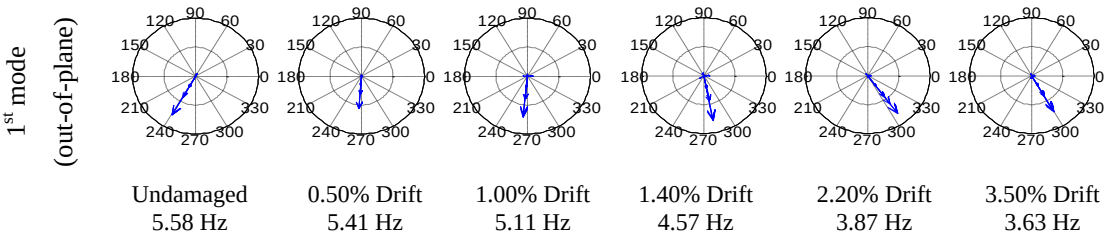

Figure 4.20 Polar plot representation of the out-of-plane mode shape

4.3.3 Comparison of Viscous Damping vs. Hysteretic Damping & Damage Observation Documentation

For the damping estimations, it can be said that NExT-ERA and SSI-DATA methods give somewhat similar results; but the overall match for the damping estimations among the methods is not as good as the frequency and mode shape estimations. The damping results by EFDD method differ more from the results obtained by the other two methods. This higher variability in damping estimations by EFDD method can be attributed to the subjectiveness of the peak-picking process. There is no increasing or decreasing trend for the damping ratio estimations with damage, as observed for the frequency and mode shape estimations at the level of excitations considered in this study. The damping ratio estimations presented in Figure 4.8 show significant variability among different excitation types, and do not have clear trends that can be used solely as a damage indicator. It is known that in real life measurements, noise always exists and SNR ratio plays an important role in accurate parameter estimation. Specifically, damping is very sensitive to measurement noise and as the noise level increases uncertainty in damping estimations also increases (Bajric et al., 2014, 2015). Another peculiarity with damping estimations is the fact that they are amplitude dependent. The damping estimations from the WN data are consistently higher than the ones estimated from the AV data for the frame at all damage states. Moreover, it would be insightful to show the change of hysteretic damping vs. estimated viscous damping coefficients as a function of damage levels (Chopra, 1995). Figure 4.21(a), shows a plot of the calculated hysteretic damping ratios of the frame ζ_{hyst} at all drift levels using base shear – top displacement response of the structural frame provided in Figure 4.3(b).

Figure 4.21(b) represents the relationship between the hysteretic and equivalent viscous damping at each drift ratios; note that viscous damping estimations presented in these figures are identified from white noise data processed with NExT-ERA method. It is known that there is not a direct/strong relation between equivalent viscous damping and hysteretic damping (a function of the area under the hysteretic force-displacement curves) at this excitation levels; but at much higher excitation levels, which is not possible to induce with the available shaker in hand, a relation between these two damping values may exist.

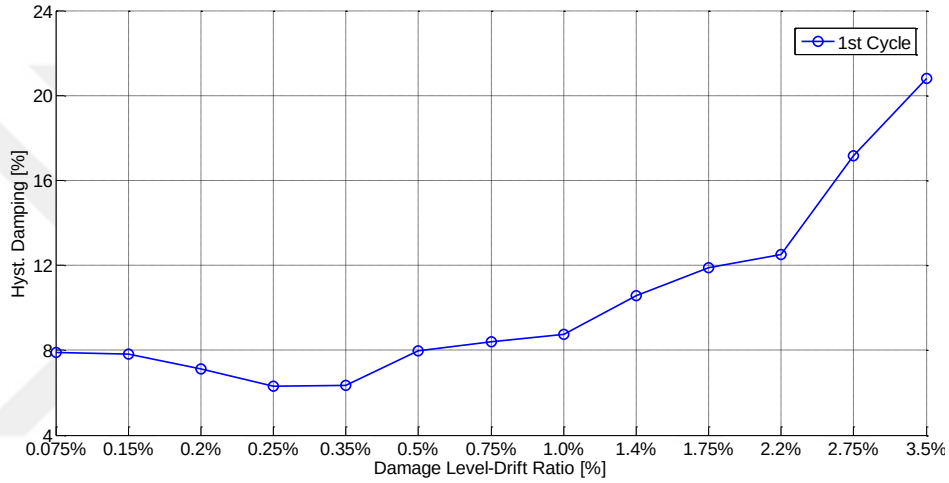

(a)

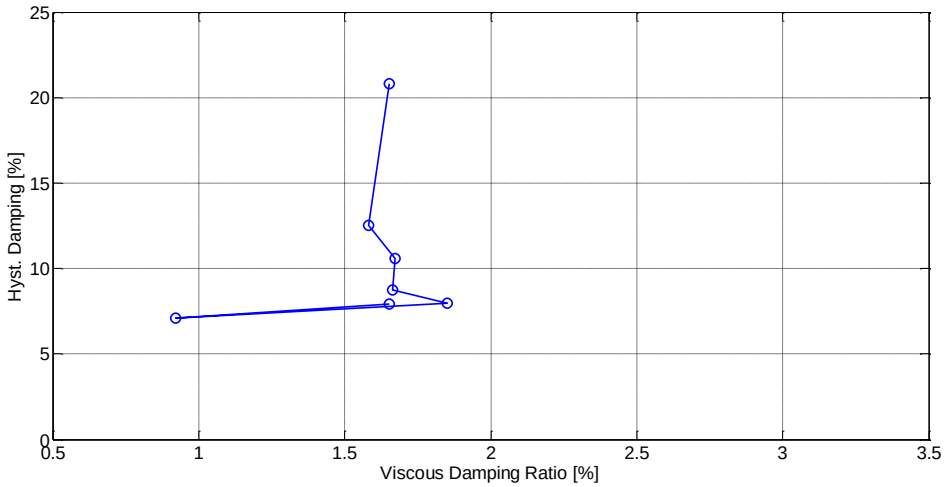

(b)

Figure 4.21 (a) Hysteretic damping at each incremental drift ratios (b) relationship between the equivalent viscous and hysteretic damping

Table 4.2 Summary of visual damage inspections at each damage state

Drifts (%)	Damage Description
0.075-0.20	Minor flexural cracks on the beam (<0.2 mm). No cracks on column.
0.25-0.50	New beam flexural cracks. Flexural column cracks. Minor cracks on the slab and beam (<0.5 mm).
0.75-1.00	Moderate damage on frame joints. New minor flexural cracks on beam (<1 mm).
1.40	Uplift between foundation - column ends. Moderate flexural cracks on slab and beam/column ends (>2 mm).
1.75-2.20	Uplift between foundation - column ends increased. Moderate - severe flexural cracks on column - beam interfaces (>3 mm).
2.75-3.50	Severe flexural damage on frame (>5 mm). Spalling and crushing at base of column concrete. Buckling of reinforcing bars at column bottom ends.

The stiffness degradation values calculated at the ultimate damage state (i.e., 3.5%) is around 70%. It should be emphasized here that the quasi-static tests allowed performing detailed damage observations, the dynamic tests allowed stiffness degradations to be calculated using the modal parameter estimations. By combining static and dynamic tests, it was possible to match different damage types (from static tests) with stiffness degradations obtained through the frame dynamic response (from dynamic tests). Visual damage observations were made and documented during quasi-static tests; a summary of these observations at specific drift ratio intervals is given in Table 4.2 in a simplified form. In Chapter 5, damage observations will be documented and correlated with damage identification results in a more detailed way.

CHAPTER FIVE
DAMAGE IDENTIFICATION OF A REINFORCED CONCRETE FRAME AT INCREASING DAMAGE LEVELS BY SENSITIVITY-BASED FINITE ELEMENT MODEL UPDATING

5.1 Introduction

In this chaper, finite element model updating based damage identification study work is performed on the half-scale RC portal bare frame presented in Chapter 4. At each progressively increasing damage state, through the minimization of an objective function, the stiffness reduction factors of the individual damaged elements are obtained. The updating procedure is carried out in two steps: (i) The initial FE model is updated to obtain the reference model using the experimentally identified modal parameters corresponding to the undamaged frame, and (ii) using this reference model, the procedure is repeated at each damage state to identify the damage, its location and extent. In this study, structural damage is defined as relative stiffness reduction (i.e. reduction in the Young's modulus). Number of design variables used for the updating procedure is reduced to obtain a well-conditioned inverse problem by taking into account: (a) symmetry conditions, (b) detectability metrics (sensitiveness) extracted from the Jacobian matrix, and (c) internal moment levels in the frame elements.

5.2 Damage Identification of the Reinforced Concrete Frame

In this section, the FE model updating technique is applied to the RC frame of which its OMA results presented in Section 4. The residuals used in updating process are based on the natural frequencies and mode shapes identified by accelerometer data. Three-dimensional linear elastic model of the bare RC frame is developed using Bernoulli–Euler beam elements; FEDEASLab finite element analysis program is used for all modeling and analysis needs. The model parameters of the initial FE model are determined from the measured geometric dimensions and the results of the uni-axial compressive strength tests of cubic samples conducted on the 28th day.

Accordingly, Young's modulus of 32 GPa and a density of 25 kN/m^3 are used for the concrete. Since in real-life situations perfect fixity at supports are usually very difficult to attain, the support conditions in the initial FE model are set to be simple supports at the column ends together with 3 rotational springs about x (in-plane), y (out-of-plane), and z (vertical) axes. Other nodes in the FE model are unconstrained, and the lumped mass assumption is made. At supports, the initial rotational spring stiffnesses are set to 9807 kNm/rad by a trial and error procedure for bringing the numerical modal analysis results close to the experimentally identified ones; nevertheless fine adjustments of these springs are obtained through the optimization run in Section 5.2.1. Thus, model updating is applied on the initial model using the optimization method to obtain the reference model. For that, the modal parameters estimated at the undamaged state are used.

The initial FE model is composed of 12 substructures (9 for the frame elements and 3 for rotational springs). The sub-structuring takes into account the neighboring finite elements and/or the geometrically symmetric frame elements which are expected to be affected similarly during updating (e.g. substructure 1 for the bottom elements, substructure 2 for the mid-elements, and substructure 3 for the top elements of the column(s), see Figure 5.2 (b)). The tool defined as detectability index is used to investigate the sensitivity of individual elements with respect to design variables; accordingly one can use the sensitivity matrix to obtain detectability indices for individual finite elements or substructures as follows (Weber et al., 2007)

$$D_j = \left\| s_j \right\| \tag{5.1}$$

where s_j is the jth column of the sensitivity matrix. Note that each column vector in the sensitivity matrix indicates changes in modal parameters due to a unit change in an updating (design) variable. In other words, the detectability index determines sensitivity of elements (or substructures) to modal parameters in a relative way (i.e. detectable elements are more sensitive to modal parameters) and helps analyst to decide which parameters should be updated or not. The fact that a modal data is sensitive to a parameter doesn't automatically imply that this parameter has to be

included in the updating process. In another words, if the value of that parameter is already adequately representing the true value, there is no reason to update it. The detectability indices for these substructures are calculated for the first mode (out-of-plane), for the second mode (in-plane mode), and for both modes together. The results are presented in Figure 5.2(a). It is clear that the sensitivity of a substructure varies from one mode to another and some of them are insensitive to changes in some modal parameters (e.g. the rotational springs about x-axis are sensitive to the 1st mode but insensitive to the 2nd mode). By investigating the detectability index, the detectable substructures along with their numbers are determined as follows: beam ends (7-8), column bottom ends (1), column top ends (3), column mid-zones (2), beam mid-zone (9), rotational springs about x axis (10), and rotational springs about y axis (11). In this way, numbers of substructures involved in the updating procedure (i.e. design variables) are reduced from 12 to 8.

The beam-to-column bending moment capacity ratio of the test frame is approximately 40% (i.e. the columns are stronger than the beam in terms of flexural strength); moment-curvature relationship plot is shown in Figure 5.1. Therefore, it can be shown theoretically that the plastic hinges are first to occur at the beam ends (at weaker sections) rather than at the column(s) top ends. Once the plastic hinges occur at the beam ends, this puts an upper limit to the moment to be transferred from the beam ends to the column(s) top ends. Since this transferred moment is lower than the moment capacity of the column(s) top ends, minor structural damage is expected to occur in these regions. This is to be also confirmed by the damage observations presented later in the chapter. The situation at the column(s) bottom ends is different: As the moment due to the in-plane applied load increases, this moment must be counter acted by the column(s) bottom ends. Therefore, major structural damage in these regions is expected to occur (also confirmed by the damage observations).

The mid-zones of the beam and column elements are not selected for updating due to the low level of internal moments occurring in these regions; also, visual observations clearly revealed that there were only insignificant damages in these regions. Eventually, 5 design variables are found to be appropriate for damage

identification, which are beam ends (7–8), column(s) bottom ends (1), rotational springs about x axis (10), and rotational springs about y axis (11).

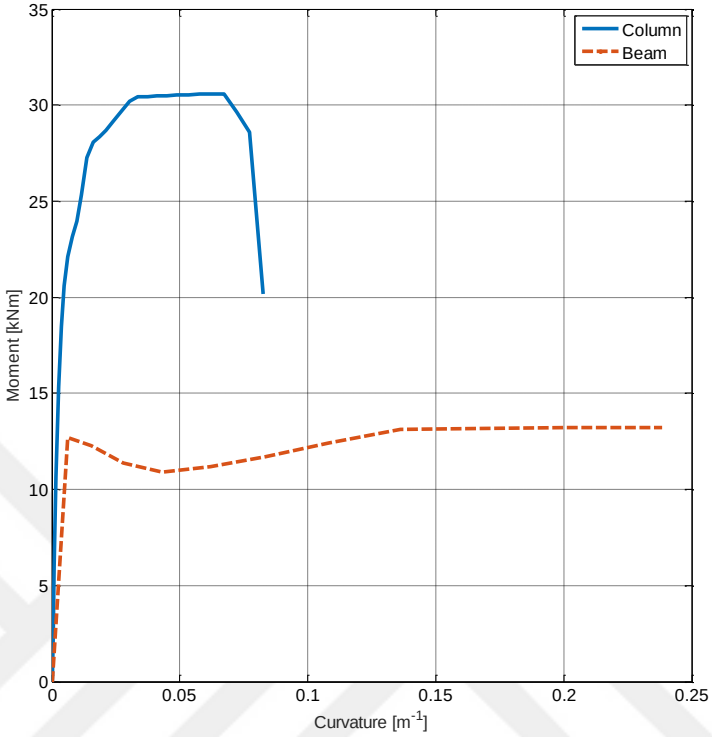

Figure 5.1 Moment-curvature plot of the column and beam member

In this study, the structural damage is defined as the relative stiffness reduction which is quantified by a reduction in element Young's modulus and spring stiffness coefficients which represents the support conditions. The damage identification procedure is performed in two steps: (1) Updating an initial FE model to obtain a reference model by using the estimated modal parameters of the undamaged frame. Within this step, the design variables are updated until a good match between the experimentally identified modal parameters of the undamaged frame and those of the FE model is achieved. (2) Once the reference model is obtained, successive updating operations are performed on it using the modal parameters estimated at progressively increasing discrete damage levels (e.g. 0.50%, 1.00%, 1.40%, 2.20%, and 3.50%). In the second step, updating at discrete damage levels is performed always on the reference model instead of on the updated model of a previous damage state. The rotational springs assigned to the supports are excluded from the design variables set

in the second step (i.e. they are not updated; but kept fixed at the values obtained in the first step). If also the rotational springs were to be included, they would attract most of the changes due to their higher sensitivities (see Figure 5.2) and would lead to unrealistic damage results for other substructures. Note that the constraints, lower and upper bounds on design variables p for substructures, are set to be ± 1.0 (i.e. $l_b = -1.0$ and $u_b = +1.0$) where (−) values mean stiffening and (+) values mean softening. Table 5.1 shows the modal parameter estimation results of the structural frame at different damage states processed by EFDD by the use of WN vibration data and they are used in model updating application. Note that frequency values are little bit different from the results shown in Table 4.1, since the NExT-ERA results are presented there in Section 4.

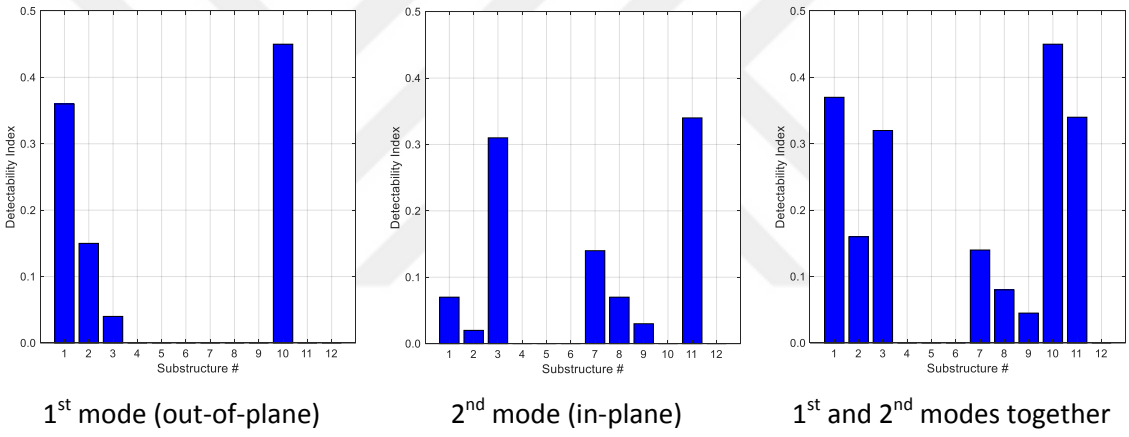

(a)

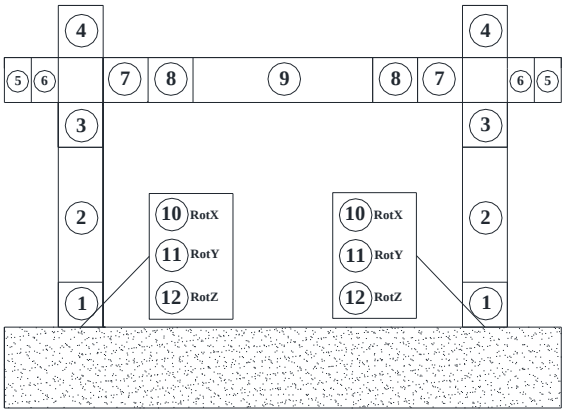

Detectable Elements

1) Column(s) bottom ends
2) Column(s) mid-zones
3) Column(s) top ends
7-8) Beam ends
9) Beam mid-zone
10) Rotational springs about x axis (RotX)
11) Rotational springs about y axis (RotY)

(b)

Figure 5.2 (a) Detectability index and (b) detectable elements

Table 5.1 Modal parameter estimation results of the frame by EFDD method by the use of WN vibration data

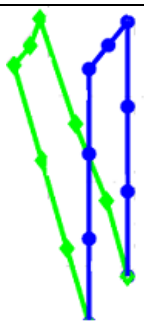		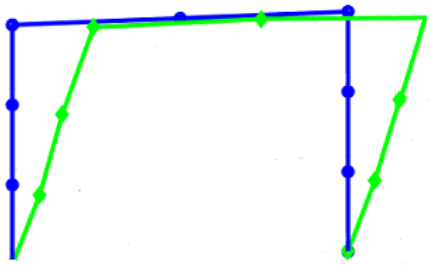	
1st mode (out-of-plane)		2nd mode (in-plane)	
Drift Level	Frequency [Hz]	Drift Level	Frequency [Hz]
Undamaged	5.58	Undamaged	15.10
0.50%	5.41	0.50%	13.55
1.00%	5.11	1.00%	11.11
1.40%	4.57	1.40%	11.04
2.20%	3.87	2.20%	9.62
3.50%	3.63	3.50%	8.25

5.2.1 Updating for the Reference Undamaged State

The substructures beam ends (7-8), column(s) bottom ends (1), rotational springs about x axis (10), and rotational springs about y axis (11) are selected as design variables for updating the initial FE model. Here, a common design variable is defined for the adjacent elements at the beam ends (i.e. only one variable instead of two for the elements designated as 7-8 in Figure 5.2). The results for the optimization problem are summarized in Table 5.2. The algorithm updated only the rotational springs without updating other elements in the model which is due to their relatively higher sensitivities. The spring stiffnesses about x and y axes after updating became 5894 kNm/rad and 7444 kNm/rad, respectively. It is seen from Table 5.2 that the first and second natural frequencies of the reference FE model (updated model, 3rd column) and the experimentally identified values (2nd column) match very well. Also, modal assurance criterion (MAC) values are calculated to compare the mode shapes before (6th column) and after (7th column) updating (Allemang, 2003). There is a very marginal improvement in the MAC values calculated between the experimentally estimated mode shapes and the mode shapes of the FE model (before

and after updating) which indicates that the considered mode shapes are not sensitive to the updating parameters.

Table 5.2 Results of updating the initial FE model to obtain the reference model using the modal data estimated at the undamaged state

(1) Initial FE Model Freq.	(2) Undamaged Frame Freq.	(3) Updated FE Model Freq.	(4) Freq. Differences Before Updating (1 - 2)	(5) Freq. Differences After Updating (3 - 2)	(6) MAC Before Updating (1 - 2)	(7) MAC After Updating (3 - 2)
[Hz]	[Hz]	[Hz]	[%]	[%]	[-]	[-]
6.16	5.58	5.58	10	0	0.99	0.99
15.70	15.10	14.98	4	1	0.95	0.96

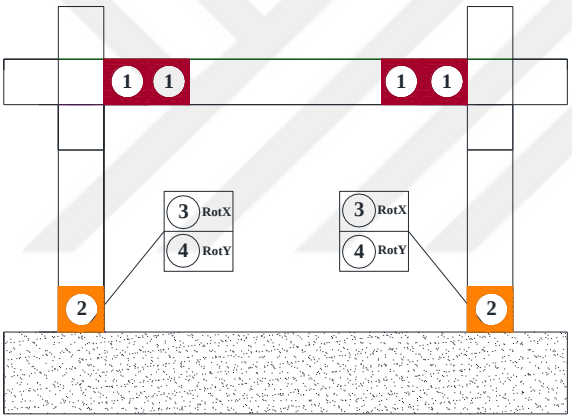

Design Variables

① Beam ends
② Column(s) bottom ends
③ Rotational springs about x axis (RotX)
④ Rotational springs about y axis (RotY)

*Substructures ① and ② are also selected as design variables but not updated by the algorithm.

	Initial	Ref. Model (Updated)
③ RotX (kNm/rad):	9807	5894
④ RotY (kNm/rad):	9807	7444

As an outcome of the reference state updating, the modal properties of the calibrated FE model for the first 3 modes are represented in Table 5.3; for the sake of better visualization, mode shapes of the FE model extracted in SAP2000 environment is shown. Note that the modes used for reference state updating corresponds to the 1st and 3rd structural modes of the FE model; whereas 2nd mode couldn't be extracted experimentally by OMA techniques due to low SNR and rank of the problem which is specified in Section 4.3.1. Since the electro-dynamic shaker excitation is applied in a single point with single in plane -X direction in WN test,

rank of the problem is limited to one; thus only the in-plane mode (15.10 Hz) is identified with a high confidence rate experimentally.

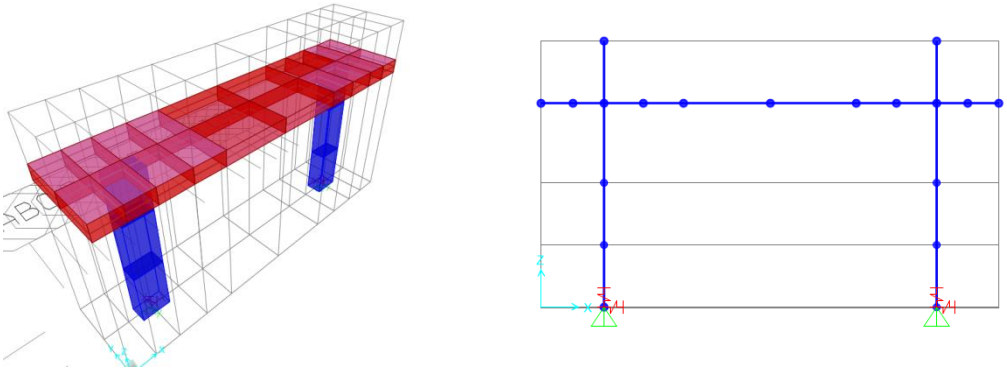

Reference FE model

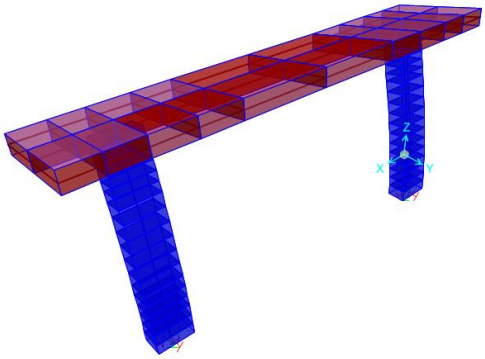

(1. mode: out of plane) – 5.58 Hz –

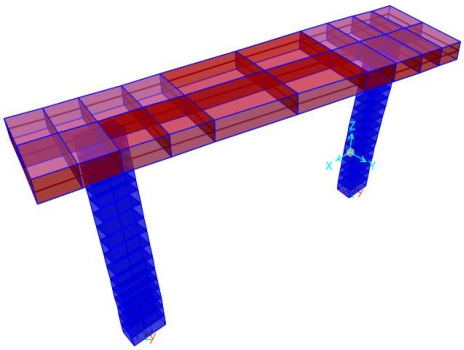

(2. mode: torsional mode) – 9.40 Hz –

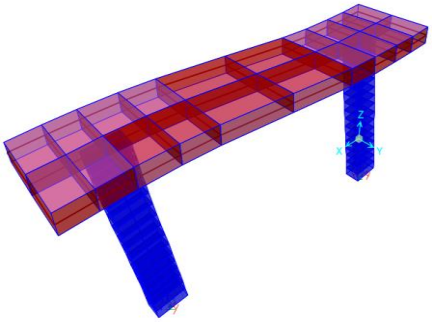

(3.mode: in-plane lateral) – 14.98 Hz –

Figure 5.3 Modal parameters of reference (calibrated) FE model

5.2.2 Damage Identification at Increasing Damage Levels

The reference model obtained in the previous section is updated by using two design variables (the one assigned to the beam ends and the one to the column(s) bottom ends, the spring stiffnesses are kept fixed after the reference model is

obtained) using the estimated modal parameters at gradually increasing discrete damage levels. For each damage states, residual vector has 2 r_f + 17 x 2 r_s = 36 components. Note that the weighting factors were set to 1 for the in-plane and the out-of-plane natural frequencies and for the in-plane mode shapes only; whereas the out-of-plane mode shapes are excluded from the optimization process by setting their weighting factor to zero due to high estimation uncertainty seen in these modes (17 components related to out-of-plane mode shape residuals are equal to zero at each iterations). For the updating of reference FE model for incremental damage states, the dimensionless damage factors were constrained in range [0,1]. The damage factors are evaluated relative to the reference state; for each incremental damage states, the estimated modal parameters shown in Figure 5.3 are used in objective function for damage identification. The solution of the optimization problem and the calculated dimensionless stiffness reduction factors (in terms of p in percent) at different damage levels with respect to the reference state (undamaged) are presented in Table 5.3. It is clear that the natural frequencies of the updated FE model (3rd column) and the experimentally identified ones (2nd column) match almost perfectly. Especially for the 3.50% drift level, the effectiveness of the method can be clearly seen since the frequency differences calculated before and after updating are decreased significantly from 82% to 1% (4th and 5th columns). On the other hand, changes in the MAC values calculated before and after updating (6th and 7th columns) remain almost the same due to their low sensitivities to the design variables. In Table 5.3, the dimensionless stiffness reduction factors indicate that the severity of the structural damage increases as the drift level increases, which is due to accumulation of damage on the beam and column(s) ends. In order to investigate the solution space of the optimization problem, contour plots of the objective function with respect to the changes in the design variables are calculated. In these plots, x and y axes represent the design variables used for the beam and column(s) bottom ends (i.e. two design variables), whereas the z axis (contours) is the value of the objective function for a particular design parameter pair. Since only two design variables are used for the frame updating, the contour plots for different damage levels can be plotted in Figure 5.4. In these plots, the region with the darkest color indicates the global minimum (i.e. solution of the optimization problem). It can be

inferred that the objective function has a flat surface in the vicinity of the solution which means that the global minimum lies within a wide interval (especially at low damage states); therefore, the solution to the optimization problem is not unique. Yet as the damage level increases, the region indicating the global minimum narrows down (the areas with darker blue zones shrink), indicating that the solution becomes closer to a unique one. This indicates that the chosen design parameters can be used to represent the damage patterns observed at higher drift ratios.

Table 5.3 Updating the reference model for increasing damage levels using the estimated modal data (damage identification results)

Drifts (%)	(1) Reference FE Model Freq.	(2) Damaged Frame Freq.	(3) Updated FE Model Freq.	(4) Freq. Diff. Before Updating (1 - 2)	(5) Freq. Diff. After Updating (3 - 2)	(6) MAC Before Updating (1 - 2)	(7) MAC After Updating (3 - 2)
	[Hz]	[Hz]	[Hz]	[%]	[%]	[-]	[-]
0.50	5.58	5.41	5.41	3	0	0.99	0.99
	14.98	13.55	13.64	11	1	0.96	0.96
1.00	5.58	5.11	5.10	9	0	0.98	0.98
	14.98	11.11	11.22	35	1	0.98	0.98
1.40	5.58	4.57	4.55	22	0	0.98	0.98
	14.98	11.05	11.17	36	1	0.98	0.98
2.20	5.58	3.87	3.85	44	0	0.97	0.97
	14.98	9.62	9.73	56	1	0.99	0.98
3.50	5.58	3.64	3.62	54	0	0.99	0.98
	14.98	8.25	8.33	82	1	0.99	0.98

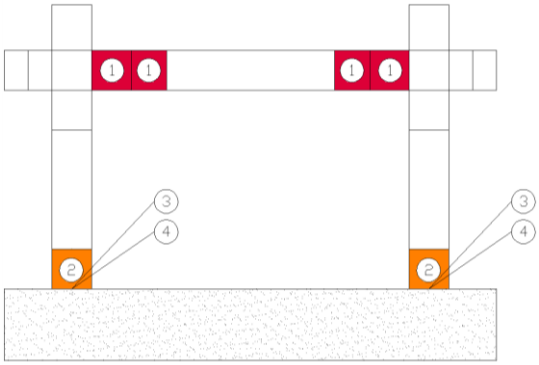

Design Variables

① Beam ends
② Column(s) bottom ends
③ Rotational springs about x axis (RotX)
④ Rotational springs about y axis (RotY)

Drifts (%)	Stiffness reduction factors with respect to the reference state (p%)	
	①	②
Reference	0	0
0.50	49	15
1.00	81	35
1.40	78	58
2.20	85	75
3.50	91	79

*Rotational spring stiffnesses ③ and ④ are not selected as design variables.

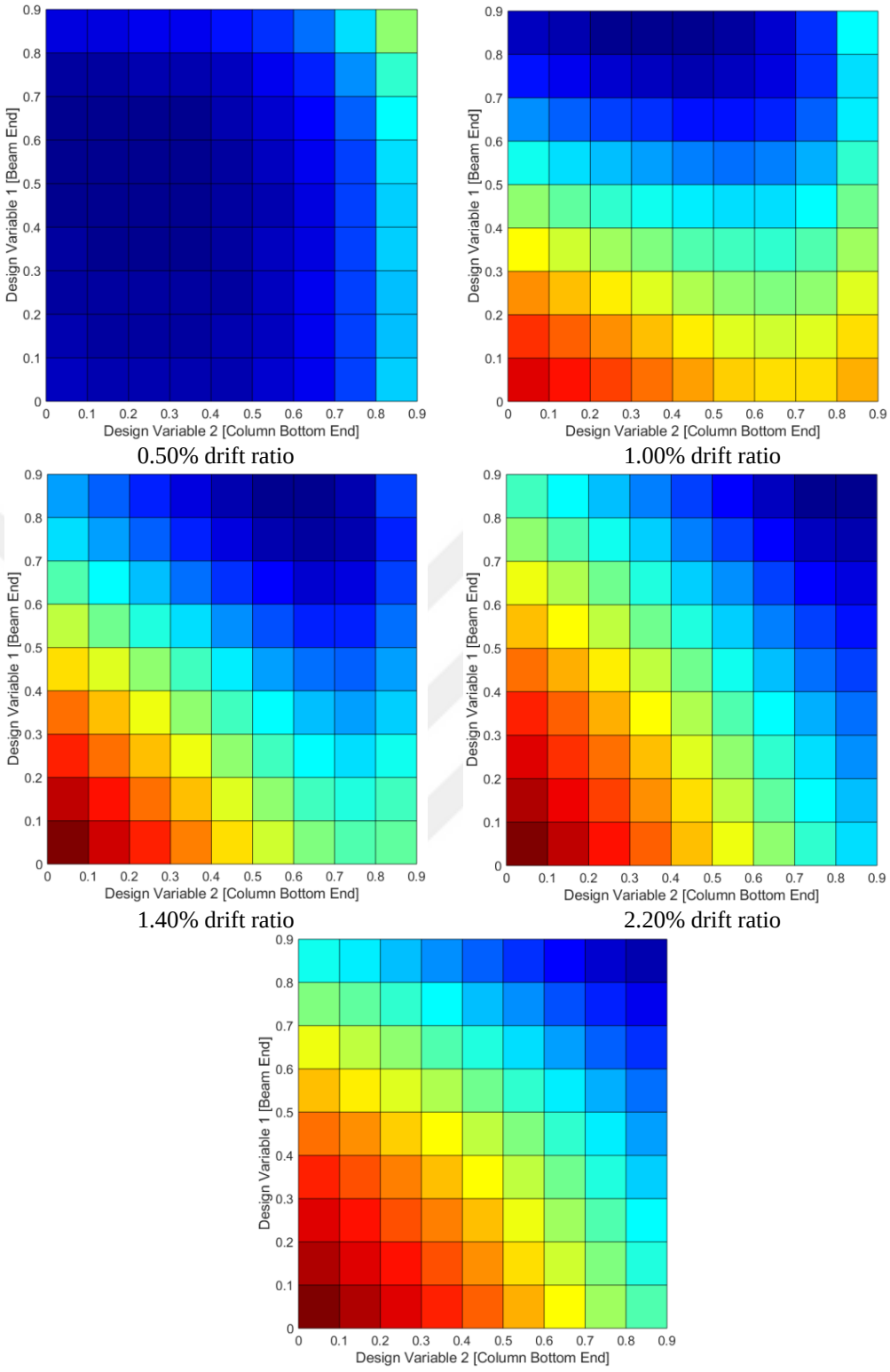

Figure 5.4 The contour plots of the two-parameter objective function for increasing damage levels

5.2.3 Visual Damage Inspections at Increasing Damage Levels

The damage identification results presented in Section 5.2.2 are also supported by visual damage inspections made during the quasi-static tests. These inspections are tried to be correlated with stiffness degradations (SD) corresponding to the in plane modes with respect to the undamaged case can be approximated by the following equation

$$SD_i = \frac{(f_{und})^2 - (f_{dam,i})^2}{(f_{und})^2} \quad (5.2)$$

where subindice 'i' represents various states (i=ND, 0.2%, 0.5%, 1.0% etc.). Note that the stiffness degradation values are calculated using the frequency estimations. At different drift levels for different frames are matched with the detailed visual damage inspections (refer to Table 4.2). The results are aggregated into three dimensional plots and are presented in Figure 5.5 for the structural frame; stiffness degradations are calculated as 8%, 18%, 46%, 47%, 60%, 70% for 0.2%, 0.5%, 1.0%, 1.4%, 2.2%, 3.5% drift ratios, respectively. In these figures, damage types are categorized for column (subplot a), beam (subplot b) members in two distinct groups, and subplots (c) show the zones of the RC frame. The bars with red colors indicate that a particular damage type (as indicated on the longitudinal axis) occurred for the first time or that damage type increased significantly at that particular drift ratio (as indicated on the transversal axis). The bars with yellow colors indicate that no significant change in the existing damage type occurred and the bars with green colors indicate that a particular damage type has not yet occurred at that drift ratio. These figures are useful in determining what damage type (also its extent, and its location) has more pronounced effect on the stiffness degradation as a function of increasing structural damage.

According to results presented in Figure 5.5, the damages at beam ends due to the flexural action were effective until 0.2% drift ratio, and these damages resulted in ~8% stiffness degradation. With increasing drift ratio, up to 1.0%, the damage at

column ends started to be more pronounced in loss of in-plane stiffness; nevertheless beam ends are also considered to be increased at this drift ratio. The largest change in stiffness degradation (~28%) was observed within the 0.5%-1.0% drift ratio interval due to mainly column damages (Figure 5.5(a), damage types 1a, 2a, and 3a). Beyond the 1.0% drift ratio, no additional flexural cracks are observed on beam ends; this is consistent with the damage identification results presented in Table 4.2. Towards the end of the test, the separation at the column-foundation interface can be seen as the critical factor in stiffness degradation and at these drift ratios, concrete is crushed and spalled at column bottom ends.

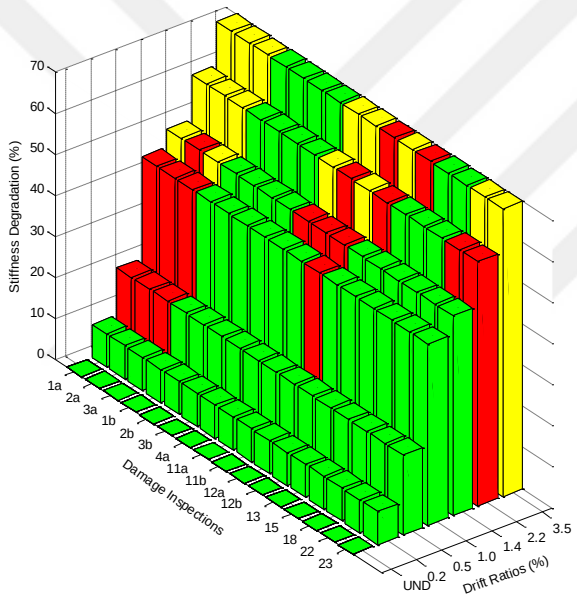

1a) Flexural cracks at column bottom ends.
2a) Flexural cracks at column top ends.
3a) Flexural cracks at column central zone.
1b) Shear cracks at column bottom ends.
2b) Shear cracks at column top ends.
3b) Shear cracks at column central zone.
4a) Shear cracks at column-beam joint region.
11a) Crushing of cover concrete at left column bottom end.
11b) Crushing of cover concrete at right column bottom end.
12a) Uplift between left column and foundation.
12b) Uplift between right column and foundation.
13) Reinforcements at column bottom ends become visible.
15) Buckling of reinforcements at column bottom ends.
18) Rupture of reinforcement at column bottom ends.
22) 2 mm crack width at column ends.
23) 5 mm crack width at column ends.

(a) Column

Figure 5.5 Combined stiffness degradation - visual damage inspections plots for the structural frame

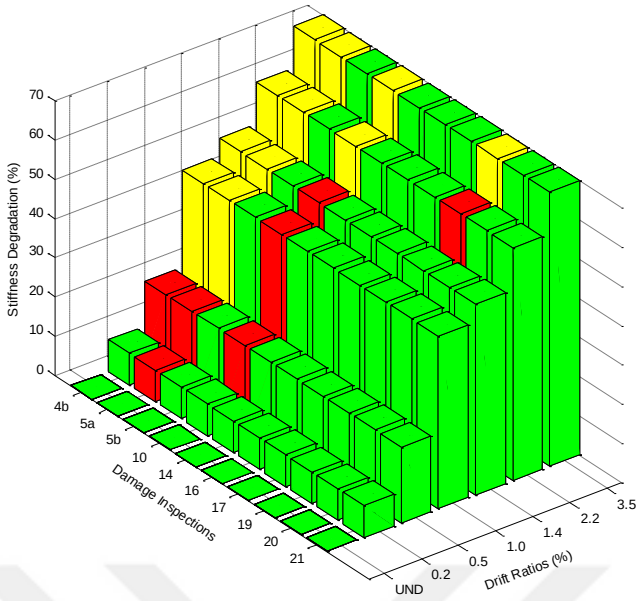

4b) Flexural cracks at beam-column joint region.
5a) Flexural cracks at beam ends.
5b) Flexural cracks at beam central region.
10) Flexural cracks at slab.
14) Reinforcements at beam ends become visible.
16) Buckling of reinforcement at beam ends.
17) Rupture of reinforcement at beam ends.
19) 2 mm crack width at beam ends.
20) 5 mm crack width at beam ends.
21) 10 mm crack width at beam ends.

(b) Beam

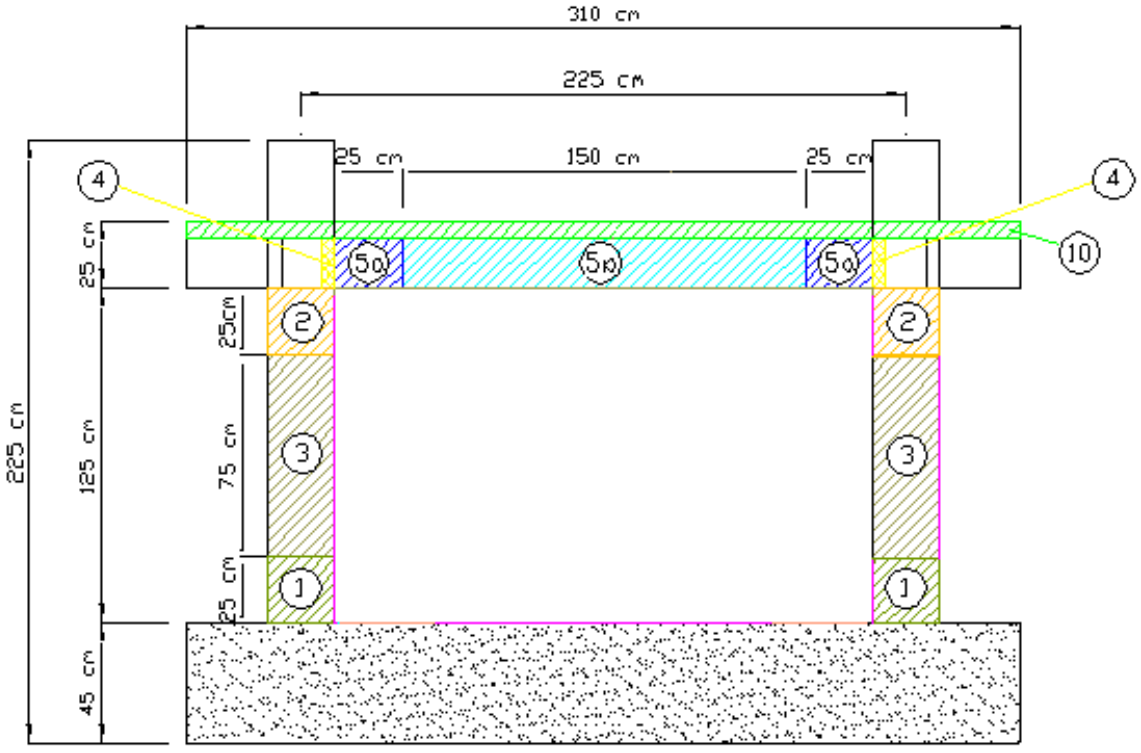

(c) Zones of RC structural frame

Figure 5.5 continues

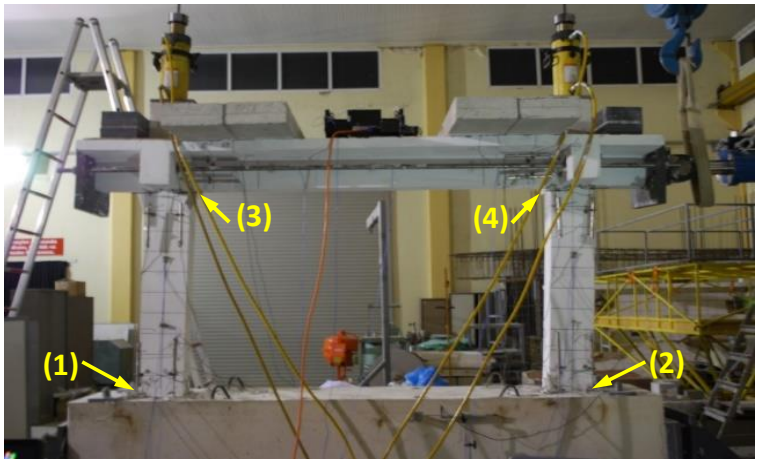

(a) General view of the frame at 3.50% drift ratio

(b) Damage on the beam ends

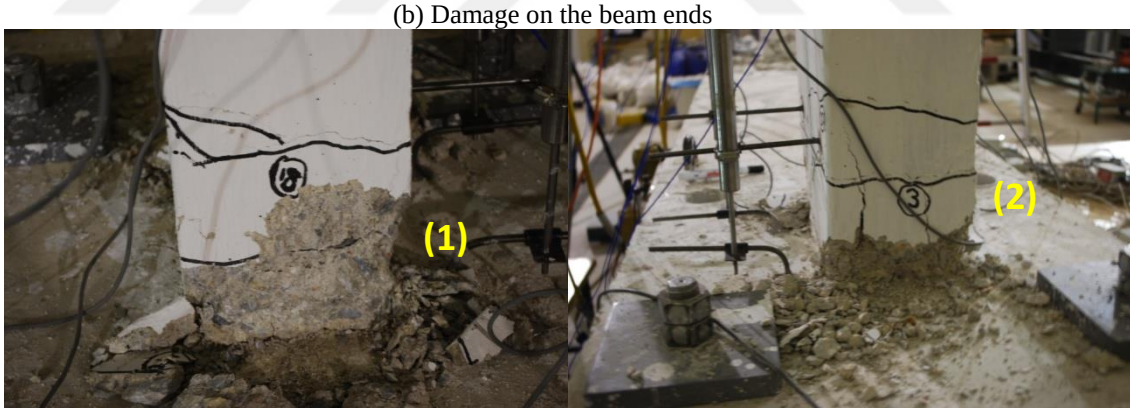

(c) Damage on the column(s) bottom ends

Figure 5.6 Observed damages on the beam ends and the column(s) bottom ends at the ultimate damage level (3.50% drift ratio) (Personal archive, 2016)

Figure 5.6(a) shows the damage state of the frame at 3.50% drift ratio (i.e. the maximum drift level where the chosen design parameters are more representative). In the ultimate damage state, extensive and deep cracks are observed on the beam ends (Figure 5.6b) and the column(s) bottom ends (Figure 5.6c). At this drift ratio, the

largest crack width on the beam ends is measured around 3 ~ 4 mm and on the column(s) bottom ends deep cracks and spalling of concrete are observed. In this damage level, the natural frequencies of the frame are reduced by 35% and 45% for the first and the second modes with respect to the undamaged state, respectively. Specifically, structural damage is mainly concentrated on the on the column(s) bottom ends; whereas only minor damage is observed on the column(s) top ends (Figure 5.6). Stiffness degradations at higher drift levels are mainly due to the widening of the existing cracks and crushing of the cover concrete on column member(s). The pictures shown in Figure 5.6(b) and (c) are chosen to show the sides of the beam and columns which experienced the most severe structural damage, damage identification results were found consistent with damage observations. The selection of design variables is justified by the damage observations; since almost no damage is observed on the top ends of the column(s) member during the whole tests and damage on the beam member almost remain constant at higher drift ratios.

CHAPTER SIX
UNCERTAINTY ANALYSIS OF DAMAGE IDENTIFICATION RESULTS OBTAINED BY FINITE ELEMENT MODEL UPDATING

6.1 Introduction

Uncertainty quantification in model updating is an indispensable issue in model updating, since the problem is prone to *modeling* and *measurement errors*, which results to *uncertainties* in *model predictions* and the *vibration data*, respectively. Owing to inevitable measurement errors and inaccuracies in the numerical model, the identified parameters exhibit deviations from their exact values. Thus, it is therefore desirable to assess a measure of quality to the updated parameters. Generally, FE model updating can be regarded as a *parameter estimation technique*. In the problem of parameter estimation, measured values of model output is used in order to estimate the optimal model parameters. Since measurements invariably contain errors, only approximate parameter values are found and parameters are deemed to be *estimated*. The method of estimating is called the *estimator*, whereas the result of applying the method is *estimate*.

Section 6.1.1 and 6.1.2 briefly introduces the two different types of uncertainties in model updating problems; namely; '*uncertainties related to model prediction*' and '*uncertainties related to experimental data*' are explained with their sources. Problem is handled comprehensively in the review study of Simoen et al., (2015). The uncertainty quantification study in parameter estimation problems mainly utilizes concept of probability and statistics. In Section 6.2, it is aimed to investigate uncertainties in damage identification results due to errors in modal parameters. Structural damage is simulated as regional stiffness losses at the column and beam ends of a numerical frame type structure. In the damage identification stage, first 4 modal parameters are used. Two different levels of noise are added on them to simulate uncertainty in modal parameter estimations. Noise levels are controlled by coefficient of variation (C.O.V.). In order to quantify the uncertainty of the identified damage due to the variability of modal parameters, a full factorial analysis of variance (ANOVA), resulting in 16 combinations of modal input factors, is used. For

each combination of input factors, 20 noise realizations are generated using Gaussian normal distributions with standard deviations scaled to the level of modal parameters. The results are presented in two formats: (a) Spread of the identified damage factors for all 320 identification runs with their statistical measures and; (b) R^2 value of the mean and standard deviation of the identified damage factors due to the variability of each input factors. The results of this investigation demonstrate that specific modal parameters have only influence on specific damage factors.

6.1.1 Uncertainty Related to Model Prediction

In numerical simulations, the real behavior of the structural system may not be represented perfectly. The sources of model uncertainties are distinguished by many authors such as Walker et al., (2015); Der Kiureghian & Ditlevsen (2009); Soize (2010); Kennedy & O'Hagan (2001) and can be summarized as follows:

Model parameter uncertainty: This kind of uncertainty mainly arises from unknown or insufficiently known geometric properties, material properties or load characteristics. This kind of uncertainty also referred to as variable or model input uncertainty.

Model structure uncertainty: Modeling simplifications or assumptions made by the analyst creates this kind of uncertainties. Simoen et al., (2015), (p.131) gives two main examples for this category, "uncertain model context (i.e. uncertain extent of the numerical model) and assumptions of unknown validity regarding the selected model parameters boundary conditions, governing physical equations and model order". This kind of uncertainty also referred to as model form or model framework uncertainty. The discretization errors of FE modes and approximation errors are also considered as model structure error.

Model code uncertainty: This kind of uncertainty mainly arises from software or hardware errors. This type of uncertainty is assumed to only account for a negligible

part of modeling error and also referred to as technical model uncertainty or numerical uncertainty.

The discrepancies evaluated between the model predictions $\mathbf{G}_{model}(\mathbf{p}_{model})$ and the true system output **d** is defined as the modeling error in Simoen et al., (2015). The presence of modeling error implies that the structural model class never contains the true structural system.

6.1.2 Uncertainty Related to Experimental Data

Since model updating makes use of observational data, the most obvious source of uncertainty relates to measurement or experimental error. This error can be random measurement noise, or it can be a bias or systematic error caused by imperfections in the measurement equipment or setup, or during subsequent signal processing. Measurement error forms a source of discrepancy between the observed structural behavior $\overline{d}$ and the real structural response d; in the following, this difference is defined as the measurement error $\mu_D = \overline{d} - d$ (Simoen et al., 2015, p.132).

In FE model updating, the experimental data (i.e. modal characteristics) are extracted from time - domain vibration data using system identification methods. In these methods, a linear time invariant (LTI) system is selected to approximate the true structural system, which is then employed to identify the modal characteristics. Besides measurement noise, a number of factors can result in uncertainty on these extracted modal data, e.g. the finite nature of the data, filtering of the data, the selected model order and the chosen LTI model of the structure. It is clear that the measurement error is in this case partly caused by a form of model (structure) uncertainty regarding the chosen LTI system. Typically these uncertainties give rise to a bias of the model (resulting e.g. identification of spurious modes), bias of the modes, and variance errors. In most situations, making use of stabilization diagrams and careful selection of the model order can

resolve the bias errors; however the variance errors on the modes cannot be reduced (Simoen et al., 2015, p.132).

6.2 Problem Definition, FE Model of the Structure and Damage Scenario

In this section, the uncertainty in the damage identification results due to variability of modal parameters is investigated by using the first 4 eigenmodes. The uncertainty of the identified damage is quantified through full factorial analysis of variance (ANOVA) technique. In this study, the identified modal parameters of the damaged structure are generated numerically using the 3D model of the test structure presented in Chapter 5. Differently from the study presented in this section, three design variables is used, namely; for beam ends, column bottom ends and column top ends. Here, the damage is simulated as a reduction in bending rigidity (EI) for column(s) bottom ends, column top ends and beam ends with the rate of 30%, 40%, 50%, respectively.

In Table 6.1, reference FE model of the structure, design variables, modal frequencies for both the undamaged and damaged cases are presented. Similar to FE model presented in Section 5, support conditions of the undamaged frame were represented with simple support conditions complemented with the same rotational spring elements used in previous section (Rot-X = 5894 kNm/rad; Rot-Y = 7444 kNm/rad; Rot-Z = 20000 kNm/rad). Note that, for the damage identification study presented in Section 5, the definition of Rot-Z was required due to structural stability; however, since no mode related to Rot-Z been updated in previous section, its value wasn't mentioned there and arbitrary value was assumed. For the problem specified here, same value Rot-Z= 20000 kNm/rad is used initially, and is adjusted by the algorithm since higher structural modes are taken into account here. As the FE model of the frame has 17 free nodes, the dimension of the mode shape component is 17x3 = 51 DOFs. In practice, the main source of uncertainty in damage identification arises from modal parameter estimation errors; however, there are several other factors can be found as possible candidates; such as type of FEs used in modeling the structure, mesh size, residual types, their weights and numbers used in objective

function, number of design variables, number of sensors. This study investigates the uncertainties in damage identification due to estimation errors in modal parameters. Here, two levels of uncertainty, 0.5% and 1% coefficient of variation (COV) are considered for natural frequencies and mode shape components for these 4 modes. 20 different noise realizations were generated using Gaussian distributions with standard deviations scaled to modal parameters in the considered COV. Across the realizations, generated random errors assigned to modes are statistically independent. Dimension of a noise realization vector for one structural mode contains 2 noise levels x (1 frequency + 51 mode shape) = 104 components. Table 6.2 summarizes the input factors and their levels. Accordingly, 2 x 2 x 2 x 2 = 16 combination requires 16 x 20 = 320 identification runs in order to investigate the uncertainty in damage identification results.

Table 6.1 Finite element model and modal parameters of undamaged and damaged RC structural frame and design variables

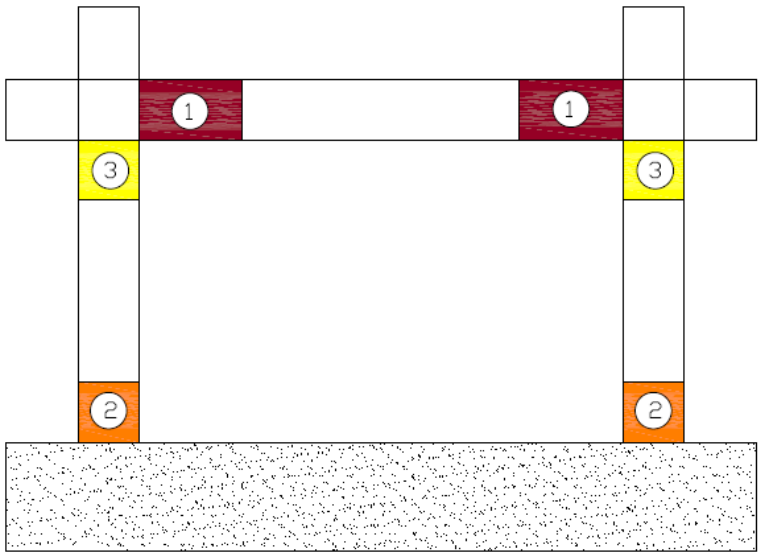

Support Conditions: Simple Support + Rotational Springs in 3 Directions
Rotational Spring Properties Rot-X=5894 kNm/rad, Rot-Y=7444 kNm/rad, Rot-Z=20000 kNm/rad

Reference (Undamaged) FE Model Frequencies	Damaged FE Model Frequencies
Mode1) 5.58 Hz	Mode1) 5.14 Hz
Mode2) 9.40 Hz	Mode2) 8.31 Hz
Mode3) 14.98 Hz	Mode3) 12.63 Hz
Mode4) 65.90 Hz	Mode4) 57.68 Hz

Design Variables: ① Beam ends; ② Column(s) bottom ends; ③ Column(s) top ends

Table 6.1 continues

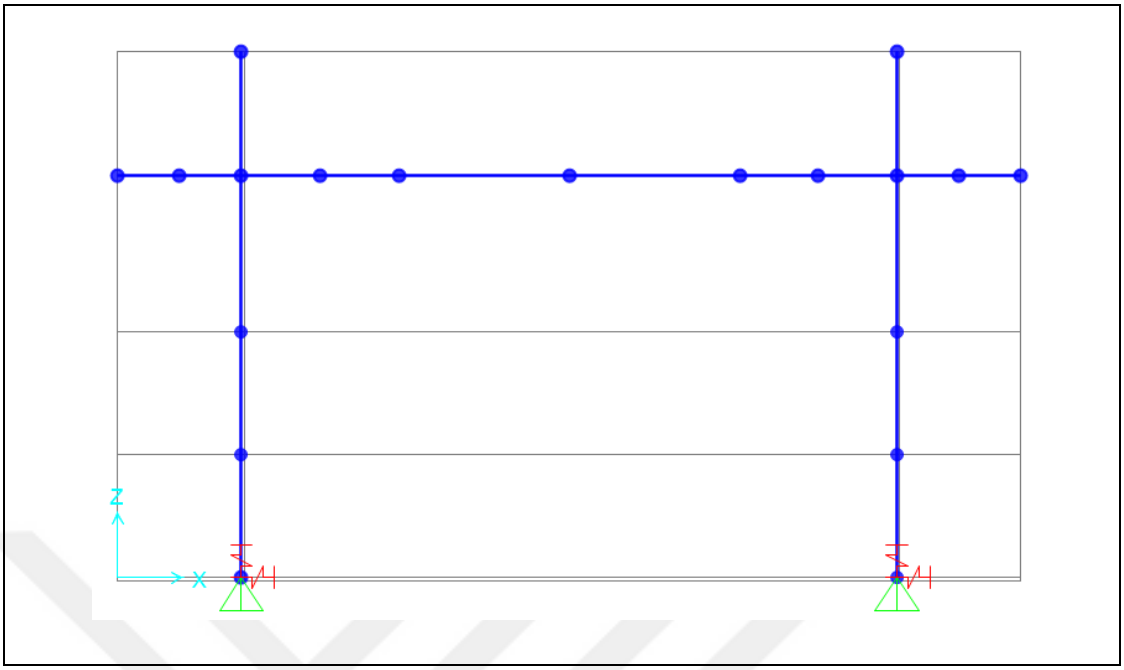

Table 6.2 Description of input factors and their levels in uncertainty study

Factor	Description	Levels
M1	Uncertainty in modal parameters of 1st mode	2 levels (0.5%, 1% COV)
M2	Uncertainty in modal parameters of 2st mode	2 levels (0.5%, 1% COV)
M3	Uncertainty in modal parameters of 3st mode	2 levels (0.5%, 1% COV)
M4	Uncertainty in modal parameters of 4st mode	2 levels (0.5%, 1% COV)

6.3 Uncertainty Quantification Results of Damage Identification

As mentioned in Section 6.2, the problem is solved by 320 identification runs using the model updating algorithm explained in Chapter 3. The damage factors were not constrained for updating the reference undamaged model to the damaged (simulated) model. The outcomes of the study (stiffness parameters) are later than used in ANOVA testing in order to understand which input factor (structural modes) contributes more to the uncertainty in damage identification. Figure 6.1 shows the spread of the identification results for each 3 substructures for all 320 identification runs. The mean values of damage factors are 0.306, 0.399, 0.505 for column bottom end(s), column top end(s) and beam end(s), respectively. Note that, the ensemble of

damage factors are obtained by varying 4 input factors (M1, M2, M3, M4), namely the first 4 structural modes polluted with two levels of noise.

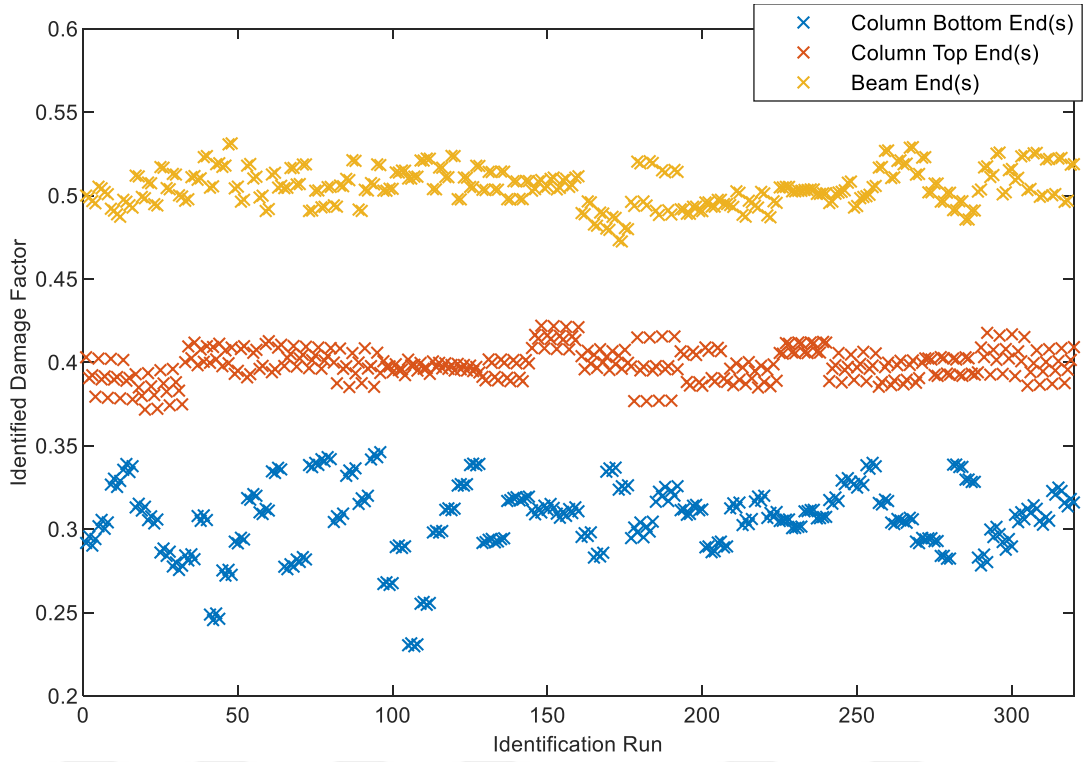

Figure 6.1 Spread of identified damage factors at column bottom end(s), column top end(s) and beam end(s) for all 320 identification runs (20 realizations)

Figure 6.2 shows the distributions of the identified damage factors (design variables) for each substructure. On each box, the central mark indicates the median, and the bottom and top edges of the box indicate the 25^{th} and 75^{th} percentiles (lower and upper quartiles), respectively. The whiskers extend to the most extreme data points not considered outliers, and the outliers are plotted individually using the '+' symbol. Table 6.3 also reports the mean and standard deviation of the 320 sets of identified damage factors for each substructure. The large standard deviation in identified damage factors shows that the residuals used in optimization problem are less sensitive to the design variables that represent these substructures.

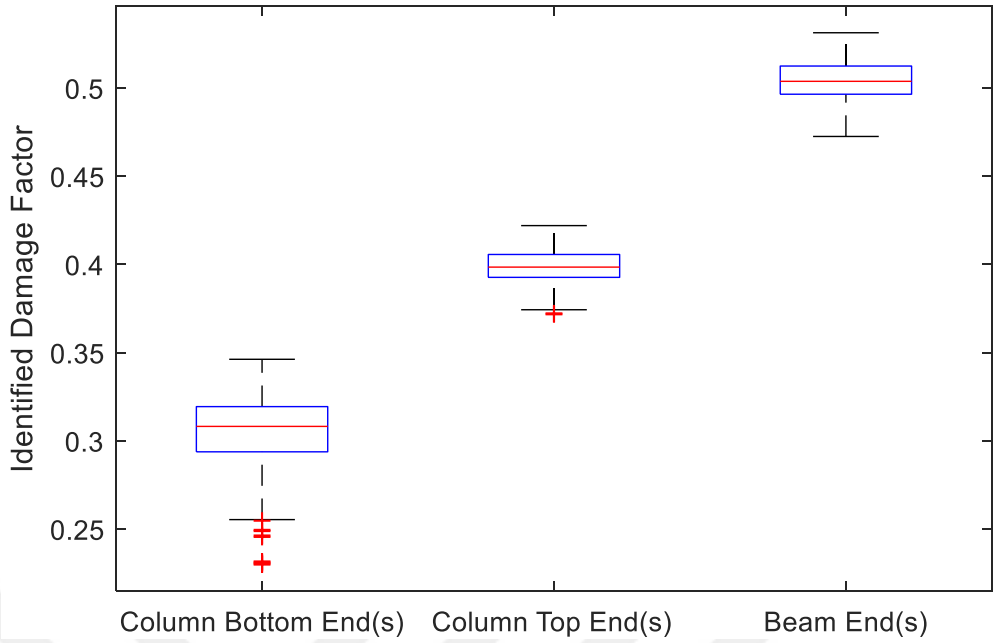

Figure 6.2 Box plot representation of identified damage factors at each substructures for 320 identification runs

Table 6.3 Mean and standard deviation (STD) of identified damage factors at each substructures for 320 identification runs

Substructures	Exact Damage [%]	Mean [%]	STD [%]
Beam End(s)	50	50.5	1.11
Column Top End(s)	40	39.9	0.94
Column Bottom End(s)	30	30.6	2.14

Figure 6.3 show the spread of mean and STD of identified damage factors at different substructures for all 16 combinations of input factors; however from the results presented there, it is not possible to quantify the contribution of input factors M1, M2, M3, M4 to the total uncertainty of the mean and STD of identified damage factors; therefore ANOVA technique is used for the uncertainty quantification of the mean and STD. ANOVA test helps analyst to determine the influence that independent variables (M1, M2, M3, M4) have on dependent variable (damage factors) in a regression study; accordingly the total variances of output features are decomposed into the sum of partial variances, which result different values for each independent input variables. In this technique, input factor contribution to the uncertainty is estimated by partial variances estimated by R^2 value; the input factor

with larger R^2 value for an output feature means the higher contribution to the uncertainty. The R^2 results of mean and standard deviation of the identified damage factors (obtained by 16 combinations) based on 20 noise realizations for each 3 substructures, are presented in Figure 6.4. Results are obtained by the aid of MABLAB command ‘anovan’.

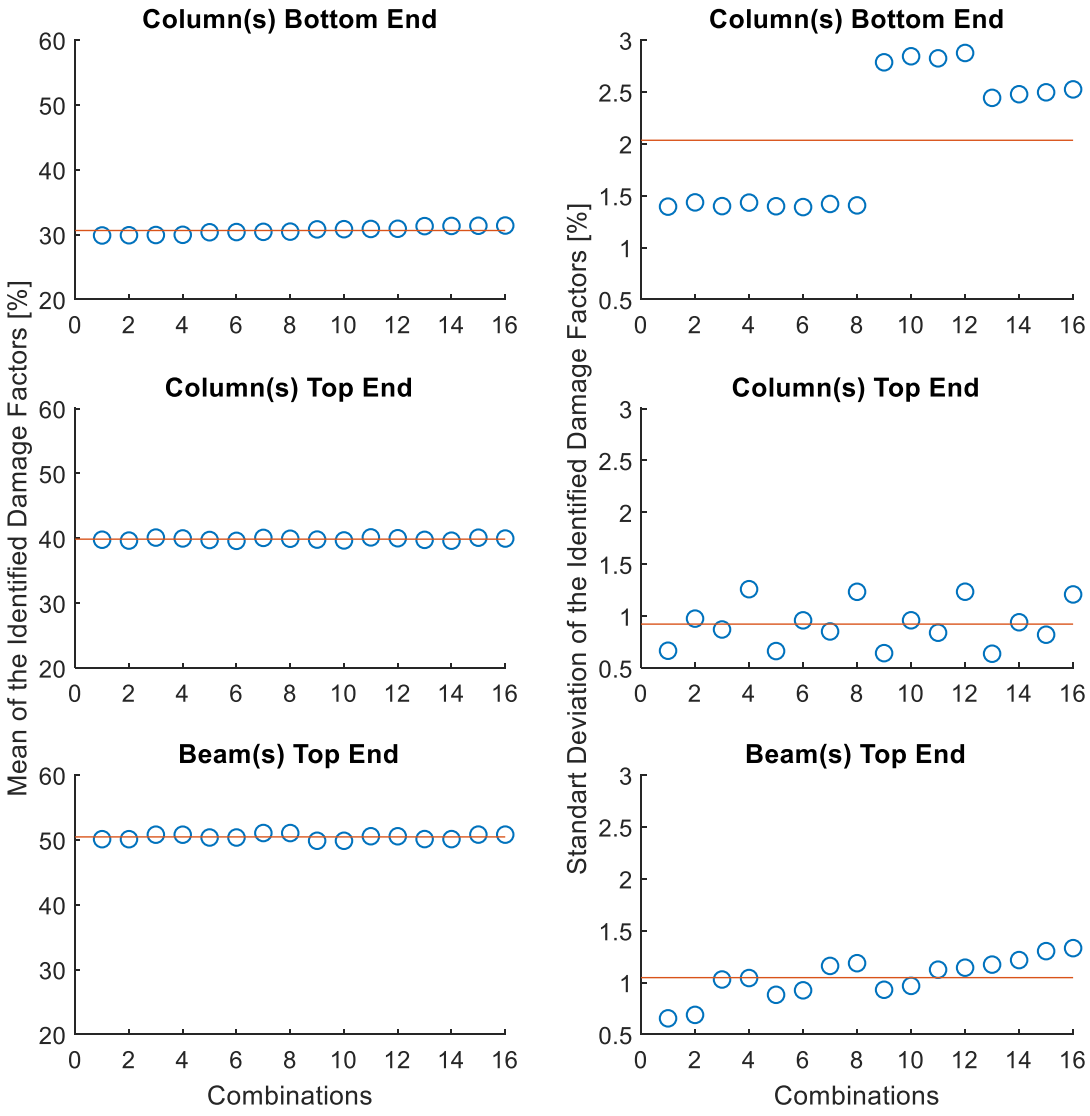

Figure 6.3 Spread of the mean and standard deviation of identified damage factors at different substructures based on 16 combinations of input factors calculated from 20 noise realizations

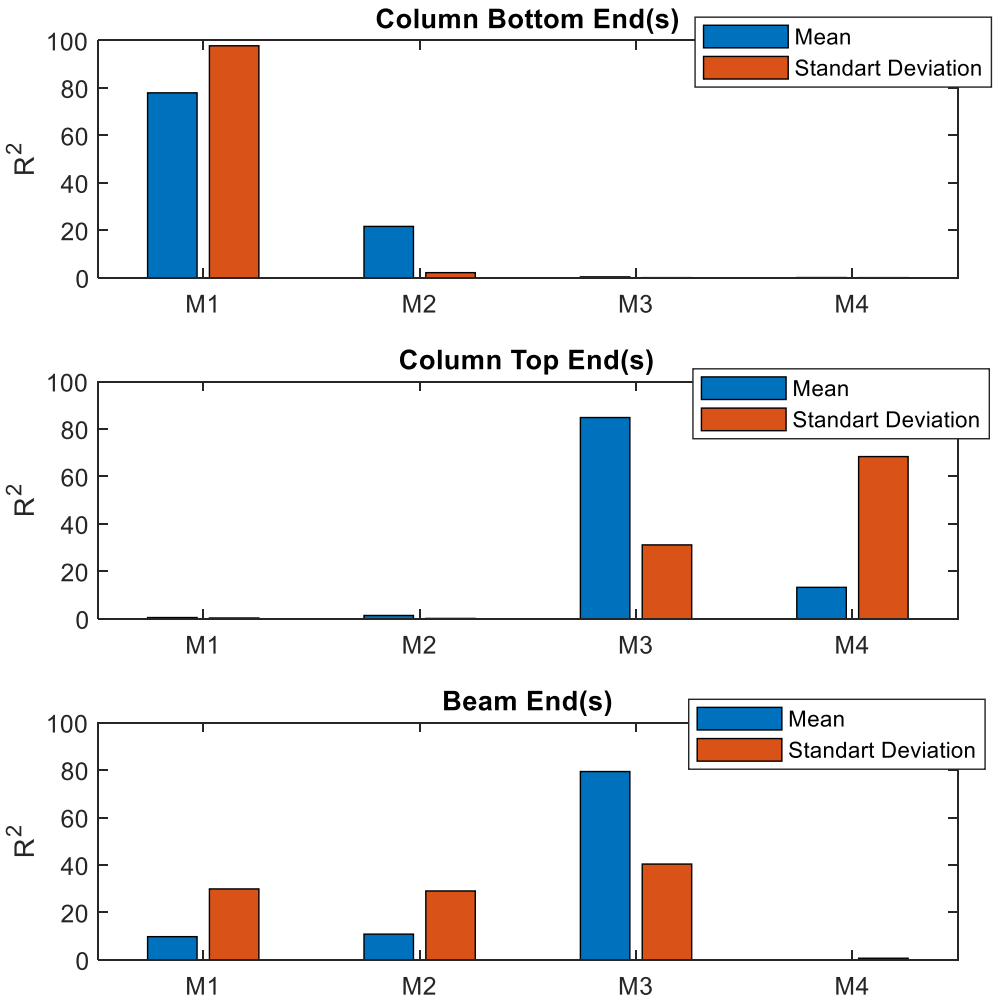

Figure 6.4 R^2 value of the mean and STD of identified damage factors at different substructures due to variability of input factors M1, M2, M3 and M4 (based on 16 combinations of input factors calculated from 20 noise realizations)

R^2 values are normalized such that their sum over all factors equates to 100. Accordingly, the variability in modal parameter M1 (out-of-plane mode) produces significant amount of uncertainty in the mean and STD value of the damage factor for column(s) bottom end; whereas the influence of higher modes to that damage factor produces less uncertainty. It can also be concluded that the uncertainty in modal parameter M2 (torsion mode) has almost no influence in the mean and STD of damage factors. In general the uncertainty in in-plane lateral mode (M3) creates significant uncertainty for damage factors column bottom end(s) and beam end(s). Similar to M2, M4 has almost no influence to the uncertainties in selected damage factors in the sense of mean and STD. As expected, results are found consistable

with the detectability index provided in Figure 5.2 in Section 5. M1 corresponds to out-of-plane mode (experimental 1st mode in Section 5); whereas M3 corresponds to in-plane lateral mode (experimental 2nd mode in Section 5).

CHAPTER SEVEN
CONCLUSIONS AND FUTURE RESEARCH

7.1 Conclusions

The research presented in this thesis mainly contributes to three subjects. (a) system identification of RC structural frame at different damage levels by the use of ambient & white noise vibration data, (b) identification of stiffness parameters of RC structure at various damage levels by the finite element model updating technique using the experimentally identified modal parameters and (c) uncertainty analysis of damage identification due to erroneous modal parameters. The major findings and contributions of this research are summarized as follows:

In the extensive experimental programme, a half-scale, single-bay, single-story RC frame was tested under single-cycle quasi-static loading along the frame in-plane direction. At the pre-determined drift levels, WN and AV tests were performed on the frame; note that in WN tests, laboratory scaled electro-dynamic shaker placed on the top of the specimen is used to excite the RC frame system over the wide frequency band. In order to perform modal parameter identification at different damage levels, three different system identification methods, namely, SSI-DATA, NExT-ERA, and EFDD are used. The findings of the study can be generalized as follows: (i) the results of three different output-only system identification methods are very close to each other for frequency and mode shape estimations under different excitation conditions. The methods used in this study can identify all modal parameters of the RC frames at different damage levels using WN data whereas it is difficult to process the AV datasets by EFDD method due to the corresponding data sets' low SNR characteristics. (ii) The identified frequencies are affected by the excitation level. The natural frequencies identified based on white-noise vibration are systematically lower than its counterpart identified by ambient vibration data for all damage states. This is most likely due to the fact that the frequency estimations are affected by the nonlinear behavior of RC frame. (iii) For the damping estimations, it can be said that NExT-ERA and SSI-DATA methods give somewhat similar results; but the overall consistency of the damping estimations among different methods is

not as good as the frequency and mode shape estimations. The damping results by EFDD method are more different than the values estimated by the other two methods. This higher variability observed in damping estimations by EFDD method can be attributed to the subjectiveness of the peak-picking process. (iv)Damping ratio estimations are amplitude dependent and are sensitive to SNR. The AV data results in lower and the WN data results in higher damping estimations. (v) As expected, for both AV and WN data, the natural frequencies identified by all the methods consistently have a decreasing trend as the frame get damaged.

As a complementary study, FE model updating technique is applied for damage identification. Method is based on the minimization of modal parameters of FE model and experimentally identified. The effectiveness of the algorithm is first shown on simulation example of dimensional (3D) structural frame. In this simulation study, damage is modelled with reduction in translational spring coefficients located at two structural nodes, damaged spring coefficients are successfully identified by the algorithm. Next, the estimated modal parameters are then used to identify the structural damage of the RC frame through the sensitivity-based finite element model updating technique. The FE model of the frame is developed in MATLAB based FEDEASLab software by using 3D frame elements and rotational springs at the supports. Damage identification is performed by minimizing an objective function formulated by the difference between the experimentally identified and the FE predicted modal parameters, i.e. modal residuals are based on the natural frequencies and mode shapes. The least squares problem is solved with the trust region Gauss-Newton method. Updating procedure is performed in two steps: first a reliable reference FE model is obtained using the modal estimation results at the undamaged state, and then the reference model is updated for successive damage states. In these steps, the structural damage is defined by relative stiffness reduction. In order to ensure a well-conditioned optimization problem, the design variables are first reduced to 4 and then to 2 for obtaining FE models representing the reference and different damage states, respectively, by taking into account: (a) the symmetry conditions in geometry, (b) the detectability matrix derived from Jacobian matrix, and (c) the moment capacity ratio of beam and

column members. Results indicate that the sensitivity varies from element to element and from mode to mode. Such as, some elements are insensitive to certain modes (i.e. rotational springs are only sensitive to the modes associated to the axis in which the springs rotate). The elements with higher sensitivities are the ones affected the most by the updating algorithm which does not automatically imply that the design parameters associated with these elements must be included in the design parameters set. If these elements are already representative of the true values, excluding them from the updating procedure (not updating them) is considered to be beneficial for obtaining more accurate damage identification results (i.e. representative of the actual observed damage). The identification results clearly show that structural damage severity consistently increases as the frame is subjected to higher drift ratios, as expected. The first significant stiffness loss of the frame is identified at 1.00% drift ratio (i.e. 35% and 81% for column(s) bottom ends and beam ends, respectively). Beyond this drift ratio (from 1.40% to 3.50%), the stiffness reduction factor for the column(s) bottom ends increases to 79% while no significant change at the beam ends occurs (a change of only 81% to 91% occurs). In other words, beyond 1.00% drift ratio, structural damage concentrates on the column(s) bottom ends with a small increase on the beam ends. It is shown that the solution to the objective function has a flat surface in the vicinity of the optimal solution at low drift levels, but then concentrates to a narrower region as the drift level increases. This shows that the chosen design parameters set (one for the beam and one for the column(s) bottom ends) does not provide a unique solution especially for low level damage states; but tends to provide a unique one for high level damage states. The damage identification results are also supported by visual damage inspections made on the R/C frame at the end of each drift level. At the ultimate damage level, large cracks are clearly visible on the beam and column(s) bottom ends which are strongly supported by the damage identification results.

In SHM, the estimation errors on modal parameters are found influential on damage identification results; this motivated author to perform and uncertainty analysis. The damaged frame structure is simulated by stiffness reduction in 3 locations (beam ends, column(s) top and bottom end(s)), and its first 4 modal

parameters used in FEMU algorithm are polluted with two noise levels, namely with 0.5% and 1.0% COVs. This allowed 2 x 2 x 2 x 2 = 16 different combinations of input factors (modal parameters); therefore each different combination of modal parameters were used to identify the simulated damage in these substructures. For each combination of these 4 modal parameters polluted with 2 different noise characteristics, 20 identification runs are performed with statistically independent realizations, which results totally 16 x 20 = 320 identification runs. Results are quantified through the analysis of variance (ANOVA) and following observations are made. Compared to M2 and M3, uncertainty in modal parameters of out-of-plane mode (M1) affects significantly both the mean and standard deviation of the identified column bottom end(s) damage; whereas uncertainties in lateral in-plane mode mainly influences both the mean and standard deviation of identified damage of the column top end(s) and beam end(s). Uncertainties in torsional and vertical in-plane modes (M2 and M4) didn't find effective on the mean and standard deviation value of the identified damage. The sensitivity index results (detectability) extracted from Jacobian matrix presented in Chapter 5 is complemented with the findings obtained in uncertainty study.

7.2 Recommendations for Future Research

The following research suggestions are offered for future studies:

As an alternative or addition to the mode shape vectors, damage identification by FEMU can be carried out by combining dynamic test data with modal strain or static deflection data in the residual vector. Note that, modal strains are very sensitive to the local damage where they are measured; whereas they are insensitive for the farther locations. Yet, difficulties are existing in combination of these two different kind of data. Since the engineering structures generally have nonlinear behavior under excessive loadings, static and dynamic stiffnesses are different. It should be noted that this study aims to focus on the capabilities of a linear model updating technique applied to a progressively damaged frame structure. It is known that there are also nonlinear model updating techniques which update parameters of hysteretic

material models. Being able to update nonlinear model parameters may prove itself more useful in quantification of structural damage.

In this thesis, damage identification results are obtained under the assumption that mass is known and not altered. Alteration of mass as a damage indicator can be considered together with stiffness degradation.

The effects of modeling and measurement errors on damage identification results can be quantified in a more comprehensive way. The uncertainties in estimation of structural modal parameters due to measurement errors are mainly depending on various components, e.g. spatial density measurements, measurement noise, length of measurement data, amplitude of input excitation. On the other hand FE modeling assumptions, e.g. type of finite elements, number and/or selection of design variables, number of residuals, weighting factors creates modeling errors which results uncertainties in model updating. Uncertainty quantification assessment can be performed by taking into account these factors in ANOVA. The effects of modeling and measurement errors on damage identification results can also be investigated by non-probabilistic interval-based methods or probabilistic Bayesian FE model updating methods.

The damage assessment of infilled frames will be investigated in upcoming studies. Regarding the behavior of infilled frame structures, special attention is required to infills as the entire structural behavior in the sense of overall stiffness, strength and ductility are adjusted, especially under seismic excitations. In this thesis, FEMU method is integrated in MATLAB based FEDEASLab environment for damage identification and localization; however, current capability of the program is limited in updating of translational, rotational springs and 3D beam elements having 6 translational, 6 rotational DOFs. The software can further be extended by implementation a four node shell element definition which is required to model the infill walls. Alternatively, this problem may be handled by modeling the infilled walls as code-conformed diagonal struts.

As a supplementary tool of the FE model updating for damage identification, damage model based on remnant stiffness definitions of cracked RC elements subjected to bending moments can be derived; and the obtained value can be compared with the ones obtained from dynamic results based on FEMU.

REFERENCES

Allemang, R. J. (2003). The modal assurance criterion–twenty years of use and abuse. *Sound and Vibration, 37* (8), 14-23.

Astroza, R., Ebrahimian, H., Conte, J. P., Restrepo, J. I., & Hutchinson, T. C. (2016). System identification of a full-scale five-story reinforced concrete building tested on the NEES-UCSD shake table. *Structural Control and Health Monitoring*, *23* (3), 535-559.

Bakir, P. G., Reynders, E., & De Roeck, G. (2008). An improved finite element model updating method by the global optimization technique 'Coupled Local Minimizers'. *Computers & Structures*, *86* (11-12), 1339-1352.

Baruch, M. (1978). Optimization procedure to correct stiffness and flexibility matrices using vibration tests. *AIAA Journal*, *16* (11), 1208-1210.

Belleri, A., Moaveni, B., & Restrepo, J. I. (2014). Damage assessment through structural identification of a three-story large-scale precast concrete structure. *Earthquake Engineering & Structural Dynamics*, *43* (1), 61-76.

Bendat, J. S., & Piersol, A. G. (2011). *Random data: Analysis and measurement procedures* (Vol. 729). Hoboken, New Jersey: John Wiley & Sons.

Berman, A. (1979). Mass matrix correction using an incomplete set of measured modes. *AIAA Journal*, *17* (10), 1147-1148.

Berman, A., & Nagy, E. J. (1983). Improvement of a large analytical model using test data. *AIAA Journal*, *21* (8), 1168-1173.

Brincker, R. (2014). Some elements of operational modal analysis. *Shock and Vibration*, 2014, 11.

Brincker, R., & Andersen, P. (2006). Understanding stochastic subspace identification. *Proceedings of the 24th IMAC, St. Louis*, 126.

Brincker, R., & Ventura, C. (2015). *Introduction to operational modal analysis*. Chichester, United Kingdom: John Wiley & Sons.

Brincker, R., & Zhang, L. (2009). Frequency domain decomposition revisited. In *Proc. 3rd International Operational Modal Analysis Conference (IOMAC'09)*, 615-626.

Brincker, R., Zhang, L., & Andersen, P. (2001). Modal identification of output-only systems using frequency domain decomposition. *Smart Materials and Structures*, *10* (3), 441.

Brownjohn, J. M., & Xia, P. Q. (2000). Dynamic assessment of curved cable-stayed bridge by model updating. *Journal of Structural Engineering*, *126* (2), 252-260.

Caesar, B. (1987). Updating system matrices. In *International Modal Analysis Conference, 5 th, London, England*, 453-459.

Caicedo, J. M. (2011). Practical guidelines for the natural excitation technique (NExT) and the eigensystem realization algorithm (ERA) for modal identification using ambient vibration. *Experimental Techniques*, *35* (4), 52-58.

Caicedo, J. M., Dyke, S. J., & Johnson, E. A. (2004). Natural excitation technique and eigensystem realization algorithm for phase I of the IASC-ASCE benchmark problem: Simulated data. *Journal of Engineering Mechanics*, *130* (1), 49-60.

Carvalho, J., Datta, B. N., Gupta, A., & Lagadapati, M. (2007) A direct method for model updating with incomplete measured data and without spurious modes. *Mechanical Systems and Signal Processing*, *21* (7), 2715-2731.

Conn, A. R., Gould, N. I., & Toint, P. L. (2000). *Trust region methods* (Vol. 1). Philadelphia, USA: Siam, MOS-SIAM Series of Optimization.

CSI, S. V. (2018). *Integrated finite element analysis and design of structures basic analysis reference manual*. Computers and Structures Inc, Berkeley (CA, USA).

Das, S., Saha, P., & Patro, S. K. (2016). Vibration-based damage detection techniques used for health monitoring of structures: a review. *Journal of Civil Structural Health Monitoring*, *6* (3), 477-507.

De Roeck, G. (2019). *Model–Based Methods of Damage Identification of Structures Under Seismic Excitation*. Retrieved April 25, 2019, from https://link.springer.com/chapter/10.1007%2F978-3-030-13976-6_10

Der Kiureghian, A., & Ditlevsen, O. (2009). Aleatory or epistemic? Does it matter?. *Structural Safety*, *31*(2), 105-112.

Doebling, S. W., Farrar, C. R., & Prime, M. B. (1998). A summary review of vibration-based damage identification methods. *Shock and Vibration Digest*, *30* (2), 91-105.

El-Borgi, S., Choura, S., Ventura, C., Baccouch, M., & Cherif, F. (2005). Modal identification and model updating of a reinforced concrete bridge. *Smart Structures and Systems*, *1* (1), 83-101.

Fang, H., Wang, T. J., & Chen, X. (2011). Model updating of lattice structures: A substructure energy approach. *Mechanical Systems and Signal Processing*, *25* (5), 1469-1484.

Fang, S. E., Perera, R., & De Roeck, G. (2008). Damage identification of a reinforced concrete frame by finite element model updating using damage parameterization. *Journal of Sound and Vibration*, *313* (3-5), 544-559.

Felber, A. J. (1994). *Development of a hybrid bridge evaluation system.* Phd Thesis, University of British Columbia, Vancouver.

Ferrari, R., Froio, D., Rizzi, E., Gentile, C., & Chatzi, E. N. (2019). Model updating of a historic concrete bridge by sensitivity-and global optimization-based Latin Hypercube Sampling. *Engineering Structures*, *179*, 139-160.

Foti, D., Diaferio, M., Giannoccaro, N. I., & Mongelli, M. (2012). Ambient vibration testing, dynamic identification and model updating of a historic tower. *NDT & E International*, *47*, 88-95.

Fox, R. L., & Kapoor, M. P. (1968). Rates of change of eigenvalues and eigenvectors. *AIAA Journal*, *6* (12), 2426-2429.

Friswell, M., & Mottershead, J. E. (2013). *Finite element model updating in structural dynamics.* Dordrecht, Netherlands: Kluwer Academic Publisher.

Giraldo, D. F., Song, W., Dyke, S. J., & Caicedo, J. M. (2009). Modal identification through ambient vibration: Comparative study. *Journal of Engineering Mechanics, 135* (8), 759-770.

Goksu, C., Inci, P., Demir, U., Yazgan, U., & Ilki, A. (2017). Field testing of substandard RC buildings through forced vibration tests. *Bulletin of Earthquake Engineering, 15* (8), 3245-3263.

Guo, Y. L., Ni, Y. Q., & Chen, S. K. (2017). Optimal sensor placement for damage detection of bridges subject to ship collision. *Structural Control and Health Monitoring, 24* (9).

Hu, S. L. J., Li, H., & Wang, S. (2007). Cross-model cross-mode method for model updating. *Mechanical Systems and Signal Processing, 21* (4), 1690-1703.

Ibrahim, S. R. (1977). Random decrement technique for modal identification of structures. *Journal of Spacecraft and Rockets, 14* (11), 696-700.

ISO/IEC 17025 Standard (2006). *General requirements for the competence of testing and calibration laboratories*.

Jacobsen, N. J., Andersen, P., & Brincker, R. (2008). Applications of frequency domain curve-fitting in the EFDD technique. In *Proceedings IMAC XXVI Conference*.

James, G. H., Carne, T. G., & Lauffer, J. P. (1995). The natural excitation technique (NExT) for modal parameter extraction from operating structures. *Modal Analysis-the International Journal of Analytical and Experimental Modal Analysis, 10* (4), 260-277.

Ji, X., Fenves, GL., Kajiwara, K., & Nakashima, M. (2010). Seismic damage detection of a full-scale shaking table test structure. *Journal of Structural Engineering, 137*(1), 14-21.

Juang, J. N., & Pappa, R. S. (1985). An eigensystem realization algorithm for modal parameter identification and model reduction. *Journal of Guidance, Control, and Dynamics*, *8*(5), 620-627.

Kammer, D. C. (1991). Sensor placement for on-orbit modal identification and correlation of large space structures. *Journal of Guidance, Control, and Dynamics*, *14* (2), 251-259.

Kennedy, M. C., & O'Hagan, A. (2001). Bayesian calibration of computer models. *Journal of the Royal Statistical Society: Series B*, *63*(3), 425-464.

Leyder, C., Dertimanis, V., Frangi, A., Chatzi, E., & Lombaert, G. (2018). Optimal sensor placement methods and metrics–comparison and implementation on a timber frame structure. *Structure and Infrastructure Engineering*, *14* (7), 997-1010.

Maia, N. M. M., Silva, J. M., He, J., Lieven, N. A. J., Lin, R. M., Skingle, G. W., ... & Urgueira, V. A. M (1997). *Theoretical and Experimental Modal Analysis*. Baldock, UK: Wiley.

MATLAB (2017) The MathWorks Inc., MA, USA.

Meo, M., & Zumpano, G. (2005). On the optimal sensor placement techniques for a bridge structure. *Engineering Structures*, *27* (10), 1488-1497.

Moaveni, B., Conte, J. P., & Hemez, F. M. (2009). Uncertainty and sensitivity analysis of damage identification results obtained using finite element model updating. *Computer‐Aided Civil and Infrastructure Engineering*, *24* (5), 320-334.

Moaveni, B., He, X., Conte, J. P., Restrepo, J. I., & Panagiotou, M. (2010). System identification study of a 7-story full-scale building slice tested on the UCSD-NEES shake table. *Journal of Structural Engineering*, *137* (6), 705-717.

Moaveni, B., Stavridis, A., Lombaert, G., Conte, J. P., & Shing, P. B. (2012). Finite-element model updating for assessment of progressive damage in a 3-story infilled RC frame. *Journal of Structural Engineering*, *139* (10), 1665-1674.

Modak, S. V. (2014). Direct matrix updating of vibroacoustic finite element models using modal test data. *AIAA Journal*, *52* (7), 1386-1392.

Mottershead, J. E., & Friswell, M. I. (1993). Model updating in structural dynamics: A survey. *Journal of Sound and Vibration*, *167* (2), 347-375.

Mottershead, J. E., Link, M., & Friswell, M. I. (2011). The sensitivity method in finite element model updating: A tutorial. *Mechanical Systems and Signal Processing*, *25* (7), 2275-2296.

Nozari, A., Behmanesh, I., Yousefianmoghadam, S., Moaveni, B., & Stavridis, A. (2017). Effects of variability in ambient vibration data on model updating and damage identification of a 10-story building. *Engineering Structures*, *151*, 540-553.

Overchee, V., & Moor, B. L. (1996). *Subspace identification for linear systems*. Dordrecht: Kluwer Academic Publishers.

Peeters, B., & De Roeck, G. (1999). Reference-based stochastic subspace identification for output-only modal analysis. *Mechanical Systems and Signal Processing*, *13* (6), 855-878.

Petersen, Ø. W., & Øiseth, O. (2017). Sensitivity-based finite element model updating of a pontoon bridge. *Engineering Structures*, *150*, 573-584.

Rodrigues, J., Brincker, R., & Andersen, P. (2004). Improvement of frequency domain output-only modal identification from the application of the random decrement technique. In *Proc. 23rd International Modal Analysis Conference, Deaborn, MI*, 92-100.

Sehgal, S., & Kumar, H. (2016). Structural dynamic model updating techniques: A state of the art review. *Archives of Computational Methods in Engineering*, *23* (3), 515-533.

Simoen, E., De Roeck, G., & Lombaert, G. (2015). Dealing with uncertainty in model updating for damage assessment: A review. *Mechanical Systems and Signal Processing*, *56*, 123-149.

Sohn, H., Farrar, C. R., Hemez, F. M., Shunk, D. D., Stinemates, D. W., Nadler, B. R., & Czarnecki, J. J. (2003). A review of structural health monitoring literature: 1996–2001. *Los Alamos National Laboratory, USA.*

Soize, C. (2010). Generalized probabilistic approach of uncertainties in computational dynamics using random matrices and polynomial chaos decompositions. *International Journal for Numerical Methods in Engineering*, *81*(8), 939-970.

Song, M., Yousefianmoghadam, S., Mohammadi, M. E., Moaveni, B., Stavridis, A., & Wood, R. L. (2018). An application of finite element model updating for damage assessment of a two-story reinforced concrete building and comparison with lidar. *Structural Health Monitoring*, *17* (5), 1129-1150.

Standard: ANSI/ASA S2.47. (1990). American national standard vibration of building-guidelines for the measurement of vibrations and evaluation of their effects on building. Acoustical Society of America.

Stavridis, A., Koutromanos, I., & Shing, P. B. (2012). Shake-table tests of a three-story reinforced concrete frame with masonry infill walls. *Earthquake Engineering & Structural Dynamics*, *41* (6), 1089-1108.

Sun, R., Perera, R., Sevillano, E., & Gu, J. (2018). Parameter identification of composite materials based on spectral model by using model updating method. *International Journal of Polymer Science*, *2018*, 1-9.

Teughels, A. (2003). *Inverse modelling of civil engineering structures based on operational modal data.* Phd Thesis, University of Leuven, Leuven.

Teughels, A., & De Roeck, G. (2005). Damage detection and parameter identification by finite element model updating. *Revue Européenne de Génie Civil*, *9* (1-2), 109-158.

Teughels, A., Maeck, J., & De Roeck, G. (2002). Damage assessment by FE model updating using damage functions. *Computers & Structures*, *80* (25), 1869-1879.

Walker, W. E., Harremoës, P., Rotmans, J., Van Der Sluijs, J. P., Van Asselt, M. B., Janssen, P., & Krayer von Krauss, M. P. (2003). Defining uncertainty: a conceptual basis for uncertainty management in model-based decision support. *Integrated assessment*, *4*(1), 5-17.

Weber, B., Paultre, P., & Proulx, J. (2007). Structural damage detection using nonlinear parameter identification with Tikhonov regularization. *Structural Control and Health Monitoring*, *14* (3), 406-427.

Wei, F. S. (1990). Analytical dynamic model improvement using vibration test data. *AIAA Journal*, *28* (1), 175-177.

Welch, P. (1967). The use of fast Fourier transform for the estimation of power spectra: a method based on time averaging over short, modified periodograms. *IEEE Transactions on Audio and Electroacoustics*, *15* (2), 70-73.

Weng, S., Xia, Y., Xu, Y. L., & Zhu, H. P. (2011). Substructure based approach to finite element model updating. *Computers & Structures*, *89* (9-10), 772-782.

Yang, Y. B., & Chen, Y. J. (2009) A new direct method for updating structural models based on measured modal data. *Engineering Structures 31* (1), 32-42.

Yi, T. H., Li, H. N., & Zhang, X. D. (2012). Sensor placement on Canton Tower for health monitoring using asynchronous-climb monkey algorithm. *Smart Materials and Structures*, *21* (12), 125023.

Yu, L., & Yin, T. (2010). Damage identification in frame structures based on FE model updating. *Journal of Vibration and Acoustics*, *132* (5), 051007.

Zhang, J., Maes, K., De Roeck, G., Reynders, E., Papadimitriou, C., & Lombaert, G. (2017). Optimal sensor placement for multi-setup modal analysis of structures. *Journal of Sound and Vibration*, *401*, 214-232.

APPENDIX-1: List of Symbols

CHAPTER TWO

$\tilde{\mathbf{y}}(f)$	vector of response in frequency domain
$\tilde{\mathbf{x}}(f)$	vector of inputs in frequency domain
$\tilde{\mathbf{H}}_{yx}(f)$	frequency response function
$\mathbf{C}_x$	correlation matrix
$\mathbf{x}(t)$	vector of inputs in time domain
$\hat{\mathbf{e}}(f)$	vector of white noise sources
$\mathbf{A}$	mode shape matrix discrete time state-space matrix
$\hat{\mathbf{A}}$	estimated mode shape matrix
$\mathbf{q}(t)$	vector of modal coordinates
OSP_{index}	optimal sensor placement index
$\{X_i\}$	random vector added on mode shape vector
ε	uncertainty parameter
σ	standard deviation used to create $\{X_i\}$
T	measurement duration
f	modal frequencies of the structure
ξ	damping factor
$\mu(\tau)$	moving average
$\sigma(\tau)^2$	standard deviation
$w(\tau)$	tapering window
a(k), b(k)	filter constants
na, nb	number of IIR and FIR filter coefficients
f_I	cut-off frequency
$\hat{\mathbf{R}}(\tau)$	unbiased cross correlation function
k	discrete time operator
N	total number of data points

T	size of averaging window
$\mathbf{Y}$	data series matrix
τ	time shift
$\mathbf{x}_0(t),\ \mathbf{y}_0(t)$	zero padded versions of $\mathbf{x}(t),\ \mathbf{y}(t)$
$[\lambda_n]$	diagonal matrix of eigenfrequencies
$[\mu_n]$	matrix of discrete time poles
$\boldsymbol{\Gamma}$	modal participation matrix observability matrix
$\boldsymbol{\gamma}_n$	modal participation vectors
$\mathbf{H}$	block row matrix form of correlation functions
(q_n)	absolute scalar measure of modal participation factor
$\mathbf{H}_1$	block Hankel matrix
$\mathbf{H}_2$	one block Hankel matrix with only a single block row
$\mathbf{A}_C$	companion matrix
ω_n	angular frequencies of structure
$\mathbf{M}$	mass matrix
$\mathbf{C}$	damping matrix
$\mathbf{K}$	stiffness matrix
$\mathbf{y}(t)$	vector of displacements
$\dot{\mathbf{y}}(t)$	vector of velocity
$\ddot{\mathbf{y}}(t)$	vector of acceleration
$\mathbf{F}(t)$	externally applied force vector
$\mathbf{R}_{\ddot{y},\ddot{y}_i}(\tau)$	vector of correlation functions
$\dot{\mathbf{R}}_{\ddot{y},\ddot{y}_i}(\tau)$	first order derivative of correlation function
$\ddot{\mathbf{R}}_{\ddot{y},\ddot{y}_i}(\tau)$	second order derivative of correlation function
A, B, C, D	discrete-time state-space matrices
$\mathbf{R}_{mxm}$, $\mathbf{S}^T_{sxs}$	matrices of left and right eigenvectors of $\mathbf{H}(0)$
$\boldsymbol{\Sigma}_g$	diagonal matrix of singular values
$[\boldsymbol{\varphi}']$	eigenvector of discrete time system

$\boldsymbol{\Psi}$	matrix holding the mode shapes in the columns
$\boldsymbol{\Lambda}$	matrix holding the discrete time poles
$\mathbf{T}_{11}, \mathbf{T}_{21}, \mathbf{T}_{12}, \mathbf{T}_{22}$	block Toeplitz matrices
$\mathbf{O}$	projection matrix
$\mathbf{X}$	matrix of Kalman states
$\mathbf{G}_y(\mathrm{k})$	the half spectrum of spectral density matrix at k^{th} frequency interval
$\mathbf{G}_y(f)$	spectral density matrix of the response
$\mathbf{R}_q(\tau)$	auto-correlation function of the modal coordinate
u_c	mode shape on the channel c
$\mathbf{G}_q(f)$	spectral density matrix of modal corrdinates
$g_n^2(f)$	autospectral densities of $\mathbf{G}_q(f)$

CHAPTER THREE

$\mathbf{p} \in \mathbb{R}^n$	vector of design parameters
m	the number of residuals
m_f	the number of frequency residuals
m_s	the number of mode shape residuals
$\mathbf{r}_j$	j^{th} residual in the optimization problem
$z_j(\mathbf{p})$	the quantity of modal parameters belongs to FE model
$\tilde{z}_j$	the components of experimental modal data
$\mathbf{r}_f(\mathbf{p}), \mathbf{r}_s(\mathbf{p})$	the eigenfrequency and mode shape residuals
ϕ_i	numerical mode shapes
$\overline{\phi}_j$	experimental mode shapes
λ_i	numerical eigenvalues
$\overline{\lambda}_j$	experimental eigenvalues
ϕ_j^l	mode shape component of the j^{th} mode shape vector ϕ_j

ϕ_j^{ref}	reference mode shape component of the j^{th} mode shape vector ϕ_j (belong to the finite element model)
$\tilde{\phi}_j^{l}$	mode shape component of the j^{th} mode shape vector $\tilde{\phi}_j$ (belong to the experimentally identified)
$\tilde{\phi}_j^{ref}$	reference mode shape component of the j^{th} mode shape vector $\tilde{\phi}_j$ (belong to the experimentally identified)
$\mathbf{W}$	diagonal weighting matrix
w_j	weighting factor of $\mathbf{r}_j$
$\mathbf{X}$	physical variables to be updated
$\mathbf{X}^e$, $\mathbf{X}_{ref}^e$	the physical parameter value in element e and its reference value
a_x^e, a^e	dimensionless correction factor
$\mathbf{K}$	global stiffness matrix
$\mathbf{K}^U$	stiffness matrix of elements properties remain unchanged
n^e	the number of elements (or group of elements) which are updated
$\mathbf{K}^e$	updated element stiffness matrix
$\mathbf{K}_{ref}^e$	reference element stiffness matrix
$\mathbf{N}$	matrix of damage function
$f(\mathbf{p})$	objective (cost) function
$q_k(\mathbf{z})$	quadratic model function of $f(\mathbf{p})$
$\mathbf{z}_k^{GN}$	Gauss-Newton iteration step vector
∇ (.)	gradient operator
∇^2(.)	hessian operator
Δ	radius of the trust region
J	Jacobian matrix

CHAPTER FOUR

f_i, f_j	frequencies for successive model orders
ξ_i, ξ_j	damping ratios for successive model orders
$\oplus$	a pole with stable frequency, damping and mode shape
.d	a pole with stable frequency and damping
.v	a pole with stable frequency and mode shape
.f	a pole with stable frequency only
ζ_{hyst}	hysteretic damping ratios of the frame

CHAPTER FIVE

D_j	detectability index
s_j	jth column of the sensitivity matrix
l_b , u_b	lower and upper bounds applied on design variables
f_{und}	natural frequency of undamaged structure
$f_{dam,i}$	natural frequency of damaged structure at state 'i'

CHAPTER SIX

$\mathbf{G}_{model}$	model or transfer operator
$\mathbf{p}_{model}$	numerical model parameters
$\overline{d}$	observed structural behaviour
d	real structural response
μ_D	measurement error